

Membrane Type 1 Matrix Metalloproteinase Cleaves Low Density Lipoprotein Receptor to Regulate Lipid Metabolism

by

Maggie Wang

A thesis submitted in partial fulfillment of the requirements for the degree of

Master of Science

Medical Sciences - Pediatrics
University of Alberta

© Maggie Wang, 2022

Abstract

Low-density lipoprotein receptor (LDLR) mediates clearance of plasma LDL cholesterol (LDL-C) and protects against the development of atherosclerosis. Our previous studies demonstrated that membrane type-1 matrix metalloproteinase (MT1-MMP/MMP14) cleaves LDL receptor (LDLR) and exacerbates the development of atherosclerosis. In this study, we investigated the determinants in LDLR and MT1-MMP that were critical for MT1-MMP-induced LDLR cleavage. We performed site-directed mutagenesis to generate LDLR and MT1-MMP mutations and observed that deletion of various functional domains in LDLR, including the ligand-binding repeats (LBR), the epidermal growth factor precursor homology domain, the clustered O-glycosylation region, and the C-terminal cytoplasmic tail, did not affect MT1-MMP induced cleavage of the receptor. Furthermore, removal of four predicted MT1-MMP cleavage sites on LDLR had no effect on cleavage by MT1-MMP. In addition, we observed multiple cleaved fragments of LDLR in the cell culture medium. In MT1-MMP, deletion of the catalytic domain or the MT-loop, but not the hemopexin (HPX) domain or the C-terminal cytoplasmic tail of MT1-MMP, significantly decreased MT1-MMP's ability to cleave LDLR. Further Ala-scanning analysis revealed the important role of Ile at position 167 within the MT-loop in MT1-MMP's action on LDLR. Replacement of Ile167 with polar residues in MT1-MMP caused a significant loss in LDLR cleavage, whereas mutation of Ile167 to a non-polar amino acid residue had no effect.

In addition, MT1-MMP cleaves extracellular matrix (ECM) components, such as type I collagen, and plays a critical role in maintaining homeostasis of ECM. Considering the crucial role of ECM in the progression of liver fibrosis, we studied MT1-MMP's effects on this process. To do so, we fed MT1-MMP hepatocyte specific knockout (*Mmp14^{LKO}*) mice and the control

Mmp14^{Flox} mice with a high fat, high fructose, and high cholesterol Gubra amylin liver NASH (GAN) diet for 42 weeks. We did not observe any significant difference between *Mmp14^{LKO}* and *Mmp14^{Flox}* mice in body weight, blood glucose levels, plasma levels of total cholesterol (TC), high density lipoprotein cholesterol (HDL-C), non-HDL-C, and triglyceride (TG). The ratio of liver weight to body weight, Oil-Red O staining, and hematoxylin and eosin (H&E) staining were also comparable in the two genotypes. Histologically, the liver samples of both *Mmp14^{LKO}* and *Mmp14^{Flox}* mice did not show notable fibrosis even though they appeared to have serious steatosis. Analysis of liver lipid levels revealed that lacking hepatic MT1-MMP did not change TC and TG levels. mRNA levels of genes encoding factors important for lipid metabolism (*Srebp1c*, *Fasn*, *Srebp2*, *Pcsk9*, *Ppara*, and *Cpt1a*), inflammation (*Tnfa*, *Il1b*), and fibrosis (*Tgfb*, *Colla1*) were also not altered in the liver of *Mmp14^{LKO}* mice compared to that of *Mmp14^{Flox}* mice.

In conclusion, our studies indicate that MT1-MMP does not require a specific cleavage site on LDLR and may cleave LDLR at multiple sites. However, an amino acid residue with a hydrophobic side chain at position 167 in MT-loop is critical for MT1-MMP-induced LDLR cleavage. Furthermore, lacking hepatic MT1-MMP does not appear to alter the development of liver steatosis in mice or promote liver fibrosis in mice fed the GAN diet. These data combined with our previous findings suggest that MT1-MMP may be a promising therapeutic target to lower plasma cholesterol levels and pave the way for the design of highly selective MT1-MMP inhibitors.

Preface

This thesis is an original study conducted by Maggie Wang for her MSc Thesis. Chapter 3 of this thesis is from: “Identification of amino acid residues in MT1-MMP important for its ability to cleave LDLR”, and is in process of publication in “Frontiers in Cardiovascular Medicine”. Co-authors to this section are: Adekunle Alabi, Hong-mei Gu, Xiao-dan Xia, Gui-qing Wang, Dawei Zhang. Data on Figures 7 and 9 was provided by Adekunle Alabi. Maggie Wang is the first co-author, supplied data and topic, and wrote the first draft for this paper.

Chapter 4 of this research project received approval from the animal ethics committee for protocol AUP00000456.

Acknowledgements

I want to show my sincerest gratitude to Dr. Dawei Zhang for helping me to reach greater heights during my MSc degree. I have learned a tremendous amount of theoretical and practical skills from Dr. Zhang's insightful teachings and supportive nature. I have diversified my knowledge and abilities as a biomedical researcher through the Zhang lab's resources I had access to. Outside the lab, Dr. Zhang pushed me in the right direction by making connections at hosted research events, so I could broaden my horizons.

I would also like to thank the members of the Zhang lab for contributing to my journey in completing this project. Hongmei Gu and Yishi Shen were vital to teaching and supplying the training I needed to carry out my experiments and complete my project successfully.

Outside of Zhang lab, I want to thank Dr. Zamaneh Kassiri and Dr. Richard Lehner for providing insightful information on further steps I can take in my research to make it outstanding. They have guided and supported me from their busy schedules to ensure I am set up for success. In the department of Pediatrics, I want to acknowledge Ms. Mikhaila Skehor, Dr. Sujata Persad, and Ms. Trish Kryzanowski, who helped me navigate the technicalities of my degree. In addition, they have provided me with valuable information on scholarships and research related events to make my MSc fruitful.

Finally, I want to thank the funding sources, The Maternal and Child Health Scholarship and the 75th Anniversary Award, for supporting and making my research happen.

Table of Contents

Abstract	ii
Preface	iv
Acknowledgements.....	v
List of Abbreviations	x
Chapter 1: Background	1
1.1 Atherosclerosis	1
1.2 The Development of Liver Fibrosis.....	3
1.2.1 NAFLD	3
1.2.2 Pathology of Liver Fibrosis	5
1.2.3 Hepatic Stellate Cells in Liver Fibrosis	6
1.2.4 TGF- β and MT1-MMP's Role in Liver Fibrosis.....	7
1.3 Low Density Lipoprotein Receptor	9
1.3.1 LDLR Structure	9
1.3.2 Regulation by SREBP-2	12
1.4 Membrane Type 1 Matrix Metalloproteinase	15
1.4.1 The Roles of MT1-MMP	15
1.4.2 MT1-MMP Substrates	15
1.4.3 Structure of MT1-MMP	16
1.4.4 Regulation of MT1-MMP	19

1.4.4.1 Transcriptional Regulation of MT1-MMP	19
1.4.4.2 Post-translational Regulation of MT1-MMP	20
1.4.4.3 Endocytosis	20
1.4.4.4 Autocatalysis	20
1.4.4.5 Endogenous Inhibitors	21
Rationale/Hypothesis	22
Chapter 2: Methods and Materials	25
2.1 Materials	25
2.2 Site-Directed Mutagenesis	25
2.3 Transformation.....	26
2.4 DNA Purification	28
2.5 Cell Transfection	28
2.6 Whole Cell Lysis	28
2.7 Immunoblotting	29
2.8 Migration Assays	30
2.9 Immunofluorescence	30
2.10 Animal	31
2.11 Special Animal Diet and Experimental Use	31
2.12 Histological Staining	32
2.13 Blood Glucose, Total Cholesterol, Triglyceride, HDL-C measurements.....	32

2.14 Lipid extraction	33
2.15 BCA Assay	34
2.16 Real Time Reverse Transcription Polymerase Chain Reaction	34
2.17 Statistical Analysis	35
Chapter 3: MT1-MMP Mediated Degradation of LDLR	36
3.1 Introduction	36
3.2 Results.....	39
3.2.1 Specific Sites on LDLR for MT1-MMP Mediated Cleavage.....	39
3.2.2 The Requirement of Domains in MT1-MMP for LDLR Shedding.....	46
3.2.3 Mutational Analysis of the MT-Loop	49
3.2.4 Detailed Mutational Analysis of Ile167.....	55
3.3 Discussion & Conclusion.....	58
Chapter 4: Determining Hepatic Membrane Type 1 Matrix Metalloproteinase's Effect on ECM Degradation in Liver Fibrosis.	62
4.1 Introduction.....	62
4.2 Results.....	64
4.2.1 Physical Parameters and Plasma Lipids of <i>Mmp14^{Flox}</i> and <i>Mmp14^{LKO}</i>	64
4.2.2 Histological Stains of <i>Mmp14^{Flox}</i> and <i>Mmp14^{LKO}</i> livers	67
4.2.3 Liver TC and TG	69
4.2.4 Gene Expression	71

4.3 Discussion	73
Chapter 5: Discussion, Conclusions, and Future Directions	75
References	80

List of Abbreviations

α-SMA	Alpha smooth muscle actin
APS	Ammonium persulfate
Arg	Arginine
Asp	Aspartate
CCl₄	Carbon tetrachloride
cDNA	Complementary DNA
CM	Chylomicron
Col1a1	Collagen type 1 gene
CPT1a	Carnitine palmitoyltransferase 1A
CVD	Cardiovascular disease
DMEM	Dulbecco's modified eagle medium
DNA	Deoxyribonucleic acid
ECM	Extracellular matrix
ER	Endoplasmic reticulum
FASN	Fatty acid synthase
FBS	Fetal bovine serum
FH	Familial hypercholesterolemia
GAPDH	Glyceraldehyde 3-phosphate dehydrogenase
GAN	Gubra amylin liver NASH
Glu	Glutamic acid
Gly	Glycine

H&E	Hematoxylin and eosin
HDL	High density lipoprotein
HDL-C	High density lipoprotein cholesterol
HEK293	Human embryonic kidney 293
HMGCR	3-hydroxy-3-methyl-glutaryl-coenzyme A reductase
HPX	Hemopexin
HSC	Hepatic stellate cells
IL-1β	Interleukin 1 beta
IL-6	Interleukin 6
Ile	Isoleucine
INSIG	Insulin induced gene 1 protein
LAP	Latency associated proprotein
LBR	Ligand binding repeats
LKO	Hepatocyte specific knock out
LDL	Low density lipoprotein
LDL-C	Low density lipoprotein cholesterol
Leu	Leucine
MFB	Myofibroblast
MMP	Matrix metalloproteinase
MT-MMP	Membrane type matrix metalloproteinase
MT1-MMP (or MMP14)	Membrane type 1 matrix metalloproteinase
NAFLD	Non-alcoholic fatty liver disease
NASH	Non-alcoholic steatohepatitis

oxLDL	Oxidized LDL
PBS	Phosphate buffered saline
PCSK9	Proprotein convertase subtilisin/kexin type 9
PCR	Polymerase chain reaction
PEI	Polyethylenimine
PEMT	Phosphatidylethanolamine N-methyltransferase
PPAR-α	Peroxisome proliferator-activated receptor- alpha
Pro	Proline
SCAP	Sterol regulatory element-binding protein cleavage-activating protein
SDS	Sodium Dodecyl Sulfate
SLC	Small latent TGF- β complex
SMC	Smooth muscle cells
SREBP-1c	Sterol regulatory element-binding protein-1c
SREBP-2	Sterol regulatory element-binding protein-2
RNA	Ribonucleic acid
RT-PCR	Real time reverse transcription polymerase chain reaction
TAA	Thioacetamide
TβRI	TGF- β type 1 receptor
TβRII	TGF- β type 2 receptor
TC	Total cholesterol
TE buffer	Tris-EDTA buffer
TIMP	Tissue inhibitor of metalloproteinase
TG	Triglyceride

TGF-β	Transforming growth factor beta
Thr	Threonine
Tnf-α	Tumour necrosis factor alpha
Trp	Tryptophan
Tyr	Tyrosine
Val	Valine

Chapter 1: Background

Cardiovascular disease (CVD) is the leading cause of mortality and morbidity worldwide, where approximately 17.9 million people succumb to the disease each year. CVD is a collection of disorders affecting the heart, brain, and peripheral tissues, such as myocardial infarction, coronary heart disease, stroke, and peripheral arterial disease. CVD has both genetic and behavioural components that increase the risk towards heart disease (WHO, 2022). Behavioural factors include a sedentary lifestyle, alcohol and tobacco use, and high caloric intake. These factors can lead to metabolic disorders such as diabetes, obesity, and fatty liver disease which are linked to CVD (Heart&Stroke, 2022; WHO, 2022). Atherosclerosis is one such disorder that is a major contributor to CVD.

1.1 Atherosclerosis

Before the start of the 20th century, mortality caused by high blood cholesterol was not common. Only when population and general life expectancy increased across the world did atherosclerosis become a common morbidity for CVD (Bentzon et al., 2014). Atherosclerosis is primarily a lipoprotein-driven disease. While lifestyle, diet, alcohol intake, and smoking play a factor, high levels of plasma cholesterol, particularly low-density lipoprotein cholesterol (LDL-C), is the primary driving force for developing atherosclerosis (Bentzon et al., 2014; Lu & Daugherty, 2015).

Atherosclerosis is caused by dysregulation in lipid regulatory pathways and the pro-inflammatory response. One such lipid metabolic disorder is familial hypercholesterolemia (FH), where the main mechanism to clear plasma low density lipoprotein (LDL) is disrupted (Defesche et al., 2017; Goldstein & Brown, 2009; Lu & Daugherty, 2015).

In conditions of high blood LDL-C, LDL accumulates in the arterial intima and can be oxidized to oxidized LDL (oxLDL). oxLDL then stimulates the immune response and can induce smooth muscle

cells (SMC) and endothelial cells to express adhesion molecules for binding with circulating monocytes. They can also induce chemo-attractants and growth factors for monocyte migration and differentiation into macrophages upon entering the sub-endothelial space (Bentzon et al., 2014) (**Figure 1**). In mice and humans, both macrophages and SMC can uptake LDL-C and turn into foam cells (Wang et al., 2019). Lipid-laden foam cells undergo apoptosis and release apoptotic remnants, such as cell debris and cholesterol crystals, which contribute to the necrosis core formation. Lipid deposits, otherwise known as xanthomas, are not harmful and typically can be reversed. However, persisting high levels of plasma cholesterol, lipid laden macrophages, and SMCs in the sub-endothelial walls compromise the inflammatory response and set a continuous cycle of inflammation and lipid accumulation (Bentzon et al., 2014; Lu & Daugherty, 2015).

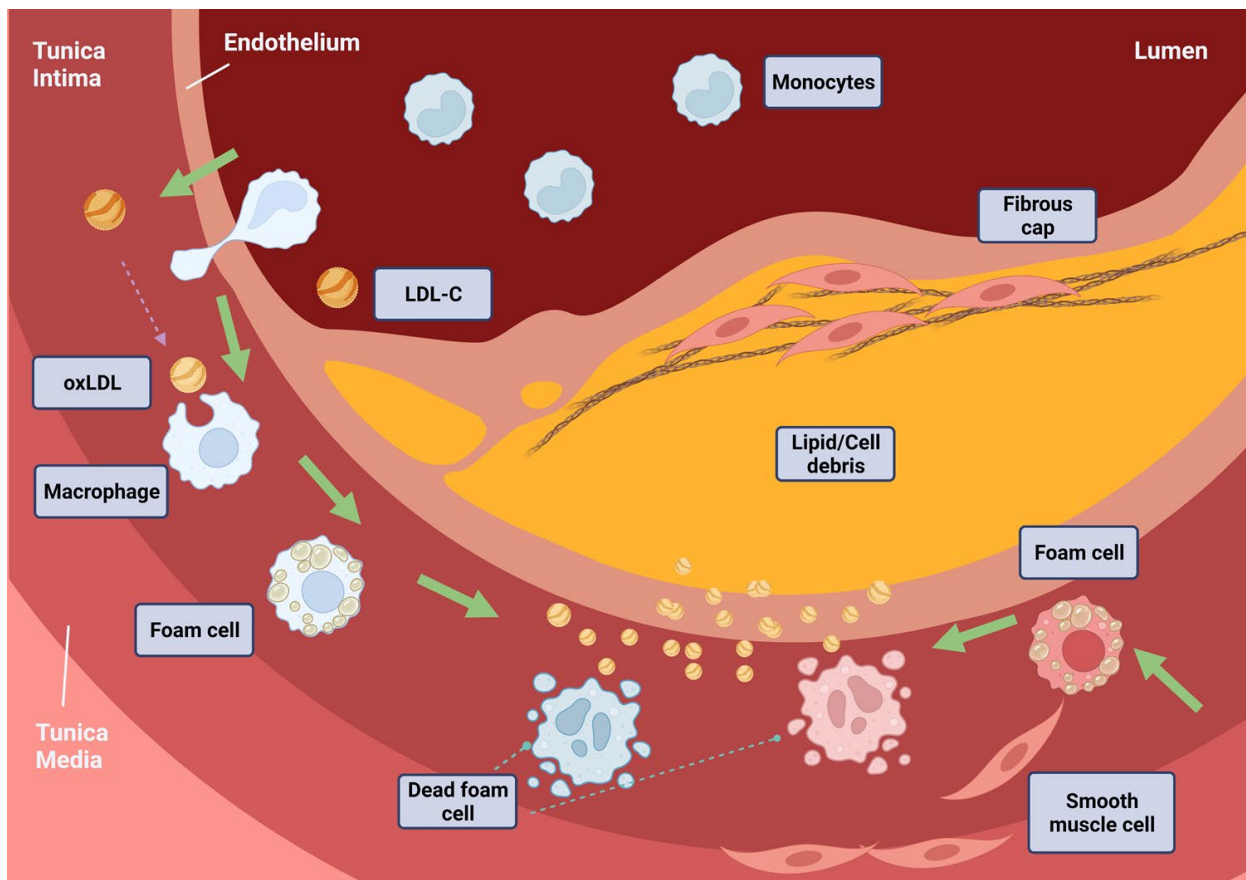


Figure 1. Schematic of the development of an atherosclerotic plaque in the arterial wall. Accumulated LDL in the intima is oxidized into oxLDL. The presence of oxLDL activates the innate and

adaptive immune response. Monocytes respond to cytokines, then migrate and cross the endothelial cell layer and into the intima, where they differentiate into macrophages. Macrophages phagocytose the accumulated oxLDL and become foam cells. SMC from the tunica media can also uptake oxLDL and become foam cells. Lipid laden foam cells go through cell apoptosis or necrosis, releasing cell debris and consequently contributing to growing plaque. (Figure made by Maggie Wang on BioRender)

1.2 The Development of Liver Fibrosis

1.2.1 Non-alcoholic Fatty Liver Disease

The liver plays a critical role in lipoprotein metabolism, such as secretion of very-low-density lipoprotein (VLDL), clearance of LDL and chylomicron (CM) remnants, and production of high-density lipoprotein (HDL) (Acharya et al., 2021). Under normal conditions, the turnover of hepatic triglyceride (TG) is regulated by balancing TG synthesis versus TG secretion and fatty acid oxidation (Buzzetti et al., 2016). However, under conditions of dyslipidemia and obesity, fatty acid input to the liver exceeds the capacity of fatty acid oxidation, thereby causing fat to accumulate and propagating the development of non-alcoholic fatty liver disease (NAFLD) (**Figure 2**). NAFLD is defined as the accumulation of TG in the liver of patients without excessive alcohol intake (Buzzetti et al., 2016; Engin, 2017; Francque et al., 2021; Friedman et al., 2018; Rosselli et al., 2014). Accumulation of TG is characterized by hepatic fat levels being greater than or equal to 5% of liver weight or liver steatosis in greater than or equal to 5% of hepatocytes (Francque et al., 2021). Endogenous causes of NAFLD are exhibited through dysregulation in factors associated with TG synthesis, utilization, and secretion from the liver. For example, defects in VLDL secretion from the liver were observed to promote hepatic steatosis. VLDL is produced by the liver and assembled from a combination of apolipoprotein (apo) B100, TG, phospholipids, and cholesteryl-ester (CE) before subsequently being secreted into circulation. The constituents of fatty acids and free cholesterol used in VLDL synthesis are either derived from *de novo* synthesis or the re-uptake of circulating lipoproteins (Ghosh et al., 2022; Newberry et al., 2021). Studies

on certain liver-specific knockout mice with impaired VLDL secretion were observed to develop liver steatosis, fibrosis, and hepatic carcinoma (Newberry et al., 2021). On the other hand, external risk factors for NAFLD are typically caused by diet, where excess caloric intake has been observed to increase the risk of steatosis and liver cell damage, as indicated by increased levels of serum alanine aminotransferase (Buzzetti et al., 2016; Panera et al., 2014; Petta et al., 2013). High calorie diets in humans and animal models typically consist of a combination of fats, cholesterol, and sugars, where each component can affect the pathophysiology of NAFLD. For example, fructose is a lipogenic and pro-inflammatory dietary factor that was observed to be associated with TG accumulation in the liver. Studies done on mice and humans have shown that an increased fructose consumption also caused upregulation of pro-inflammatory factors, such as tumour necrosis factor alpha (TNF- α), contributing to the increased risk of liver fibrosis (Buzzetti et al., 2016; Friedman et al., 2018).

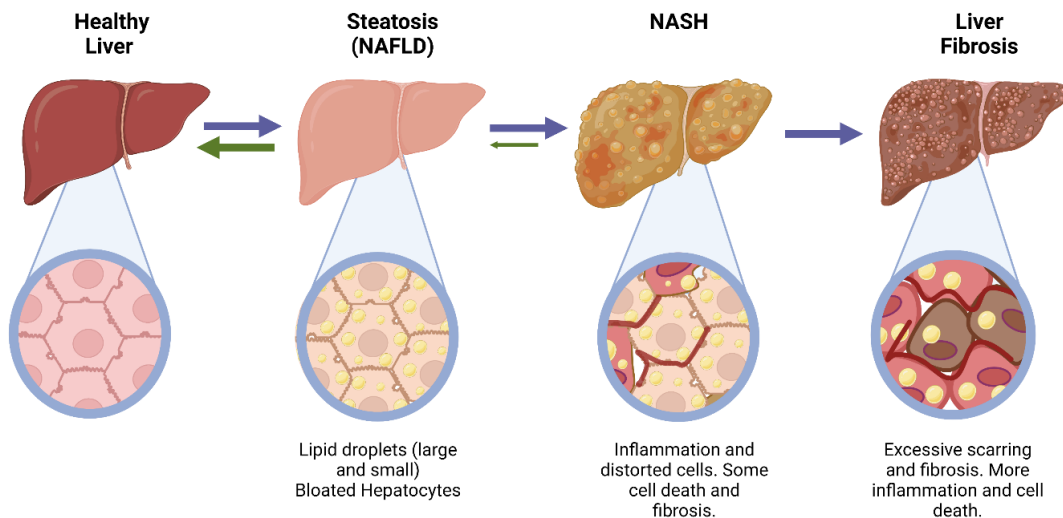


Figure 2. Progression of healthy liver to liver fibrosis. Diet-induced fatty liver appears larger and lighter in colour than healthy liver due to lipid-laden hepatocytes. At the steatosis stage, the damaged liver is still reversible to a healthy liver. Persistent high lipid conditions and inflammation can cause

NAFLD to progress into NASH. At NASH, there is greater inflammation, cell death, and beginnings of fibrosis. NASH is semi-reversible. However, once NASH progresses into liver fibrosis, as indicated by severe liver fibrosis and scarring, it becomes irreversible. The final stages would be liver cirrhosis or the development of hepatocellular carcinoma. Liver transplant is needed at the final stage. (Figure made by Maggie Wang on BioRender)

NAFLD is typically reversible to normal liver by managing diets and drug treatments (Henriksson & Andersen, 2020). However, persistent liver steatosis causes an accumulation of hepatocellular injury, thus subjecting the liver to increasing levels of inflammation. Increased levels of pro-inflammatory cytokines and reactive oxygen species result in histological changes such as hepatocyte necrosis, apoptosis, neutrophil chemotaxis, and activation of pro-fibrotic cells, which can result in non-alcoholic liver steatohepatitis (NASH) and eventually liver fibrosis. Currently, NASH and liver fibrosis are largely irreversible (Buzzetti et al., 2016; Chiang et al., 2011; Jahn et al., 2019; Musso et al., 2013).

1.2.2 Pathology of Liver Fibrosis

Liver fibrosis is defined by the accumulation of extracellular matrix (ECM) proteins, increased inflammation, portal hypertension, and eventual liver failure (Dewidar et al., 2019; Friedman et al., 2018). In normal physiological conditions, fibrogenesis is a wound healing response. For example, damaged tissues are initially sequestered when there is an acute liver injury. ECM components are secreted into the Space of Disse, an area between the periphery of hepatocyte and endothelial cells for nutrient exchange with circulation, to isolate the damaged tissue (Acharya et al., 2021; Schwabe et al., 2020; Yanguas et al., 2016). However, persistent, or chronic liver injury tips the balance between fibrillar ECM synthesis and degradation, resulting in a significant increase in fibrillar ECM components. In fibrotic ECM, type 4 collagen is replaced by type 1 and type 2 collagen (Acharya et al., 2021; Dewidar et al., 2019; Yanguas et al., 2016). Increased fibrotic ECM deposition can distort liver structure through fibrous scarring, constrict vessels causing portal hypertension, and failure in the liver regenerative process as

hepatocytes become replaced with ECM (Acharya et al., 2021; Yanguas et al., 2016). Therefore, the transition from a healthy liver to liver fibrosis involves structural and functional changes to liver cells, activation of pro-inflammatory and pro-fibrotic pathways, and changes to ECM composition (Acharya et al., 2021; Dewidar et al., 2019; Gressner et al., 2007).

1.2.3 Hepatic Stellate Cells in Liver Fibrosis

All liver cells contribute to the progression of liver steatosis to liver fibrosis. However, hepatic stellate cells (HSC) are the main driving force behind the production of fibrotic ECM, even though HSC accounts for only 15% of total resident liver cells (Acharya et al., 2021; Gressner et al., 2007). Under normal conditions, HSC is a retinoid storing cell that accounts for 85% of liver vitamin A (Gressner et al., 2007). Stimulation from pro-inflammatory cytokines like TNF- α and transforming growth factor beta (TGF- β), activates HSC from its quiescent form to fibrosis inducing myofibroblasts (MFB). HSC contributes to 82-96% of all MFBs in fatty liver disease models and 80-95% of collagen producing myofibroblast in mouse model studies (Acharya et al., 2021; Schwabe et al., 2020).

Under initial HSC differentiation, HSC undergoes a conformational change. Changes include developing a fibroblast shape, loss of vitamin A, increasing cell surface expression of receptors for growth factors and cytokines, and a proliferative and migratory phenotype (Dewidar et al., 2019; Yanguas et al., 2016). In addition, perpetuating pro-fibrotic and pro-inflammatory stimuli enhance MFB to increase the production of ECM components and stimulate the immune response. High levels of TGF- β , type 1 collagen, and alpha smooth muscle actin (α -SMA) thus indicate HSC activation for liver fibrosis (Acharya et al., 2021; Krstic & Santibanez, 2014; Mu et al., 2002; Yanguas et al., 2016).

While HSC is the dominant factor for fibrotic ECM production, other liver cell types also contribute to liver fibrosis pathology. For example, hepatocytes make up around 60% of total liver cells and play an important role in the urea cycle, drug detoxification, and synthesis of plasma proteins

(Acharya et al., 2021). In pathology, hepatocytes can contribute to fibrogenesis by undergoing epithelial-to-mesenchymal transition (EMT). EMT is a reversible process in which epithelial cells lose their apical-basal polarity and develop a mesenchymal phenotype. In the case of hepatocytes, they acquire the mesenchymal properties for synthesizing ECM components (Acharya et al., 2021; Dewidar et al., 2019; Wang et al., 2006). Additionally, hepatocytes are a source of lipid peroxides and apoptotic bodies that can induce type 1 collagen production. Hepatocellular cell apoptosis was thus found to contribute to increase inflammation and liver fibrosis (Yanguas et al., 2016).

Another example of non-HSC cells is Kupffer cells, the resident liver macrophages. Under pro-inflammatory and pro-fibrotic conditions, Kupffer cells activate and transdifferentiate HSC into MFB. In liver fibrosis, Kupffer cells affect ECM turnover by producing pro-fibrotic factors like TGF- β as well as regulating ECM cleavage enzymes such as matrix metalloproteinases (MMP) and their endogenous inhibitors (Fabregat & Caballero-Diaz, 2018).

Recent studies have also shown that the expression of MMPs was increased in liver injury, which may contribute to ECM remodelling (Calabro et al., 2014). Levels of membrane type 1 matrix metalloproteinase (MT1-MMP) are increased in all liver cells, including hepatocytes. During liver injury, MMP may promote clearance of fibrillar matrix around hepatocytes (Benyon & Arthur, 2001; Knittel et al., 1999). Irregular MMP activity can contribute to the imbalance between ECM deposition and degradation in liver fibrosis. Non-HSC liver cells thus also contribute to the pro-fibrotic and inflammatory pathology of liver fibrosis.

1.2.4 TGF- β and MT1-MMP's Role in Liver Fibrosis

TGF- β 1, more commonly known as just TGF- β , is a tissue specific cytokine that is involved in cell proliferation, wound healing response, cell differentiation, inflammation, and pathological fibrosis (Acharya et al., 2021; Nakerakanti & Trojanowska, 2012). The pro-inflammatory and pro-fibrotic

cytokine is a part of a 33 member family and is commonly investigated for its role in organ fibrosis. Research done in liver fibrosis found TGF- β to be the most potent stimulus for fibrillar collagen production (Dewidar et al., 2019; Fabregat & Caballero-Diaz, 2018; Yanguas et al., 2016).

TGF- β is initially secreted as an inactive precursor which must undergo proteolytic cleavage for activation. In the first step towards activation, the inactive precursor non-covalently associates with the latency associated proprotein (LAP) to form a small latent TGF- β complex (SLC). As part of the SLC, inactive TGF- β can then be deposited in the ECM which it then binds to the latent TGF- β binding protein and thus be retained on the ECM. Activation of latent TGF- β occurs by proteolytic cleavage of the latent TGF- β binding protein by furin-like proteases, which results in the subsequent dissociation of TGF- β from LAP. Localized TGF- β activation can also occur through interactions with specific integrins (Dewidar et al., 2019; Takawale et al., 2015). For example, MT1-MMP is found to directly and indirectly, by matrix metalloproteinase 2 (MMP2) actions, activate latent TGF- β through an interaction with membrane bound integrins (Krstic & Santibanez, 2014; Quintero-Fabian et al., 2019; Wang et al., 2006; Yanguas et al., 2016). Integrin $\alpha\beta 8$ was found to bind with the latent TGF- β complex through interactions with the integrin binding Arg-Gly-Asp (RGD) motif on the LAP. Upon binding, MT1-MMP can then come in and form a complex with integrin $\alpha\beta 8$ and latent TGF- β for TGF- β 's activation (Fabregat & Caballero-Diaz, 2018; Mu et al., 2002). Mu et al. have shown that MMP inhibitors, such as GM6001, significantly decreased TGF- β activation in MT1-MMP induced cells. Furthermore, soluble forms of integrin $\alpha\beta 8$ and MT1-MMP cannot activate TGF- β , indicating the importance of cell surface localization of the MT1-MMP/integrin $\alpha\beta 8$ /latent TGF- β complex (Mu et al., 2002). Post-activation, TGF- β can bind to TGF- β type 2 receptor (T β RII) to mediate pro-fibrotic activity. Upon ligand binding, T β RII phosphorylates TGF- β type 1 receptor (T β R1) at a glycine-serine rich domain resulting in a conformational change that sensitizes T β R1 to bind and phosphorylate SMAD2/3. This activates the downstream SMAD signalling pathway thereby regulating TGF- β target genes that contribute to

hepatocyte cell death and progression to NASH and liver fibrosis (Acharya et al., 2021; Dewidar et al., 2019; Mu et al., 2002; Takawale et al., 2015).

Beyond liver fibrosis, patients can progress to liver cirrhosis and hepatocellular carcinoma. Both require liver transplantation as there is no treatment to reverse disease progression at end stage liver disease (Acharya et al., 2021; Dewidar et al., 2019; Friedman et al., 2018).

However, studies on treatments targeting pro-fibrotic and pro-inflammatory factors of NASH and liver fibrosis are currently underway. For example, fibroblast growth factor 21 (FGF21) analogues, such as Pegbelfermin, are found to downregulate TGF- β and thus inhibit activation of HSC. In a study done by Henriksson and Anderson, FGF21 analogues decreased fibrotic markers including type 1 collagen and α -SMA in the methionine-choline deficient diet fed mouse models. Furthermore, FGF21 analogues decreased liver steatosis in mice and increased beta oxidation. Due to FGF21 analogue's promising results, FGF21 analogues are currently in clinical development as a potential treatment for steatosis, NASH, and liver fibrosis (Henriksson & Andersen, 2020). As NASH and liver fibrosis are largely irreversible, targeting physiological processes contributing to pathology is of interest to mitigate disease progression (**Figure 2**).

1.3 LDLR

Human low density lipoprotein receptor (LDLR) is an 839 amino acid transmembrane protein that was first identified by Goldstein and Brown (Beglova & Blacklow, 2005; Goldstein & Brown, 2009; Jeon & Blacklow, 2005). Hepatic LDLR is a main player for enacting homeostatic control over plasma cholesterol and is part of the main pathway that clears plasma lipids from circulation. LDLR is responsible for removing up to 70% of LDL-C (Xia, Alabi, et al., 2021a).

1.3.1 LDLR Structure

Starting from the N-terminus, LDLR's ectodomain consists of 7 cysteine-rich repeats known as LDLR type A modules, or more commonly, ligand binding repeats (LBR). LDLR binds to apoB100 on LDL, and apoE on VLDL, intermediate-density lipoprotein (IDL), and CM remnants (Go & Mani, 2012). Of the 7 LBR repeats, each repeat individually or in concert infers specificity for substrate binding. For example, repeats 4 and 5 interact with apoE on VLDL and CM remnants. Repeats 1 and 2 have a negligible role in interacting LDL, while deleting any repeats from 3 to 7 reduces LDL binding by 50% (Beglova et al., 2004; Go & Mani, 2012; Jeon & Blacklow, 2005; Russell et al., 1989). LBR is followed by a 400 residue long epidermal growth factor precursor homology domain (EGF) that starts with two EGF repeats, a 6 bladed beta-propeller, followed by the third EGF repeat (Jeon & Blacklow, 2005)(**Figure 3**). The EGF domain is responsible for lipoprotein release in the low pH environment of the endosome. Upon substrate binding, LDLR is endocytosed into a clathrin-coated vesicle where it is shuttled to the endosome. In the endosome's acidic environment, LDL is released and delivered to the lysosome, where it is further degraded into its constituents, such as cholesterol. Cholesterol can be delivered into various subcellular organelles, stored in lipid droplets as CE, or exported in VLDL. Meanwhile, LDLR is recycled back to the cell surface (Beglova et al., 2004; Davis, Goldstein, et al., 1987; Go & Mani, 2012; Jeon & Blacklow, 2005) (**Figure 4**). In the EGF, the beta propeller is the pH sensor that allows for LDLR to adopt an open conformation at neutral pH while folding into a closed conformation at acidic pH to release LDL. The beta propeller contains a conserved Tyr-Trp-Thr-Asp (YWTD) sequence and 3 histidine residues (H562, H586, and H190) on the surface. While the effects of individual mutation are negligible, deletion of all three histidine residues is shown to impair LDL binding and release (Beglova et al., 2004; Jeon & Blacklow, 2005). With 54% of FH mutations stemming from the EGF, the EGF is crucial for LDLR recycling (Jeon & Blacklow, 2005). Further down towards the C-terminus is the clustered O-linked glycosylation region which has no known function, followed by the transmembrane domain and a cytoplasmic tail at the C-terminus (**Figure 3**). The cytoplasmic tail contains the NPVY motif that is critical for the internalization of the receptor into clathrin coated pits. Notable

mutations on the cytoplasmic tail include Y807C, dubbed as the JD mutation, which impairs receptor internalization and causes familial hypercholesterolemia (FH). FH is characterized by elevated plasma levels of cholesterol, especially LDL-C, and increased risk of premature coronary heart disease (Davis et al., 1986; Jeon & Blacklow, 2005).

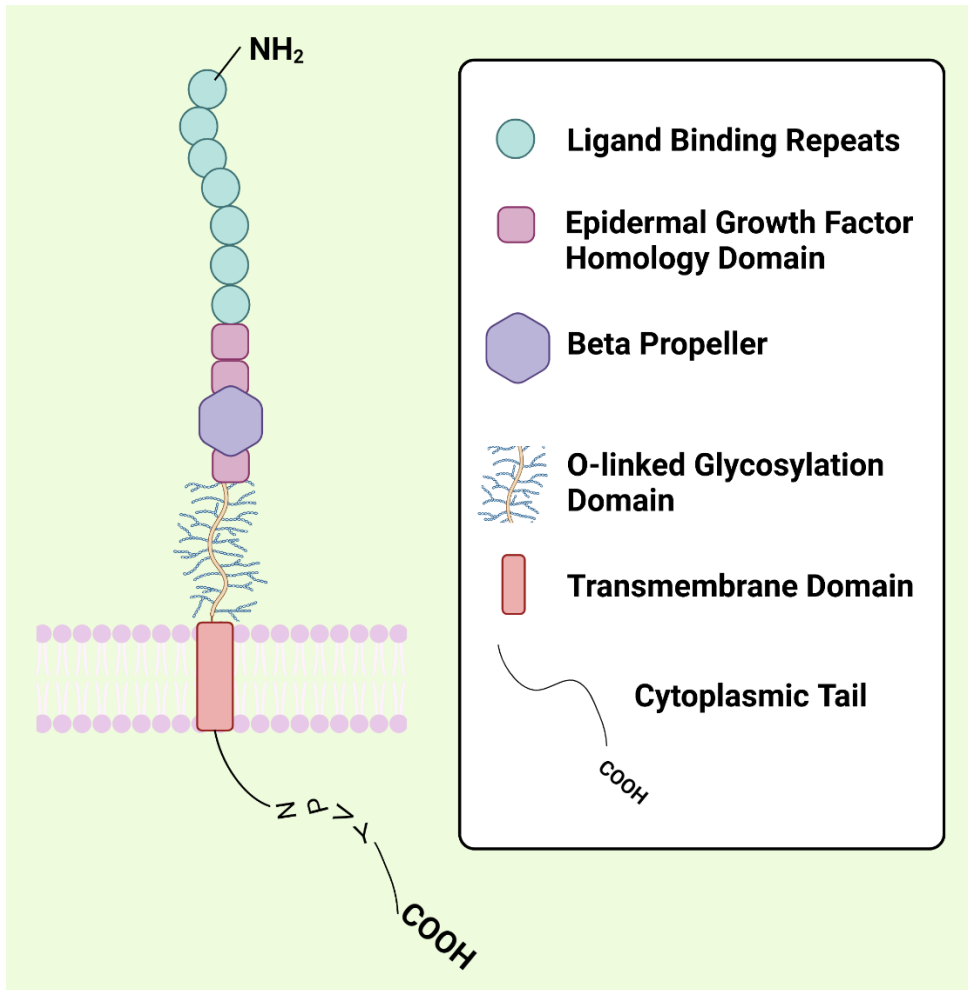


Figure 3. Structure of LDLR. From the N-terminus, LDLR consists of 7 domains in the LBR, where substrate specificity is conferred by individual domains. Following the LBR is the EGF which regulates substrate release in the endosome and recycling of LDLR back to the plasma membrane. The beta propeller after the first 2 EGF repeats is the pH sensor that allows LDLR to adopt an open substrate binding conformation at neutral pH and closed conformation at acidic pH to dissociate the substrate. Next is the O-linked glycosylation region with an unspecified function, the transmembrane domain, and

the cytoplasmic tail. The cytoplasmic tail contains the NPVY motif, which is essential for receptor-mediated endocytosis of lipoprotein particles. (Figure made by Maggie Wang on BioRender).

1.3.2 Regulation by SREBP-2

3 different isoforms of sterol regulatory binding protein (SREBP) exist in mammals, with each regulating a specific metabolic pathway. For cholesterol metabolism, SREBP-2 is a key transcription factor for regulating liver LDLR levels. SREBP-2 is ubiquitously expressed, and its transcriptional activity can be increased by pro-inflammatory factors and reduced by elevated cellular levels of oxysterols and cholesterol (Ferre et al., 2021; Luo et al., 2020; Musso et al., 2013). The general structure consists of a N-terminal basic helix-loop-helix transcription factor domain, a transmembrane domain composed of two transmembrane segments with a short luminal loop, and a C-terminal regulatory domain. SREBP-2 is initially synthesized as a ~120 kDa precursor on the endoplasmic reticulum (ER) (Luo et al., 2020; Rawson, 2003). SREBP-2 binds to the SREBP cleavage activating protein (SCAP), forming a SCAP-SREBP complex on the ER membrane (Luo et al., 2020). SCAP consists of an N-terminal domain that can bind to insulin-induced gene 1 or 2 protein (INSIG1/2), a sterol sensor in the transmembrane helices, and a C-terminal domain with tryptophan-aspartate repeats for binding to the C-terminal domain of SREBP (Ferre et al., 2021; Rawson, 2003). Under high cellular cholesterol levels, INSIG1/2 binds to the SCAP-SREBP complex to retain the complex on the ER, which suppresses the production of the transcriptional active form of SREBP-2, and ultimately factors for the cholesterol biosynthetic pathway. Under low cellular cholesterol, SREBP-2/SCAP is separated from INSIG. SCAP can be recognized by the COPII complex, shuttling the SCAP-SREBP complex from the ER to the Golgi (Luo et al., 2020; Rawson, 2003; Yang et al., 2020). In the Golgi apparatus, SREBP is cleaved by site 1 protease and site 2 protease to release its N-terminal transcriptional active form. The cleaved N-terminal domain is then translocated into the nucleus to upregulate transcription of SREBP-2's target genes, such as *LDLR*, *PCKS9*, and *HMGCR* (Brown & Goldstein, 1997; Go & Mani, 2012; Luo et al., 2020; Shimano

& Sato, 2017) (**Figure 4**). Additionally, 3-hydroxy-3-methyl-glutaryl-coenzyme A reductase (HMGCR) degradation is also prevented under sterol depletion, as HMGCR under high ER cholesterol can bind to an INSIG/ubiquitin ligase complex on the ER and be marked for proteasome-mediated degradation. Therefore, preventing HMGCR degradation also promotes cholesterol biosynthesis (Luo et al., 2020).

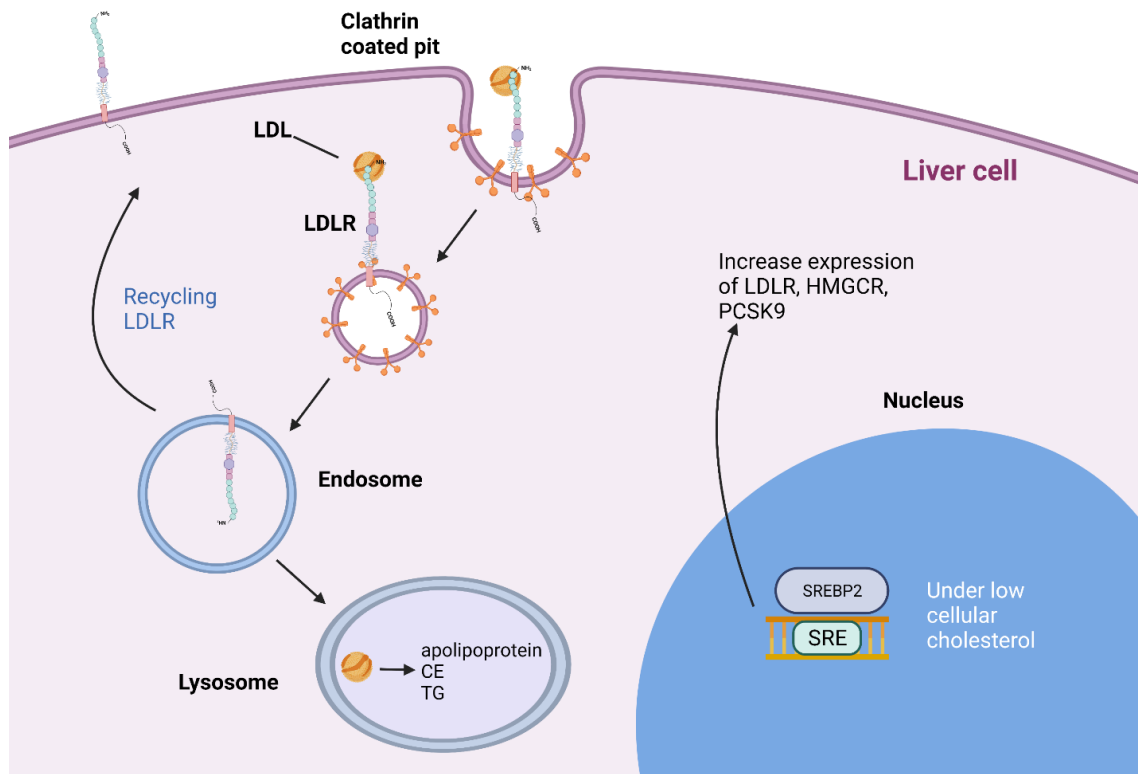


Figure 4. Mechanism for LDLR processing LDL. LDLR, as an important factor for lipid metabolism, is regulated on transcriptional and post-translational level. LDLR substrates, such as LDL with apoB100, bind to LBR and is internalised. LDL-LDLR complex is endocytosed into a clathrin coated pit and shuttled to the endosome. In the low pH environment, LDLR adopts a closed conformation and releases LDL, while the receptor is recycled back to the cell surface. LDL is then shuttled to the lysosome for degradation into its constituents. Under low cellular cholesterol levels, SREBP-2 is activated and upregulates the cholesterol pathway. (Figure made by Maggie Wang on BioRender)

On the post-translational level, proprotein convertase subtilisin/kexin type 9 (PCSK9) can regulate LDLR levels by binding to LDLR on the cell surface and directing the receptor to the lysosome for degradation. Circulating PCSK9 is primarily secreted from hepatocytes. The structure consists of a pro-domain, the catalytic domain, and the C-terminal histidine rich domain. While PCSK9's catalytic domain is the main binding site of LDLR, the positively charged C-terminal tail may also interact with the negatively charged LBR and block LDLR recycling (Go & Mani, 2012; Xia, Peng, et al., 2021).

Disruption to LDLR function and regulation can result in diseases such as FH. FH is an autosomal dominant hereditary disease defined by a dysfunctional LDLR. 1 in 250 people inherits the heterozygous mutation with one defective allele, and have double the normal amount of plasma LDL, which increases the risk for developing CVD in their 40's to 50's (Go & Mani, 2012; Jeon & Blacklow, 2005; Vuorio et al., 2017). Less common is the homozygous mutation found in 1 in a million people, that propagates development of atherosclerosis at a very young age (Vuorio et al., 2017). Statins are currently the popular lipid lowering method for people suffering from dyslipidemia. Statins work by inhibiting HMGCR, the rate limiting step in cholesterol biosynthesis, by competing with normal HMGCR substrates at the active site and altering the functional structure of the enzyme, thus decreasing cellular cholesterol levels. Sterol depletion induces SREBP-2 activation and transcription of hepatic LDLR to increase LDL uptake from plasma. While statins can efficiently lower plasma LDL-C by up to 50%, patients are also found to exhibit adverse effects in muscle toxicity and display symptoms of statin intolerance. As an alternative, PCSK9 inhibitors can also efficiently decrease plasma lipids but are financially unsustainable for majority of patients. Therefore, finding an alternative lipid lowering strategy is critical (Ahmad, 2014; Fitchett et al., 2015; Kolber et al., 2018; Vuorio et al., 2017; Xia, Alabi, et al., 2021b). As the key player in lipid homeostasis, it is essential that LDLR is functional and properly regulated.

1.4 Membrane Type 1 Matrix Metalloproteinase

1.4.1 The Roles of MT1-MMP

MT1-MMP is a ubiquitously expressed enzyme that is part of the 23 member MMP family of zinc dependant endopeptidases (Gross & Lapiere, 1962; Sato et al., 1994; Takawale et al., 2015; Xia, Alabi, et al., 2021b). The enzyme was initially discovered as an activator of pro-MMP2, another enzyme of the same family that plays a role in cancer cell invasion (Gifford & Itoh, 2019; Sato et al., 1994). Extensive research on MT1-MMP showed that MT1-MMP function and expression levels are tissue dependant, thus reflecting MT1-MMP's diverse set of physiological roles including ECM remodelling and wound healing (Fields, 2019; Mu et al., 2002; Takawale et al., 2015; Xia, Alabi, et al., 2021b). MT1-MMP has also been implicated in different pathological processes such as inflammation, rheumatoid arthritis, angiogenesis, plaque rupture, and cancer (Amar et al., 2017a; Gifford & Itoh, 2019; Xia, Alabi, et al., 2021a). In cancer, MT1-MMP plays a role in cancer cell invasion and metastases and thus found to be highly expressed in cancer tissues in renal carcinoma, astrocytic tumor, and melanoma (Lang et al., 2004; Woskowicz et al., 2013; Xia, Alabi, et al., 2021a). Given MT1-MMP's diverse role in multiple physiological and pathological processes, an in-depth understanding of MT1-MMP's structure, regulation, and function is critical.

1.4.2 MT1-MMP Substrates

MMPs are classified by their substrates and structure. MT1-MMP, encoded by the *Mmp14* gene in mice and *MMP14* gene in humans, is a collagenolytic enzyme that can degrade collagen at a neutral pH. Collagenase MMPs include MMP1, MMP8, and MMP13 (Decaneto et al., 2017; Gifford & Itoh, 2019; Xia, Alabi, et al., 2021a). MT1-MMP can cleave multiple ECM substrates such as type 3 collagen, fibronectin, and type 1 collagen, which implicates MT1-MMP's function in ECM degradation in fibrosis and cancer cell invasion. For example, MT1-MMP is found in the leading edge of invadopodium to

promote cell migration in collagen rich environments (Gifford & Itoh, 2019; Sodek et al., 2007). MT1-MMP can also indirectly cleave type 4 collagen in basement membranes by activating pro-MMP2. While tissue inhibitors of metalloproteinase (TIMP) typically act as endogenous inhibitors to MMP, certain TIMPs may also activate specific MMPs. TIMP2 can activate pro-MMP2 to its mature form. Pro-MMP2 can be activated in two ways by TIMP2. Method one is through TIMP-2 and pro-MMP2 forming a complex through their C-terminal domains and leaving the N-terminal domain of TIMP-2 free to interact with cell surface MT1-MMP. The alternative is TIMP-2 first interacting with MT1-MMP and then recruiting pro-MMP2 to complex with TIMP-2's free C terminal domain. Finally, an MT1-MMP that is not bound to TIMP-2 is recruited to activate pro-MMP2 (Sato et al., 1994; Takawale et al., 2015). In of the context of CVD, MT1-MMP increases the risk for atherosclerotic plaque rupture. Plaque rupture accounts for 75% of CVD events (Xia, Alabi, et al., 2021a). Collagen, a major substrate of MT1-MMP, provides tensile strength for plaque caps that are susceptible to proteolytic actions. Furthermore, studies have found that there was significantly more collagen in the aortic arch of *Mmp14* *-/-* *Ldlr* *-/-* mice versus *Ldlr* *-/-* mice with MT1-MMP, thus indicating MT1-MMP's role in atherosclerosis (Alabi et al., 2021; Xia, Alabi, et al., 2021b).

Aside from cleaving ECM components, MT1-MMP can also cleave non-matrix substrates such as Nieman Pick Disease Type C2 protein, heat shock protein 90-alpha, pro-inflammatory cytokines, growth factor receptors, and LDLR (Mu et al., 2002; Osenkowski et al., 2004; Takawale et al., 2015; Xia, Alabi, et al., 2021a). For the purpose of this study, we will focus on the structural and functional characteristics of MT1-MMP for its ability to target and cleave LDLR in regulating LDL uptake (Alabi et al., 2021; Xia, Alabi, et al., 2021b).

1.4.3 Structure of MT1-MMP

All MMP members have the same general structure consisting of a hemopexin domain, a hinge region, the conserved catalytic domain with a zinc binding site, a N-terminal pro-domain that conceals

the catalytic site in MMP's inactive state, and a signal peptide domain, except for MMP7, 23, and 26 that do not have a hemopexin domain (Cao et al., 1998; Dufour et al., 2008; Takawale et al., 2015). What differentiates MT1-MMP from the soluble members of the MMP family is, it is bound to the plasma membrane by the transmembrane domain, followed by a short cytoplasmic tail (Gifford & Itoh, 2019; Xia, Alabi, et al., 2021b). Like MT1-MMP, MT2-MMP, MT3-MMP, and MT5-MMP are also bound to the cell surface by the transmembrane domain. MT4-MMP and MT6-MMP on the other hand also exist on the cell surface, albeit via a glycosylphosphatidylinositol anchor. As a membrane bound MMP, MT1-MMP can be localized in specific domains on the plasma membrane for specific functions.

MT1-MMP contains 582 amino acid residues and is ubiquitously expressed. MT1-MMP protein is encoded by the *MMP14/Mmp14* gene located on chromosome 14q11.2 and 14C2, for human and mouse, respectively (Gifford & Itoh, 2019; Houghton, 2015; Sato et al., 1994; Xia, Alabi, et al., 2021a). In the full-length structure of MT1-MMP, the sequence starts with the N-terminal domain. In the inactive MT1-MMP, the N-terminal signal peptide is for targeting into secretory vesicles (Ra & Parks, 2007). Next, is the pro-peptide domain that contains the PRC⁹³GVPD cysteine switch motif and a conserved R¹⁰⁸XKR motif. For MT1-MMP activation, the R¹⁰⁸XKR motif of the pro-peptide domain is recognized and cleaved by furin like enzymes to release the pro-domain. Following is the highly conserved catalytic domain which contains a conserved zinc binding motif of HE²⁴⁰XGHXXGXXH. His239, His243, and His249 of the zinc binding motif coordinate the catalytic Zn²⁺ with a water molecule for nucleophilic action in substrate cleavage. During substrate proteolysis, Zn²⁺ is strongly polarized and forms a bridge with the conserved glutamate in position 240 (Glu240) as part of a complex that works to cleave the peptide backbone of MT1-MMP's substrates. Mutations of Glu240 can result in a catalytically inert MT1-MMP (Alabi et al., 2021; Decaneto et al., 2017; Toth et al., 2002; Xia, Alabi, et al., 2021b). It is also of note that soluble MT1-MMP, whether by auto-catalytic activities or mutations, is not catalytically active (Gifford & Itoh, 2019). Within the catalytic domain also exists an 8 residue loop P¹⁶³YAYIREG¹⁷⁰

dubbed the MT-loop (English et al., 2001). The MT-loop connects beta-strands 2 and 3 in the beta-sheet structure of the catalytic domain and structurally protrudes from the molecular surface. The MT-loop is found only in transmembrane-bound membrane-type matrix metalloproteinases (MT-MMP) and is specific for each MT-MMP member (English et al., 2001; Lang et al., 2004; Xia, Alabi, et al., 2021a). It has been observed that deleting the MT-loop does not abrogate MT1-MMP's catalytic activity, but can impair MT1-MMP's kinetic activities in targeting and acting on particular substrates (Alabi et al., 2021; English et al., 2001). Following the catalytic domain is the flexible proline-rich hinge region that can be o-glycosylated (Ra & Parks, 2007; Tochowicz et al., 2011). Next, is the hemopexin domain that consists of four beta propellers which mediate protein interactions, enzyme activation, protein localization, and endocytosis for recycling and degradation (Page-McCaw et al., 2007; Xia, Alabi, et al., 2021b). While the overall structure of the hemopexin domain is similar to other MMPs, the hemopexin domain in MT1-MMP has four propeller blades composed of 3 anti-parallel beta sheets where the outermost strands is a combination of two short sheets with a bulge in between (Tochowicz et al., 2011; Xia, Alabi, et al., 2021a). Hemopexin domain homodimerization plays a crucial regulatory role in the proteinase for collagen degradation in cell migration and invasion (Gifford & Itoh, 2019; Itoh et al., 2008; Tochowicz et al., 2011). Past the stalk is the transmembrane domain that anchors the MT1-MMP to the plasma membrane. The transmembrane domain localizes to specific domains in the plasma membrane for MT1-MMP's catalytic activity in cleaving extracellular and peripheral protein substrates. Furthermore, transmembrane domain-dependant dimerization of MT1-MMP plays a role in pro-MMP2 activation (Itoh et al., 2008; Osenkowski et al., 2004; Tochowicz et al., 2011; Xia, Alabi, et al., 2021b). Finally at the C-terminus is the cytoplasmic tail that is critical for internalization of MT1-MMP in regulating MT1-MMP's cell surface levels. Additionally, mutations in the cytoplasmic tail, such as C574A, can decrease cell invasion, migration, and/or adhesion (Houghton, 2015; Osenkowski et al., 2004; Rozanov et al., 2001; Toth et al., 2002; Xia, Alabi, et al., 2021b) (**Figure 5**).

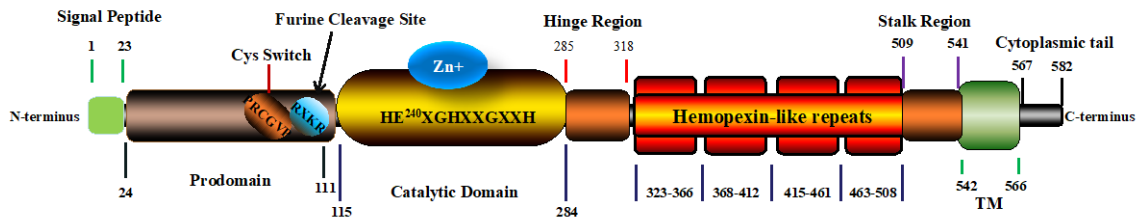


Figure 5. Structure of full length MT1-MMP. On the N terminus side, MT1-MMP starts with the signal peptide and the pro-domain. The pro-domain contains a conserved cysteine switch motif and a furin cleavage site to activate the inactive zymogen. The catalytic domain is highly conserved in all MMP members and is the site for MT1-MMP’s proteolytic function. Next is the hinge region, the hemopexin like repeats that is responsible for MT1-MMP substrate interactions, the transmembrane region that anchors MT1-MMP to the cell membrane, and finally the cytoplasmic tail that is critical for internalization of the protein. (Adapted from (Xia, Alabi, et al., 2021b))

1.4.4 Regulation of MT1-MMP

Due to the multiple physiological and pathological roles of MT1-MMP, the enzyme is regulated at the levels of transcription, proteolysis via autocatalytic mechanisms or by other proteases, endocytosis, and via endogenous inhibitors such as TIMPs (Takawale et al., 2015; Vandenbroucke & Libert, 2014; Xia, Alabi, et al., 2021a). Dysregulation of MT1-MMP premeditates many diseases.

1.4.4.1 Transcriptional Regulation of MT1-MMP

MMP14’s promoter differs from the classical MMP promoter found in *MMP1*, *MMP3*, *MMP9*, and *MMP13*, as *MMP14* does not have a TATA box. Instead, transcriptional levels of *MMP14* are regulated by the non-canonical SP1 binding site on *MMP14*’s promoter. SP1 is important for basal transcription of *MMP14* which can be induced by factors such as oxLDL and pro-inflammatory cytokines

(Gifford & Itoh, 2019; Xia, Alabi, et al., 2021b). As *MMP14* is heavily reliant on SP1, mutations in the promoter can cause up to a 90% decrease in promoter activity (Gifford & Itoh, 2019; Lohi et al., 2000).

1.4.4.2 Post-translational Regulation of MT1-MMP

At the post-translational level, MT1-MMP is synthesized as an inactive 60 kDa zymogen on the ER (Gifford & Itoh, 2019; Pahwa et al., 2014; Xia, Alabi, et al., 2021a; Zucker et al., 2002). To be fully activated, cleavage of MT1-MMP's pro-domain in the trans-Golgi and subsequent trafficking of the activated enzyme to the cell surface is necessary (Zucker et al., 2002). While the structure of MMPs varies, they are all activated by the disruption of the cysteine switch, a bond between the catalytic zinc and a cysteine in the pro-domain. Removal of the pro-domain can occur via cleavage by furin-like enzymes which targets R¹⁰⁸XKR. This conserved motif is similar in all MT-MMP and is located at the C-terminus end of the pro-domain. Activation by the proteolytic mechanism results in a shortened mature MT1-MMP (Gifford & Itoh, 2019; Takawale et al., 2015). On the other hand, super-oxides *in vitro* are also found to activate MMPs by reducing the S-H bond of the cysteine switch which causes the pro-domain to uncover the catalytic site (Takawale et al., 2015).

1.4.4.3 Endocytosis

The process of endocytosis is a regulatory mechanism for membrane proteins to either be sent to the lysosome for degradation or recycled back to the plasma membrane. MT1-MMP undergoes clathrin mediated endocytosis to regulate its cell surface levels. The cytoplasmic tail has been implicated as a mediator for MT1-MMP internalization, where the Leu-Leu-Tyr⁵⁷³ motif in the cytoplasmic tail is required to interact with the $\alpha 2$ subunit in adaptor protein 2 of the clathrin vesicle complex. MT1-MMP mutants without a functional cytoplasmic tail are found to be retained on the cell surface (Gifford & Itoh, 2019; Osenkowski et al., 2004; Toth et al., 2002).

1.4.4.4 Autocatalysis

MT1-MMP can self-regulate its own cell surface level by cleavage of the ectodomain and generating soluble fragments through autocatalysis. In this mechanism, MT1-MMP first cleaves its ectodomain at Gly284-Gly285 in the hinge region, generating an inactive 44 kDa membrane bound fragment that consists of the hemopexin domain, the stalk, the transmembrane domain, and the C-terminal cytoplasmic tail. The second cleavage occurs between Ala255-Ile256, a peptide sequence in the catalytic domain that generates a soluble 18 kDa catalytically inert fragment with some unresolved function (Itoh et al., 2008; Osenkowski et al., 2004; Pahwa et al., 2014; Xia, Alabi, et al., 2021b). It is of note that E240A, a catalytically inert mutation abolishes MT1-MMP's autocatalytic activities, while C574A, a mutant in the cytoplasmic tail retains it. Impaired autocatalysis is observed in catalytically inert mutations and soluble MT1-MMP fragments which indicates the importance of a functional catalytic domain (Rozanov et al., 2001; Toth et al., 2002; Xia, Alabi, et al., 2021b).

1.4.4.5 Endogenous Inhibitors

TIMPs are a group of endogenous competitive inhibitors of MMPs that work by competitively inhibiting the enzyme at the catalytic domain. MT1-MMP can be inhibited by TIMP-2, TIMP-3, and TIMP-4 at varying degrees except TIMP-1 which does not inhibit MT1-MMP (Takawale et al., 2015; Vandebroucke & Libert, 2014). TIMP-2 has different roles depending on its expression level. TIMP-2 can interact with MT1-MMP to form a TIMP-2/MT1-MMP/Pro-MMP2 complex that activates pro-MMP2 which can also protect MT1-MMP from auto-degradation. However, TIMP-2 in excess will inhibit MT1-MMP as a competitive inhibitor, thereby regulating MT1-MMP action (Gifford & Itoh, 2019; Osenkowski et al., 2004; Xia, Alabi, et al., 2021a; Zucker et al., 2002).

Rationale and Hypothesis

Elevated plasma LDL-C is one of the primary risk factors for the development of CVD worldwide (Libby, 2021; Xia, Alabi, et al., 2021b). Hepatic LDLR is the main mechanism for plasma LDL-C clearance, where LDLR mutants account for a litany of diseases resulting from dysregulation of lipid metabolism. Therefore, strict regulation of plasma LDL clearance by LDLR is necessary. Currently, the primary lipid lower method is through statins. Statins work by inhibiting the rate-limiting enzyme HMGCR in cholesterol biosynthesis. Reduction in cellular cholesterol levels activates the transcriptional activity of SREBP-2, thus increasing *LDLR* expression (Goldstein & Brown, 2009; Luo et al., 2020; Stancu & Sima, 2001). However, statins are efficient for less than 50% of patients and 5-10% of patients develop statin intolerance due to side effects, such as muscle toxicity (Ahmad, 2014; Fitchett et al., 2015; Xia, Alabi, et al., 2021a). An alternative method to lower plasma LDL-C is via PCSK9 inhibitors, where LDL-C levels can be decreased by up to 60% (Sabatine, 2019). However, the issue is PCSK9 inhibitors are expensive and thus a financial burden on the majority of patients (Kolber et al., 2018). Therefore, the search for alternative treatments is vital.

MT1-MMP is a possible regulatory mechanism for LDLR (Alabi et al., 2021). MT1-MMP is a membrane bound metalloproteinase that was originally studied for its role in cancer cell invasion and metastases through proteolytic degradation of the ECM and cytoskeleton reorganization. MT1-MMP can directly cleave the ECM by targeting type 1 collagen or by activating another MMP on the cell surface. MT1-MMP activates pro-MMP2 to mature MMP2, thereby cleaving type 4 collagen in the basement membrane to permit cell invasion (Iida et al., 2004; Sato et al., 1994; Woskowicz et al., 2013). Aside from MT1-MMP's well established role in promoting cancer cell migration and invasion, our lab also found hepatic MT1-MMP to have an important regulatory role in lipid metabolism, specifically, its ability to cleave LDLR. Our *in vitro* cell studies revealed that MT1-MMP knockdown in multiple cell lines increased cell surface LDLR expression, while overexpression of MT1-MMP decreased LDLR and

increased soluble LDLR (sLDLR) which positively correlates to circulating LDL-C levels (Alabi et al., 2021; Mayne et al., 2018; Mayne et al., 2007; Shimohiro et al., 2014). *In vivo* animal studies showed that overexpression of hepatic MT1-MMP decreased hepatic LDLR and increased development of atherosclerosis in *ApoE*^{-/-} mice. Conversely, knockdown of hepatic MT1-MMP increased LDLR levels while decreasing sLDLR and atherosclerotic burdens in *ApoE*^{-/-} mice (Alabi et al., 2021).

Targeting MT1-MMP has the potential to be a new lipid-lowering strategy. However, specificity for MT1-MMP has been a major issue for inhibitors as the catalytic domain is highly conserved (Xia, Alabi, et al., 2021b). Past clinical trials of all broad-spectrum MMP inhibitors for cancer failed due to adverse off-target effects (Fields, 2019). As each member of the MMP family play various essential physiological roles, non-specific targeting is detrimental, as exhibited by skeletal dysplasia and mortality within 4 weeks after birth for *Mmp14* global KO mice (Amar et al., 2017b; Xia, Alabi, et al., 2021b). Recently, it has been reported that exo-sites, regions outside the catalytic domain, are less conserved and involved in substrate recognition (English et al., 2001; Lang et al., 2004; Woskowicz et al., 2013). It is of interest to elucidate the function of these exo-sites for substrate specificity in generating specific inhibitors.

The first part of this project is to determine the specific sites on LDLR for MT1-MMP targeting and cleavage, as well as sites on MT1-MMP that allows it to recognize and cleave LDLR. Given that the MT-loop is specific for MT1-MMP, we will also determine the residue that induces LDLR targeting and cleavage (**Figure 6**).

For the second part of this project, we will shift the focus to hepatic MT1-MMP's effect on the development of liver fibrosis as MT1-MMP plays a critical role in fibrotic ECM degradation and TGF- β activation. Thus, we will subject control (*Mmp14*^{Flox}) and hepatocyte MT1-MMP specific knock out (*Mmp14*^{LKO}) mice on an *ad libitum* high fructose, high fat, and high cholesterol Gubra amylin liver

NASH (GAN) diet for 42 weeks. At endpoint, we will determine the effect of hepatic MT1-MMP on the development liver fibrosis (**Figure 6**).

Our findings will reveal the potential of targeting hepatic MT1-MMP as a novel lipid lowering therapy for patients whose disease cannot be effectively managed by current treatments.

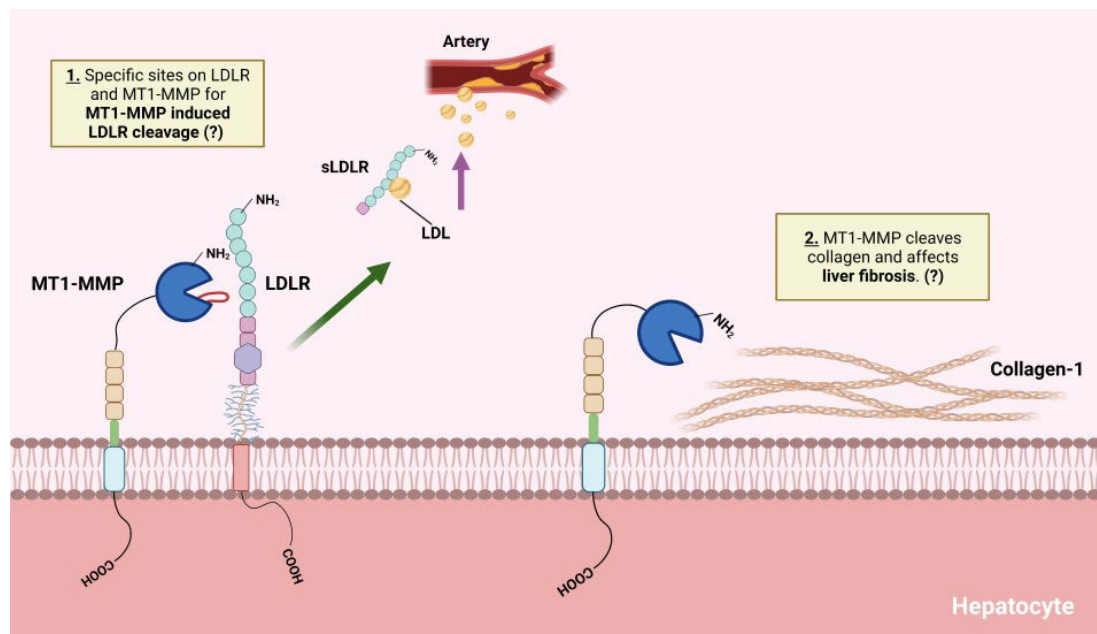


Figure 6. Project objectives. The objective for this project is to 1) ascertain the determinants on LDLR and MT1-MMP for MT1-MMP mediated LDLR cleavage. 2) As MT1-MMP plays a role in ECM degradation, we want to determine MT1-MMP's role in the development of liver fibrosis. (Made on Bio Render)

Chapter 2 Methods and Materials

2.1 Materials

Cell culture medium, fetal bovine serum (FBS), Lipofectamine 3000, GeneJet and PureLink™ Hipure plasmid miniprep kit were obtained from ThermoFisher Scientific. Complete EDTA-free protease inhibitors were purchased from Roche. Mouse monoclonal anti-Na⁺/K⁺-ATPase from BD Biosciences. All other reagents were obtained from Fisher Scientific unless otherwise indicated.

2.2 Site Directed Mutagenesis

Plasmid containing cDNA of the full-length MT1-MMP with an HA-tag on the hemopexin domain was used as the template to generate the mutant form of MT1-MMP. Plasmid pBudCE4.1 containing cDNA of the full-length hLDLR with an N-terminal HA-tag was used to generate the mutant forms of LDLR. Mutagenesis was performed using QuickChange Lightning site-directed mutagenesis kit (Agilent Technologies) as described in our previous studies (Gu, Adijiang, et al., 2013; Gu, Li, et al., 2013; Wang et al., 2013). LDLR deletions were generated as described previously (Zhang et al., 2008; Zhang et al., 2007). To generate the catalytic deletion of MT1-MMP (Δ CAT), an AgeI site was introduced at Tyr112 and Pro312, respectively. To delete the hemopexin-like repeats in MT1-MMP (Δ HXP), an AgeI site was introduced at Pro312 and Gly535, respectively. The resulted construct was digested with AgeI (FastDigest BshTI, Thermo Scientific) and ligated using the Quick Ligation Kit (New England Biolabs). To remove the C-terminal cytoplasmic region of MT1-MMP, a stop codon was introduced at Arg563. Oligonucleotides containing the residues to be mutated were synthesized by IDT® (Coralville, IA) and listed in Table 1. The presence of the desired mutation and the integrity of each construct were verified by DNA sequencing.

Site-directed mutagenesis was also used to generate mutants P163A, Y164A, Y166A, I167A, R168A, E169A, G170A, I167M, I167K, I167V, I167E, I167T, I167L, I167F, and V162A on MT1-MMP

(**Table 1**). Primers were purchased from IDT® (Coralville, IA). Mutagenesis was performed using QuickChange Lightning site-directed mutagenesis kit (Agilent Technologies). PCR components were commercial 10X reaction buffer, 50 ng of dsDNA template, 125 ng of forward and reverse primer, commercial dNTP mix, QuickSolution reagent, QuickChange Lightning Enzyme, and ddH₂O. Template DNA was pBudCE4.1 with WT MT1-MMP.

2.3 Transformation

XL-10 Gold Ultracompetent cells (Agilent Technologies) were used. β -mercaptoethanol from the kit was added and incubated with cells on ice. 2 μ L of DpnI treated DNA from the site-directed mutagenesis step was added to the ultracompetent cells and the cells were then incubated on ice. Cells were heat-shocked on 42 °C water bath to integrate the DNA. NZY+ broth (Fisher BioReagents) was added, and cells were incubated at 37 °C, 225 rpm, and 60 mins. Cell sample was spread on 1: 2000 (final concentration: 50 mg/mL) zeocin in low salt LB (10 g Tryptone, 5 g NaCl, 5g yeast extract, pH 8, bacto-agar) agar plates and incubated overnight.

Table 1. Primers used in site-directed mutagenesis. (A) MT1-MMP mutants, (B) MT-loop mutants, and (C) LDLR mutants primer sequences. Primers were purchased from IDT® (Coralville, IA).

MT1-MMP Mutants

A	Mutant	Sequence (5' to 3')
	E240A	5'- GGT GGC TGT GCA CGC GCT GGG CCA TGC CC -3'
	Y112-AgeI	5'-GTT CGA AGG AAG CGC ACC GGT ATC CAG GGT CTC-3'
	P312-AgeI	5'-GAT AAA CCC AAA AAC ACC GGT TAT GGG CCC AAC-3'
	Gly535-AgeI	5'-GAC GAG GAG GGC ACC GGT GCG GTG AGC GCG G-3'
	Arg563-Stop	5'-CAG TCT TCT TCT TCT GAC GCC ATG GGA C -3'
	MT-loop deletion	5'- CCA CTG CGC TTC CGC GAG GTG CAT GAG AAG CAG GCC GAC ATC ATG ATC -3'

MT-loop Mutants

B	Mutant	Sequence (5' to 3')
	P163-A	5'-CTT CCG CGA GGT GGC CTA TGC CTA CAT C-3'
	Y164-A	5'-CCG CGA GGT GCC CGC TGC CTA CAT CCG TG-3'
	Y166-A	5'-GAG GTG CCC TAT GCC GCC ATC CGT GAG GGC-3'
	I167-A	5'-GTG CCC TAT GCC TAC GCC CGT GAG GGC CAT G-3'
	R168-A	5'-CCC TAT GCC TAC ATC GCT GAG GGC CAT GAG-3
	E169-A	5'-CTA TGC CTA CAT CCG TGC GGG CCA TGA GAA G-3'
	G170-A	5'-GCC TAC ATC CGT GAG GCC CAT GAG AAG CAG-3'
	I167-L	5'-GTG CCC TAT GCC TAC CTC CGT GAG GGC CAT G-3'
	I167-V	5'-GTG CCC TAT GCC TAC GTC CGT GAG GGC CAT G-3'
	I167-M	5'-GTG CCC TAT GCC TAC ATG CGT GAG GGC CAT G-3'
	I167-F	5'-GTG CCC TAT GCC TAC TTC CGT GAG GGC CAT G-3'
	I167-E	5'-GTG CCC TAT GCC TAC GAA CGT GAG GGC CAT GAG-3'
	I167-K	5'-GTG CCC TAT GCC TAC AAG CGT GAG GGC CAT GAG-3'
	I167-T	5'-GTG CCC TAT GCC TAC ACC CGT GAG GGC CAT G-3'
	V162-A	5'-G CGC TTC CGC GAG GCG CCC TAT GCC TAC ATC-3'

LDLR Mutants

C	Mutant	Sequence (5' to 3')
	A521V	5'-CTC CAA GCC AAG GGT CAT CGT GGT GGA T-3'
	G529V	5'-GTG GAT CCT GTT CAT GTC TTC ATG TAC TGG-3'
	N645V	5'-AAC TTG TTG GCT GAA GTC CTA CTG TCC CCA-3'
	A789V	5'-CAG TAG CGT GAG GGT TCT GTC CAT TGT C-3'

2.4 DNA Purification

After overnight incubation, individual colonies were picked and incubated in 1 mL low salt LB (10g Tryptone, 5g NaCl, 5g yeast extract) in 50 µg/mL zeocin for 8 h. Depending on whether miniprep, midiprep, or maxiprep was performed, a specific volume of cell culture from the 1 mL mini-culture was added to a specific volume of low salt LB solution with 50 µg/mL zeocin, and incubated overnight on 37 °C shaker at 225 rpm.

For DNA purification, we followed manufacturers protocol for miniprep (PureLink™ HiPure Plasmid Miniprep Kit, Invitrogen Thermo Fisher Scientific), midiprep (GeneJET Plasmid Miniprep Kit, Thermo Scientific), and maxiprep (PureLink™ HiPure Plasmid Maxiprep Kit, Invitrogen Thermo Fisher Scientific).

2.5 Cell Transfection

HEK293 cells were maintained in DMEM (high glucose) containing 10% (v/v) FBS at 37 °C in a 5% CO₂ humidified incubator. Plasmid DNA was introduced into cells using Polyethylenimine (PEI) (PEI, M.W: 25000) or Lipofectamine™ 3000 as described (Shen et al., 2020). 48 h after treatment, whole cell lysate was prepared using lysis buffer B (1% Triton X-100, 150 mM NaCl, 50 mM Tris, pH 7.4) containing 1 × Complete EDTA-free protease inhibitors as described in our previous studies. Protein concentrations were determined by the BCA protein assay. An equal amount of whole cell lysate protein was subjected to SDS-PAGE and transferred to nitrocellulose membranes by electroblotting. Immunoblotting was performed using antibodies as indicated. Antibody binding was detected using IRDye-labeled goat anti-mouse or anti-rabbit IgG (Li-Cor). The signals were detected and quantified on a Li-Cor Odyssey Infrared Imaging System (Li-Cor).

2.6 Whole Cell Lysis

At endpoint, medium was collected, and cells were rinsed and then resuspended with 1 mL of 1X phosphate buffered saline (PBS). Medium and cells were then spun down for 5 mins at 500 xg at 4 °C, and the supernatant was decanted. Cells were lysed with 100 µL of lysis buffer B with 1X proteinase inhibitors (cOmplete Mini Protease inhibitor cocktail tablets, Roche diagnostics) and vortexed intermittently for 30 mins on ice. Samples were then spun down and the supernatant was collected and stored at -20 °C. For the stored medium, proteins were further concentrated via trichloroacetic acid (TCA) precipitation. 100% TCA was diluted to a final concentration of 15% TCA. Samples were incubated overnight at 4 °C and spun down the following day. Samples were then rinsed with -20 °C acetone, before being spun down again. Supernatant was decanted and the pellet was dried at room temperature. Finally, the pellet was resuspended in 9M urea and was solubilized at room temperature for a couple of hours or overnight in the 4 °C.

2.7 Immunoblotting

Whole cell lysis protein samples were run on 8% SDS-PAGE gels with 1X running buffer (Tris-base, glycine, SDS). Proteins were then transferred onto a nitrocellulose membrane via electroblotting in 1X transfer buffer (Tris-base, glycine) at 400 mA. Membranes were blocked with 5% (w/v) skim milk for 45 mins and washed with 1X PBST (1XPBS, 0.1% Tween-20). Membranes were blotted overnight at 4 °C in the primary antibodies as indicated below, washed the following day in 1X PBST, and then incubated in IRDye-labeled goat anti-mouse or anti-rabbit IgG (Li-Cor) secondary antibody for 30 mins at room temperature. After washing, the signals on membranes were detected and quantified on a Li-Cor Odyssey Infrared Imaging System (Li-Cor).

The following antibodies were used: HL-1, a mouse monoclonal anti-the linker sequence between ligand binding repeat LBR4 and LBR5 of LDLR antibody (van Driel et al., 1987; Zhang et al., 2008); a rabbit anti-MT1-MMP monoclonal antibody (Abcam, ab51074); a rabbit anti-HA polyclonal antibody (ProteinTech, 51064-2-AP); a mouse anti-HA monoclonal antibody (ProteinTech, 66006-2-Ig); and a

mouse anti-transferrin receptor monoclonal antibody (BD Biosciences, 612125). Primary antibodies HL-1, rabbit anti-MT1-MMP, rabbit anti-HA, and mouse anti-HA were diluted 1:1000. Mouse anti-transferrin receptor was diluted 1:10000. All secondary antibodies were diluted 1:10000.

2.8 Migration Assays

The experiment was carried out using the transwell migration assay (Pijuan et al., 2019). HEK293 cells were seeded on a 6-well cell culture plate and then transfected with empty plasmid or plasmid containing the wild-type or mutant MT1-MMP using Lipofectamine 3000. 24 h later, cells were trypsinized and counted. Equal number of cells in 500 μ L of serum-free DMEM medium were placed on a cell culture insert pre-coated with collagen type I (8 μ m). 500 μ L of DMEM containing 20% FBS was placed below the insert. 48 h after, the insert was rinsed briefly in 1X PBS, fixed, and then stained with crystal violet in 20% methanol. Cells on top of the insert were removed with a cotton swab. Cells on the bottom of the insert were imaged on an OMAX M837ZL-C140U3 microscope, and cell numbers were counted (10 images per insert). Relative cell number was calculated by dividing the mean cell number by image area that was measured with OMAX ToupView.

2.9 Immunofluorescence

Confocal microscopy was carried out as described previously (Gao et al., 2012; Gu et al., 2016; Gu et al., 2014). Briefly, HEK293 cells cultured on a coverslip were transfected with an empty vector, the wild-type or mutant MT1-MMP cDNA. 48 h later, cells were fixed with 3% paraformaldehyde in PBS, and then permeabilized using ice-cold methanol. After blocking, the cells were incubated with an anti-MT1-MMP polyclonal antibody (1:100) and an anti- Na^+/K^+ -ATPase monoclonal antibody (1:100). Antibody binding was detected using Alexa Fluor 488 goat anti-rabbit IgG and Alexa Fluor 568 goat anti-mouse IgG. Nuclei were stained with 4', 6-diamidino-2-phenylindole (DAPI, ThermoFisher). Coverslips were mounted on the slides with ProLong Diamond Antifade Mountant (ThermoFisher). Localization of MT1-MMP in the transfected cells was determined using a Leica SP5 laser scanning

confocal microscope (filters: 461 nm for DAPI, 519 nm for Fluor 488, 603 nm for Fluor 568) at the University of Alberta Cell Imaging Core.

2.10 Animal

Mmp14^{Flox} and *Mmp14^{LKO}* mice in C57BL/6 background were generated as described in our previous study (Alabi et al., 2021). Briefly, the Cre-lox strategy was used to inactivate MT1-MMP in the hepatocytes. *Mmp14^{Flox}* mice were crossed with transgenic mice expressing Cre recombinase under the control of the albumin promoter (The Jackson Laboratory) to inactivate MT1-MMP in hepatocytes in *Mmp14^{LKO}* mice. Mice were housed and bred in the animal facility at the University of Alberta. They were housed 3 to 5 mice per cage with unlimited access to water, at 22 °C, 43% humidity, and on a 12 h light/dark cycle. Mice were fed chow diet *ad libitum* (20% protein, 5% fat, and 48.7% Carbohydrates) (LabDiet, PICO Laboratory Rodent Diet 20, gross energy 4.11 kcal per gm). All animal procedures were approved by the University of Alberta Animal Care and Use committee (AUP00000456). Protocols followed guidelines of the Canadian Council on Animal Care.

2.11 Special Animal Diet and Experimental Use

Mice were fed for 42 weeks *ad libitum* with the GAN rodent diet (40 kcal% fat (mostly palm oil), 20 kcal% fructose and 2% cholesterol, Research diets). Food was topped up whenever supply was low in each cage. Water access was unlimited. Every 6 weeks and at endpoint, mice were fasted overnight (10-12 h) prior to body weight measurement, blood glucose test, and blood collection. Plasma was prepared from the blood by centrifugation at 6000 rpm, 20 mins, 4 °C using Centrifuge 5430 R (Eppendorf) and used to test plasma total cholesterol (TC) and plasma TG. Mice were observed for distress and possible morbidities for 24 h post blood sampling. They were then returned to the housing facility. At 42 weeks, mice were anesthetized with gaseous isoflurane for sample collection. Plasma and tissue samples were stored at -80 °C for further analysis.

2.12 Histological Staining

Mice liver samples preserved in CryoMatrix™ were sent to the HistoCore facility in Alberta Diabetes Institute at the University of Alberta for sectioning and staining. Liver samples were fixed in 10% formalin and embedded in paraffin. They were then sectioned at a thickness of 8 µm onto Histobond slides. The slides were then subjected to hematoxylin and eosin (H&E) and Picrosirius Red. Cryosectioned liver tissues were used for Oil-Red O staining. Slides were visualized at 10 X magnification on the OMAX M837ZL-C140U3 microscope.

2.13 Blood Glucose, Total Cholesterol, Triglyceride, HDL-C measurements

Blood glucose was measured directly from blood taken from the mice during blood collection and assessed using Contour Next blood glucose test strips (Ascensia Diabetes care). Plasma TC and plasma TG were measured following the manufacturer's protocol (Cholesterol E CHOD-DAOS Method, Fujifilm) (L-type Triglyceride M GPO_HMMPS, glycerol blanking method, Fujifilm). In the TC assay, Chol E buffer was added to samples and standard (Commercial standard solution, 200 mg/dL Cholesterol) to hydrolyze CE in serum to free cholesterol and fatty acids. Addition of the Chol E buffer (50 mmol/L Good's buffer solution, 1.6 U/mL cholesteryl ester hydrolase, 0.31 units/mL cholesterol oxidase, 5.2 units/mL peroxidase, 0.19 mmol/L 4-aminoantipyrine, 4.4 units/mL ascorbate oxidase, and 0.95 mmol/L 3,5-dimethoxy-N-ethyl-N-(2hydroxy-3-sulfopropyl)-aniline sodium salt (DAOS), pH 6.1) to the sample and standard (3µL) formed hydrogen peroxide which participated in a quantitative oxidative condensation reaction with DAOS and 4-amino-antipyrine in the presence of peroxidase to produce a blue pigment. Samples and standards were then incubated at 37°C for 5 mins. Afterwards, the absorbance of the pigment was measured at wavelength 600 nm on a plate reader. The TG assay uses a series of enzymatic reactions. Enzyme A reagent (50 U/mL Glycerol kinase (GK), 8.0 mmol/L adenocine 5'-triphosphate disodium salt (ATP), 5.6 U/mL glycerol-3-phosphate oxidase (GPO), 150 U/mL catalase (bovine liver), 0.4 mmol/L N-(3-sulfopropyl)-3-methoxy-5-methylaniline (HMMPS), 2.0 U/mL

ascorbate oxidase, pH 7.0) was first added to plasma samples. The samples were incubated at 37 °C for 5 mins. GK converted free glycerol to glycerol-3-phosphate (G3P), and GPO converted G3P to dihydroxyacetone phosphate. Catalase degraded the hydrogen peroxide in solution to H₂O and O₂. These reactions removed free glycerol in the plasma sample. Enzyme B reagent (250 U/mL lipase, 4.6 mmol/L 4-aminoantipyrine, and 25 U/mL peroxidase (horse radish), pH 7.1) was then added to hydrolyze TG in the samples to glycerol and free fatty acids. GK and GPO repeat their enzymatic actions with the glycerol from triacylglycerol. Standards (serial dilution of glycerol in ddH₂O) were added after enzyme B reagent was added. The hydrogen peroxide produced from this GPO reaction caused HMMP and 4-aminoantipyrine to undergo a quantitative oxidative condensation reaction mediated by peroxidase. This produced a blue pigmentation in which the absorbance was read on a SpectraMax 250 plate reader at wavelength of 540 nm.

HDL-C was extracted from plasma using the HDL and LDL/VLDL Cholesterol Assay kit (Cell BioLabs, Inc.). Precipitation Reagent from the kit was added 1:1 to mouse plasma samples. Plasma-Reagent mixture was vortexed then incubated at room temperature for 5 to 10 mins. Mixture was centrifuged at 2000 xg for 20 mins. The supernatant, which contained the HDL, was then used in the TC assay as described and measured at wavelength 600 nm on a SpectraMax 250 plate reader. Non-HDL-C was calculated by subtracting HDL-C from TC.

2.14 Lipid Extraction

Lipids were extracted from liver samples using the Folch method as described in our previous study (Alabi et al., 2021). The Folch method is an established method for extracting lipids with 2:1 chloroform:methanol (v/v). The method has been optimized over the years to increase accuracy and precision of measuring tissue lipid content. In this study, liver samples were flash frozen with liquid nitrogen and portioned into 100 mg aliquots. Liver aliquots were homogenized in 400 µL of homogenization buffer (50 mM Tris-HCl, 250 mM sucrose and 1mM EDTA, pH 7.4) using a Power Gen

500 (Thermo Fischer) homogenizer. Immediately after homogenization, BCA assay was used to determine protein concentration. All subsequent steps that involved the use of chloroform was done in and with glass. 100 μ L of crude liver homogenate was added to 900 μ L of 1X PBS and 4 mL of chloroform:methanol (2:1) in a glass tube with a Teflon cap. Samples were vortexed and spun down at 1800 rpm for 10 mins (Eppendorf Centrifuge 5810 R) to separate the sample into an aqueous upper phase and non-polar lower phase. The upper phase contained the polar contaminants that were discarded. The bottom phase, composed of chloroform and the non-polar lipids, was transferred to a new glass vial. The non-polar bottom phase was then dried under N₂ gas. Afterwards, the dried samples were resolubilized in chloroform with 2% Triton (v/v) by vortex. Then, the chloroform was completely dried down under N₂ gas. What remained was approximately 20 μ L of Triton containing the lipids. Lipids in Triton were finally resolubilized in 500 μ L ddH₂O on a 37°C water bath for 15 mins with intermittent vortex action. Aliquots of the extracted lipid samples were used for measurement of TC (3-6 μ L) and TG (3 μ L) with the commercial enzymatic kits (Cholesterol E CHOD-DAOS Method, Fujifilm; L-type Triglyceride M GPO_HMMPS, glycerol blanking method, Fujifilm) as described in 2.13.

2.15 BCA assay

BCA assay was conducted using a commercial kit (Pierce[™] BCA Protein Assay kit, ThermoScientific). The BCA assay standard was a serial dilution of BSA in ddH₂O (albumin from bovine serum minimum 98% electrophoresis, Sigma Life Science). Standard dilutions were 8 mg/mL, 4 mg/mL, 2 mg/mL, 1 mg/mL, and 0.5 mg/mL. 4 μ L of standards and samples were pipetted into 96 well plates. BCA reagent A and BCA reagent B were mixed in 50:1. 200 μ L of BCA mixed reagent solution was added to each well and then incubated at 37 °C for 30 mins. Protein quantification was measured at wavelength 562 nm on a SpectraMax 250 plate reader.

2.16 Real Time Reverse Transcription Polymerase Chain Reaction

TRIzol™ Reagent was used to extract total RNA from mouse liver tissues (50 mg). Tissue was homogenized in Power Gen 500 (ThermoFischer) homogenizer. Additional 0.2 mL chloroform was used to separate RNA into an aqueous phase. The aqueous phase was extracted, and RNA was then precipitated with isopropanol. RNA pellet was washed in 75% ethanol and pelleted down again. Supernatant was discarded and remaining RNA was dried and resolubilized in RNase-free water. cDNA was produced using the High Capacity cDNA Reverse Transcription kit (Applied Biosystems, ThermoFisher Scientific). The kit consists of MultiScribe Reverse Transcriptase, 100 mM dNTP mix, 10x RT Random Primers, 10x RT buffer. PCR reaction was done on C1000 Thermo Cycler (BIO-RAD).

The RT-PCR reaction was conducted using the cDNA template and forward and reverse primers for *Srebp2*, *Srebp1c*, *Ppara*, *Gapdh*, *Tgfb*, *Tnfa*, *Il1b*, *Il6*, *Coll1a1*, *Cpt1a*, *Mmp14*, *Pcsk9*, and *Fasn*. Primers were purchased from IDT® (Coralville, IA). The RT-PCR reaction also used PowerUp™ SYBR™ Green Master Mix (Applied Biosystems ThermoFisher Scientific). RT-PCR was set up on MicroAmp® Fast 96-well Reaction Plate (Applied Biosystems, Life Technologies). The sample plate was covered with Optical Adhesive Covers (Applied Biosystems, ThermoFisher Scientific), and samples were mixed on VWR Micro Plate Shaker and then spun to the bottom of the well on a FisherBrand™ Microplate Centrifuge. RT-PCR was finally carried out on Step One Plus Real Time PCR system (Applied Biosystems, Thermo Fisher).

2.17 Statistical Analysis

Statistical analyses were performed using GraphPad Prism version 9.0 (GraphPad Software). The significant difference between two groups were determined via Student's *t*-test and defined as * $p < 0.05$, ** $p < 0.01$, *** $p < 0.001$, and **** $p < 0.0001$. $p > 0.05$ was defined as no significance. Values of all data, unless otherwise indicated, were depicted as mean \pm S.D. All experiments, unless indicated, were repeated at least three times.

Chapter 3: MT1-MMP-Mediated Degradation of LDLR

3.1 Introduction

Plasma levels of low-density LDL-C are positively correlated to the risk of CVD. Hepatic LDLR is the main pathway that clears plasma LDL-C. Mutations in LDLR cause FH, characterized by elevated levels of plasma LDL-C and increased risk of coronary heart disease (Goldstein & Brown, 2015). Structurally, LDLR's ectodomain consists of 7 LBR at its N-terminus region for binding substrates, such as interacting with apoB100 on LDL and apoE on lipoprotein remnants. LBR is followed by the EGF domain that is required for lipoprotein release in the endosome and recycling of LDLR. Upon substrate binding, LDLR is endocytosed into a clathrin-coated vesicle, where it is then shuttled to the endosome. In the acidic environment of endosomes, LDL-C is released from the receptor and LDLR is recycled back to the cell surface. LDL-C is then shuttled to the lysosome for degradation. Further down in the primary sequence is the clustered O-glycosylation region, whose function is still elusive, followed by the transmembrane domain and a cytoplasmic tail at the C-terminus. The NPVY motif within the C-terminus is critical for the internalization of the receptor into clathrin-coated pits (Davis et al., 1986; Davis, van Driel, et al., 1987; Rudenko et al., 2002). Substitution of Tyr807 to cysteine, otherwise known as the J.D. mutation in FH, impairs LDLR endocytosis but does not affect LDLR trafficking to the cell surface or the binding of LDL to the receptor (Davis et al., 1986).

Currently, the primary lipid-lowering therapy is statins, which inhibits HMGCR, the rate-limiting enzyme in cholesterol biosynthesis. Reduction in cellular cholesterol levels activates the transcriptional activity of SREBP-2, thus increasing *LDLR* expression and LDL-C clearance (DeBose-Boyd & Ye, 2018; Goldstein & Brown, 2015; Horton et al., 2003). However, the efficiency of statin treatment is approximately 20-40%. Furthermore, about 15% of people treated with statins show intolerance to treatment and require alternative therapies to lower LDL-C (Fitchett et al., 2015). One option is targeting PCSK9, which promotes LDLR degradation (Guo et al., 2020; Horton et al., 2009; Lagace, 2014; Seidah

et al., 2014; Xia, Peng, et al., 2021). While recently approved PCSK9 inhibitors can effectively reduce plasma LDL-C levels, the treatment is expensive (Sabatine, 2019; Seidah, 2017). PCSK9 siRNA therapy may be more affordable, but it is still too financially unsustainable for all eligible patients to use in primary prevention. Therefore, the search for alternative treatments is necessary.

The ectodomain of LDLR can be cleaved by proteases to generate sLDLR, which inactivates LDLR-mediated LDL clearance. It has been reported that plasma levels of sLDLR are positively correlated to circulating LDL-C levels (Mayne et al., 2018; Mayne et al., 2007; Shimohiro et al., 2014). In our previous studies, we found that MT1-MMP promotes ectodomain shedding of LDLR, thereby increasing plasma LDL-C levels, and exacerbating the development of atherosclerosis in mice (Alabi et al., 2021; Xia, Alabi, et al., 2021a). Therefore, targeting MT1-MMP has the potential to be a new lipid-lowering strategy.

MT1-MMP belongs to MMP family that consists of 24 zinc-dependent endopeptidases in vertebrates and 23 in humans. It plays essential physiological roles in tissue remodelling and development by cleaving ECM components and non-matrix substrates (Amar et al., 2017c; Holmbeck et al., 1999; Xia, Alabi, et al., 2021a; Zhou et al., 2000). Structurally, MT1-MMP contains an N-terminal signal peptide, followed by a catalytic domain containing the conserved zinc-binding site (HE240XGHXXGXXH). Next is the flexible hinge region, followed by a hemopexin domain that links the catalytic domain, and the transmembrane domain that anchors the protein to cell membranes. The C-terminal cytoplasmic tail is involved in endocytosis of MT1-MMP (Castro-Castro et al., 2016; Feinberg et al., 2018; Houghton, 2015; Xia, Alabi, et al., 2021a). The catalytic domain is highly conserved in the MMP family members (Castro-Castro et al., 2016; Xia, Alabi, et al., 2021a). Clinical trials of all broad-spectrum MMP inhibitors that target the catalytic domain in oncology failed due to the lack of inhibitor specificity (Itoh, 2015). On the other hand, exosites that are regions outside the catalytic core domain of MMPs are less conserved and are involved in substrate selection and binding (Mori et al., 2013; Mori et

al., 2002; Yanez-Mo et al., 2008). Thus, drugs targeting exosites have a great potential to be both MMP and substrate specific.

In this study, we investigated the regions in LDLR and MT1-MMP required for MT1-MMP induced LDLR cleavage. We found that deletion of the MT-loop (amino acids 163-170) in the catalytic domain of MT1-MMP impaired its ability to cleave LDLR. Alanine scanning revealed that Ile at position 167 played an important role in MT1-MMP promoted LDLR degradation. Given that the MT-loop is specific for MT1-MMP, our findings provide a foundation for the future design of small inhibitors that can specifically target MT1-MMP's action on LDLR.

3.2 Results

3.2.1 Specific Sites on LDLR for MT1-MMP Mediated Cleavage

We have previously reported that MT1-MMP mediates shedding of the LDLR and regulates plasma LDL-C metabolism (Alabi et al., 2021). Here, we sought to identify the specific sites on LDLR for MT1-MMP-mediated cleavage. The LDLR has five distinct regions, each playing different critical roles in the functionality of the protein. To determine if any of these regions are important for MT1-MMP-mediated LDLR shedding, we made various LDLR mutants with deletions of different LDLR function domains, including the ligand binding repeat deletion ($\Delta R1-R7$), EGF-like domain deletion (ΔEGF), O-Linker sugar domain (ΔO -Linker), and C-terminal domain ($\Delta 812$) (**Figure 7A**). Each mutation was co-transfected with an equal amount of empty or the wild-type MT1-MMP-containing plasmid into HEK293 cells. We found that MT1-MMP cleaved all LDLR deletion mutants in a similar manner relative to the wild-type receptor (**Figures 7B-C**), indicating that each of these regions are not required for MT1-MMP's action on the LDLR. Another possibility is that MT1-MMP may have multiple cleavage sites on the receptor. To explore whether LDLR cleavage occurs on the cell surface or after endocytosis, we investigated if the loss of recycling property of the LDLR affected its cleavage by MT1-MMP. The J.D. mutation in LDLR is a naturally occurring mutation, in which Tyr in the NPVY motif is mutated to Cys (Y807C). This mutation impairs LDLR endocytosis, thus resulting in FH (Davis et al., 1986). Co-expression of the J.D. mutant with MT1-MMP did not prevent MT1-MMP cleavage of the protein (**Figures 7B-C**), indicating that the endocytosis of the protein does not play an essential role in MT1-MMP-mediated LDLR cleavage.

We then used the software CleavePredict (<http://cleavpredict.sanfordburnham.org>) to predict the cleavage sites of MT1-MMP on LDLR. CleavePredict is a validated free access web server for predicting the substrate cleavage pattern by MMPs. It employs MMP specific position weight matrices which is derived from statistical analysis of high-throughput phage display experimental cleavage results of

metalloproteinases (Kumar et al., 2015). The software predicted 22 putative MT1-MMP cleavage sites on LDLR, with a spread across all its extracellular domain (**Table 2**). We selected 4 locations based on the position weight matrix score and proximity to the transmembrane domain, which has been suggested to be the cleavage region of MT1-MMP on LDL receptor related protein 1 (LRP1) (Rozanov, Hahn-Dantona, et al., 2004). The selected sites were A521, G529, and N645 in the YWTD region and A789 within the transmembrane domain and near the outer layer of plasma membrane. These key residues were individually replaced with Val to disrupt each putative cleavage site, as confirmed by CleavePredict. We then co-expressed the mutant LDLR with the wild-type MT1-MMP in HEK293 cells. As shown in **Figures 7D and E**, all mutants were effectively cleaved by MT1-MMP, suggesting that each of the selected cleavage points is not required for the overall cleavage of LDLR mediated by MT1-MMP.

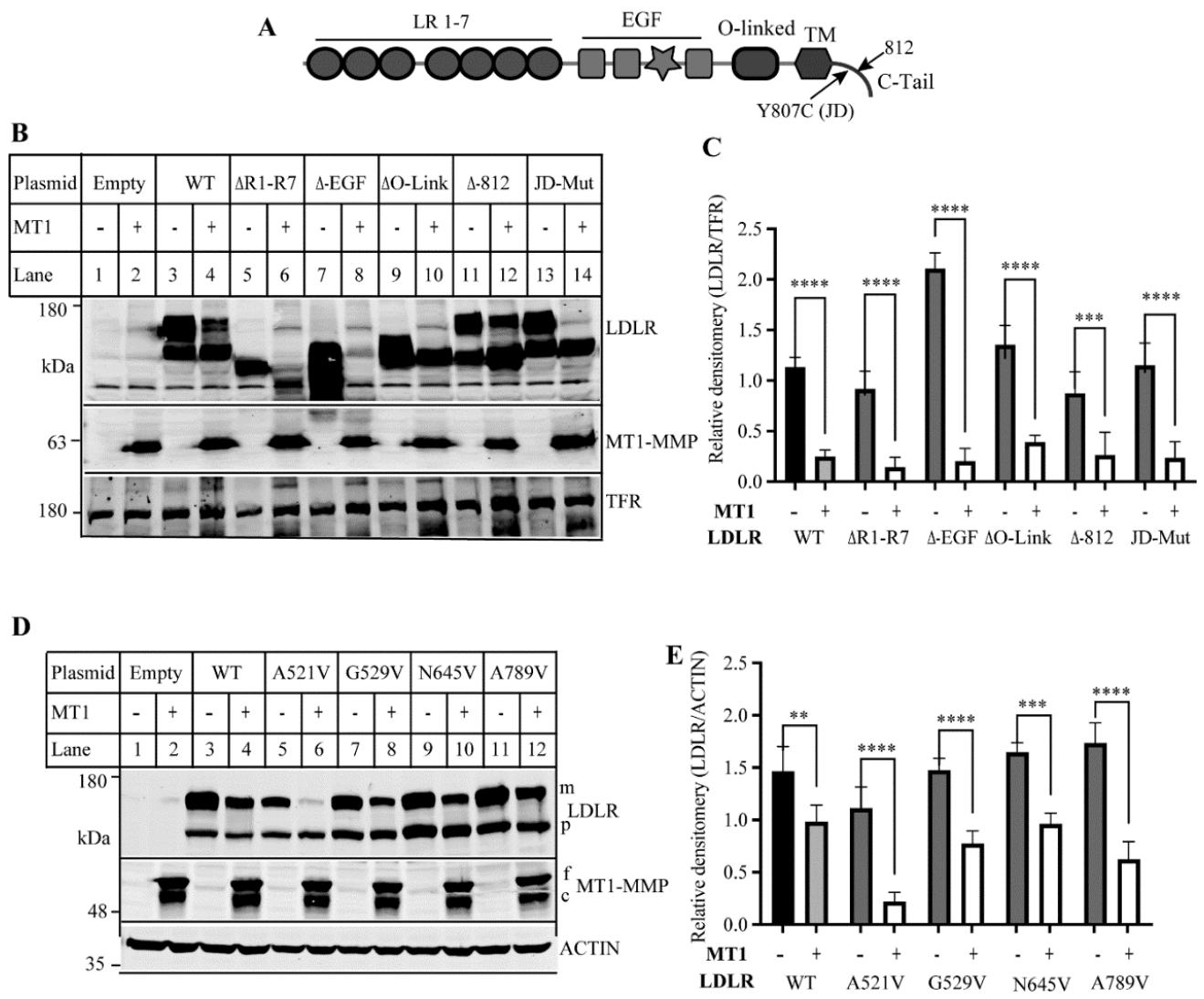


Figure 7. Effects of mutations in LDLR on MT1-MMP induced LDLR cleavage. (A) Diagram of the functional domains of LDLR. LR, ligand binding region. EGF, the epidermal growth factor precursor homology domain. O-linked, the O-linked sugars domain. TM, transmembrane domain. JD, the J.D. mutation (Y807C) identified from a FH patient. C-tail, the C-terminal cytoplasmic tail. (B to E) Immunoblotting and quantification. Equal amount of plasmid DNA containing LDLR deletion (B and C) or point mutations (D and E) and empty vector (-) or plasmid containing the wild-type MT1-MMP were transfected into HEK293 cells for 48 h. Equal amounts of total proteins in whole cell lysate was applied to SDS-PAGE and immunoblotting with antibodies as indicated. Densitometry was determined by a Li-Cor Odyssey Infrared Imaging System. Representative images are shown. TFR, transferrin receptor

(TFR). m, mature form of LDLR. p, precursor of LDLR. f, full-length MT1-MMP. c, cleaved form of MT1-MMP. Relative densitometry was defined as the ratio of the densitometry of the wild-type or mutant LDLR to that of TFR (C) or ACTIN (E) at the same condition. Values were mean \pm S.D. of ≥ 3 experiments. **, $p < 0.01$. ***, $p < 0.001$. ****, $p < 0.0001$.

Table 2. Predicted MT1-MMP cleavage sites on LDLR. Predicted MT1-MMP cleavage site on LDLR as determined by the online CleavePredict software, showing cleavage positions, residues and position weight matrix score. Selected positions were bolded.

P1 cleavage positions	Residues	PWM ^ Score
14	WTVAL-LLAAA	0.54
86	CIPQF-WRCDG	1.94
152	CGPAS-FQCNS	5.51
186	QRCRG-LYVFQ	2.87
397	KAVGS-IAYLF	1.14
400	GSIAI-LFFTN	3.05
421	SEYTS-LIPNL	2.97
425	SLIPN-LRNVV	2.30
521	SKPRA-IVVDP	4.90
529	DPVHG-FMYWT	5.37
541	GTPAK-IKGGG	1.95
554	VDIYS-LVTEN	1.17
565	QWPNG-ITLTL	5.36
584	SKLHS-ISSID	3.26
608	RLAHP-FSLAV	2.38
610	AHPFS-LAVFE	1.45
645	LLAEN-LLSPE	5.96
657	VLFHN-LTQPR	4.07
685	CLPAP-QINPH	2.54
701	ACPDG-MLLAR	0.81
707	LLARD-MRSCL	1.93
789	SSVRA-LSIVL	7.55

To further understand the cleavage pattern of LDLR by MT1-MMP, and if the metalloproteinase indeed cleaved LDLR at multiple sites, we looked at the cleaved LDLR ectodomain fragments in cell culture medium. For protein detection, we used two different anti-LDLR antibodies, HL-1, a mouse monoclonal anti-the linker sequence between ligand binding repeat LBR4 and LBR5 of LDLR antibody (van Driel et al., 1987); and 720B, a rabbit polyclonal anti-EGF-A of LDLR antibody (Zhang et al., 2008). HEK293 cells were co-transfected with MT1-MMP alone or with both LDLR and MT1-MMP. The amount of total proteins in culture medium was comparable in the two groups (**Figure 8A**). Both antibodies revealed minimal amount of bands in culture medium of cells overexpressing WT LDLR. However, there were multiple bands in the culture medium of cells overexpressing both LDLR and MT1-MMP, although the pattern of the bands was different (**Figure 8B**). Concomitantly, the mature form of LDLR appeared as a thick band in whole cell lysate of cells overexpressing WT LDLR, while LDLR was virtually undetectable when LDLR and MT1-MMP were both overexpressed (**Figure 8C**). Taken together, these findings suggest that MT1-MMP may cleave LDLR at multiple sites.

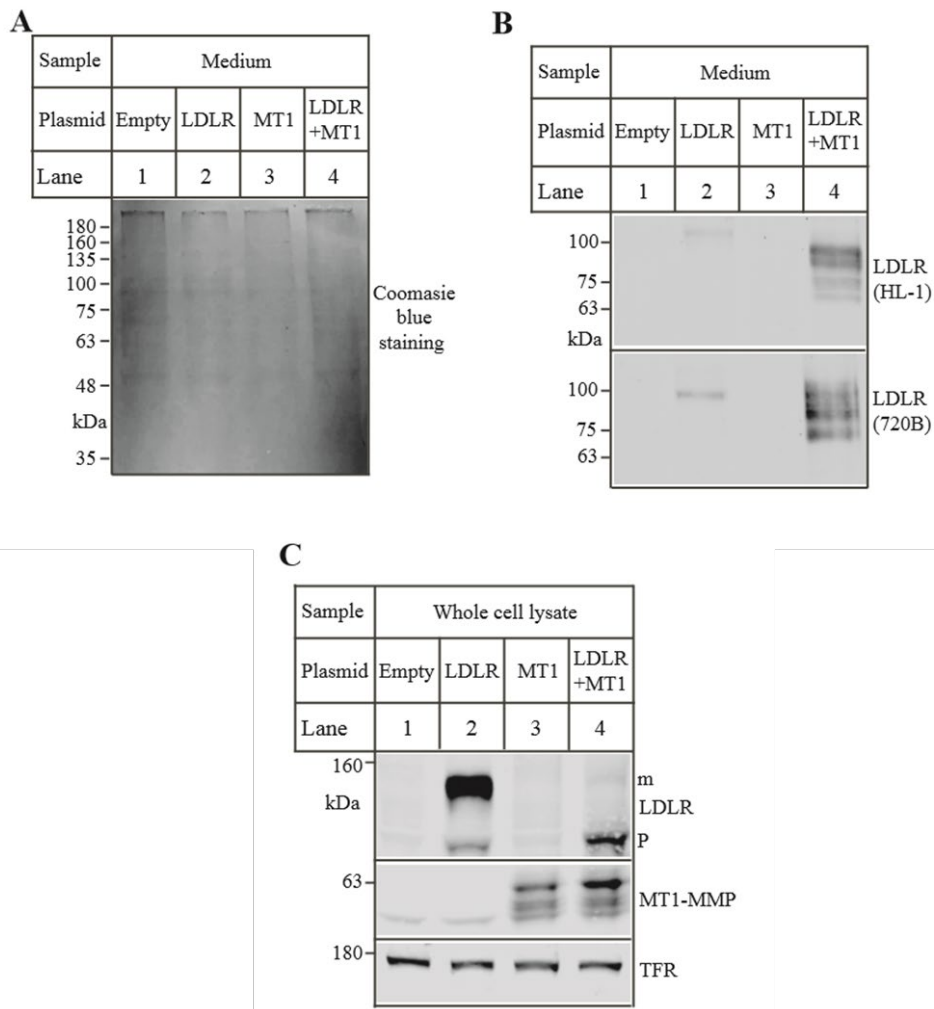


Figure 8. Cleavage of LDLR by MT1-MMP. (A) Coomassie blue staining. HEK293 cells were transfected with MT1-MMP alone, LDLR alone, or both MT1-MMP and LDLR. 48 h later, medium and cells were collected separately. Equal amounts of cell medium were applied to SDS-PAGE, followed by Coomassie blue R-250 staining (0.25% in 50% methanol (v/v) and 10% acetic acid (v/v)). The membrane was then destained in 40% (v/v) methanol with 10% (v/v) acetic acid and scanned on a Licor Odyssey Imaging System. **(B and C) Immunoblotting.** Equal amounts of cell medium (B) or whole cell lysate (C) from HEK293 cells transfected with MT1-MMP alone, LDLR alone or both MT1-MMP and LDLR for 48 h was applied to immunoblotting with antibodies indicated. m, mature form of LDLR. p, precursor of LDLR. TFR, transferrin receptor. Similar results were obtained from at least two more experiments. Representative images are shown.

3.2.2 The Requirement of Domains in MT1-MMP for LDLR shedding

Next, we determined which functional domains in MT1-MMP were critical for its ability to cleave LDLR. Thus, we deleted C-terminal cytoplasmic region (Δ C-Term), the hemopexin-like repeats (Δ HPX), the catalytic domain (Δ CAT), and the MT-loop (Δ 163-170) (**Figure 9A**). The wild-type or mutant MT1-MMP was co-expressed with the wild-type LDLR in HEK293 cells. The expression of the wild-type and mutant MT1-MMP, except for Δ HPX that did not have the tag, were confirmed by an anti-HA antibody. While a rabbit polyclonal anti-MT1-MMP antibody that recognizes the catalytic domain revealed the wild-type, Δ C-Term, Δ HPX, and Δ 163-170 but not Δ CAT MT1-MMP (**Figure 9B**). As shown in **Figures 9B and C**, Δ C-Term and Δ HPX, like the wild-type MT1-MMP, effectively cleaved the mature form of LDLR. On the other hand, the cleavage property was lost in Δ CAT MT1-MMP, reinforcing the importance of the catalytic activity of the proteinase for LDLR cleavage. This result was consistent with our previous finding of the catalytically dead E240A mutant of MT1-MMP. The E240A mutant virtually lost the ability to cleave LDLR (Alabi et al., 2021). Furthermore, deletion of the MT-loop abrogated MT1-MMP's ability to cleave LDLR. These findings indicate that the catalytic activity and the MT-loop are essential for MT1-MMP promoted LDLR shedding.

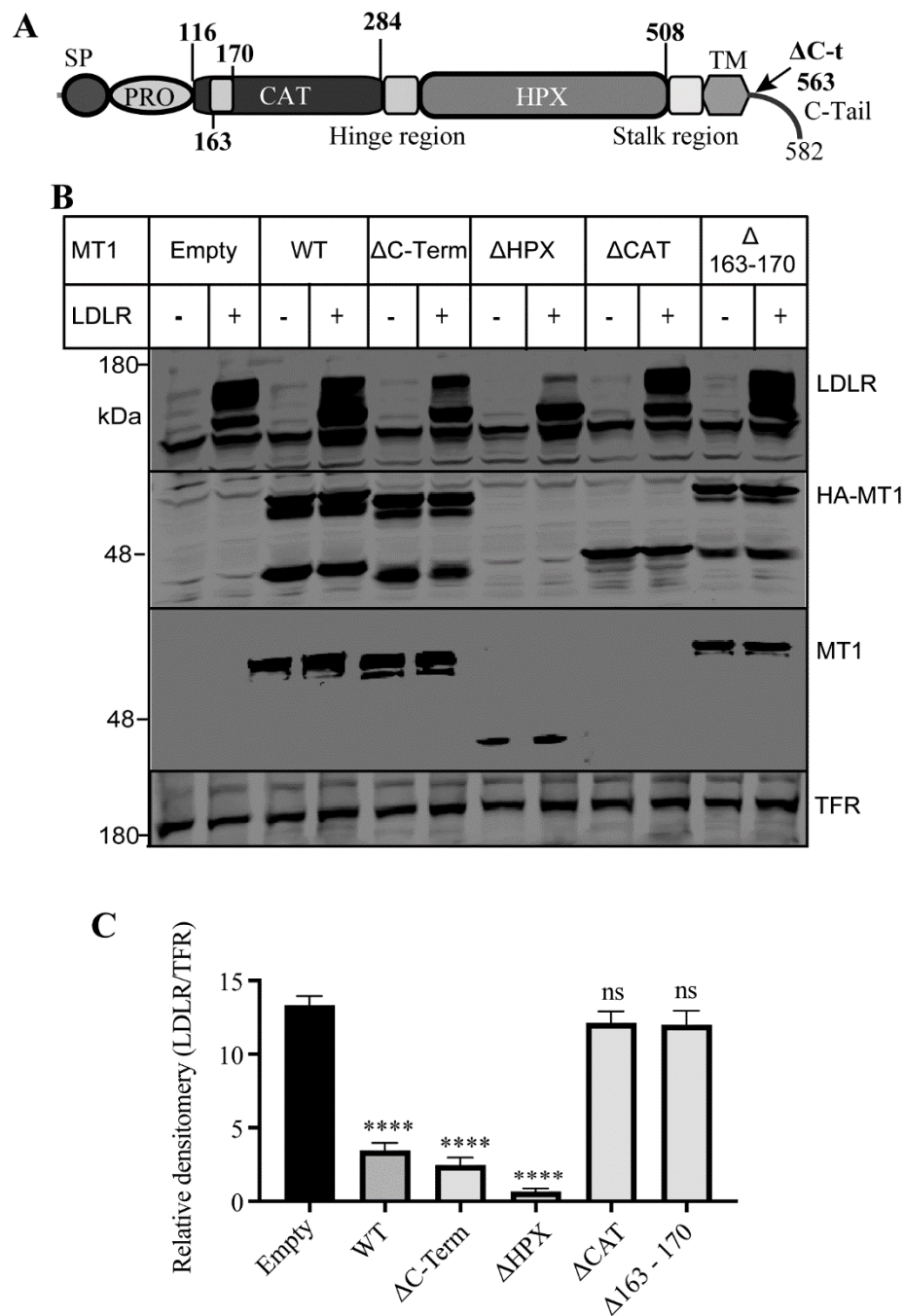


Figure 9. Effects of mutations in MT1-MMP on its ability to cleave LDLR. (A) Diagram of the functional domains of MT1-MMP. SP, signal peptide. CAT, the catalytic domain. HPX, the hemopexin domain. TM, transmembrane domain. C-Tail, the C-terminal cytoplasmic tail. **(B to C) Immunoblotting and quantification.** Equal amounts of plasmid DNA containing the wild-type or mutant MT1-MMP and empty plasmid (-) or the wild-type LDLR-containing plasmid were co-transfected into HEK293 cells for 48 h. Equal amounts of total proteins in whole cell lysates was applied to immunoblotting with antibodies

as indicated. TFR, transferrin receptor (TFR). Representative images are shown. Densitometry was determined by a Li-Cor Odyssey Infrared Imaging System. Relative densitometry was defined as the ratio of the densitometry of the mature form (m) of LDLR to that of TFR at the same condition. Values were mean \pm S.D. of ≥ 3 experiments. no significance (ns), $p > 0.05$. ****, $p < 0.0001$.

3.2.3 Mutational Analysis of the MT-loop

The MT-loop consists of seven amino acid residues and is present in all four type-I transmembrane MMPs (MT1-, MT2-, MT3-, MT5-MMP), except the two glycosyl phosphatidylinositol-anchored membrane-associated MMPs (MT4- and MT6-MMP) (**Figure 10A**). Pro163 and Tyr164 in the MT-loop are completely conserved among MT1, MT2, MT3, and MT5-MMP. Ile167 is also highly conserved except for MT3-MMP that has a hydrophobic Leu instead of Ile. We then performed alanine-scanning analysis to determine the contribution of each of these amino acid residues to MT1-MMP's action on LDLR. As shown in **Figures 10B and C**, substitution of Ile167 with Ala (MT1-MMP^{I167A}) significantly impaired MT1-MMP's ability to promote LDLR degradation, while mutation of other amino acid residues had no significant impact, indicating the important role of Ile167 in MT1-MMP promoted LDLR cleavage.

A

MT1-MMP. ATPLRFREVPYAYIREGHEKQADIMIFFAEGFHGDSTP
 MT2-MMP. ATPLVFQEVYEDIRLRQKEADIMVLFASGFHGDSSP
 MT3-MMP. VTPLTFEEVPYSELENGK-RDVDITIIIFASGFHGDSSP
 MT5-MMP. VTPLTFEEVPYHEIKSDR-KEADIMIFFASGFHGDSSP
 MT4-MMP. IAPLNFHEVA-----GSAADIQIDFSKADHNDGY P
 MT6-MMP. ESGLTFHEVDS-----PQGQEPDILIDFARAFHQDSY P

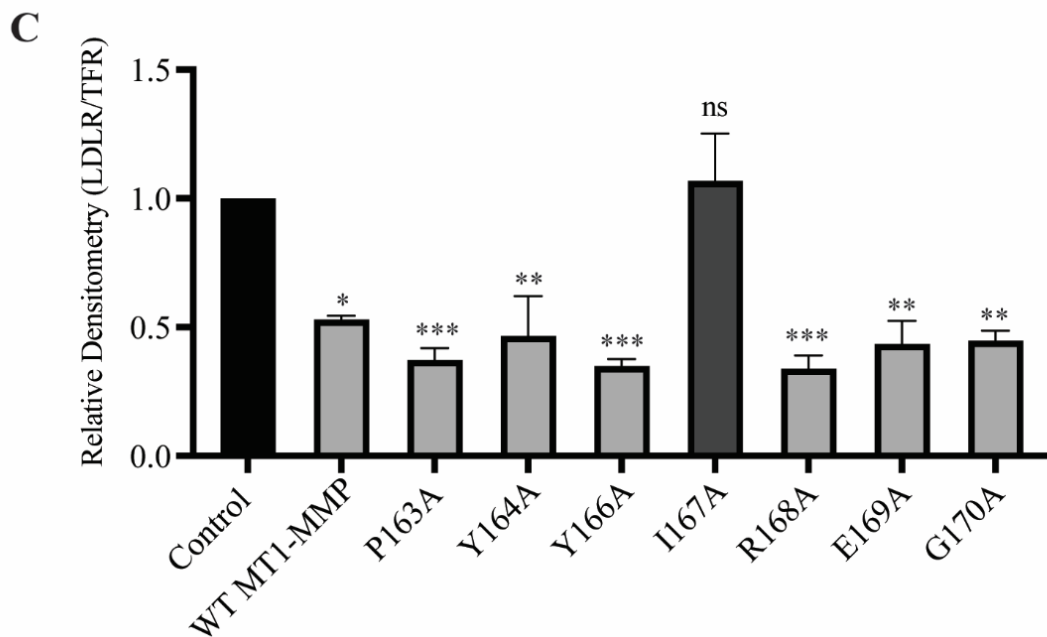
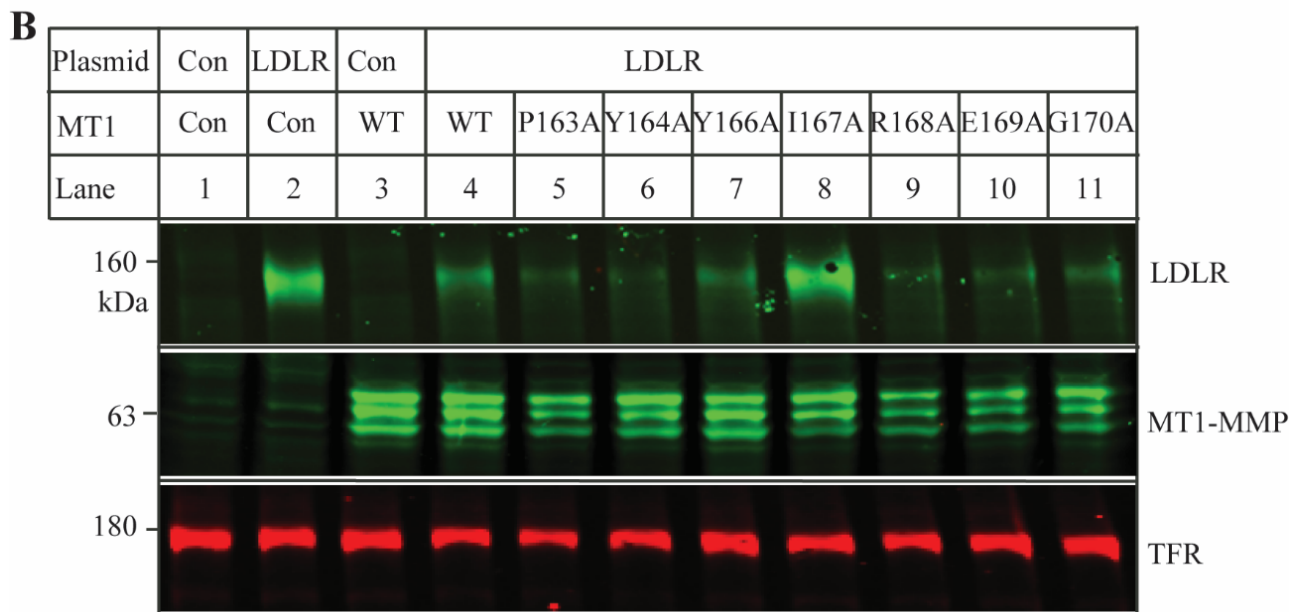


Figure 10. Mutational analysis of the MT-loop. (A) Alignment of partial sequence of different MT-MMPs. The alignment was performed using Multiple Alignment (Fast Fourier Transform (MAFFT))

FFT-NS-I, v7.429). MT1-MMP: NP_004986; MT2-MMP: NP_002419.1; MT3-MMP: NP_005932; MT5-MMP: NP_006681. MT4-MMP: NP_057239. MT6-MMP: NP_071913. The MT-loop was underlined. **(B to C) Immunoblotting and quantification.** Equal amounts of plasmid DNA containing the wild-type LDLR was co-expressed with empty vector (Con), the wild-type, or mutant MT1-MMP in HEK293 cells for 48 h. Equal amounts of total proteins in whole cell lysates was applied to immunoblotting with antibodies as indicated. TFR, transferrin receptor (TFR). Representative images are shown. Densitometry was determined by a Li-Cor Odyssey Infrared Imaging System. Relative densitometry was defined as the ratio of the densitometry of LDLR to that of TFR at the same condition. Values were mean \pm S.D. of ≥ 3 experiments. The significant difference between two groups (wild type or mutant MT1-MMP vs. the Control) was determined via Student's *t*-test. no significance (ns), $p > 0.05$. *, $p < 0.05$. **, $p < 0.01$. ***, $p < 0.001$.

We then performed confocal microscopy to assess whether mutation I167A affected the trafficking of MT1-MMP using an anti-HA antibody that recognizes HA-tagged MT1-MMP. As shown in **Figure 11A**, MT1-MMP was undetectable in cells transfected with an empty vector (Control). Both the wild-type MT1-MMP and MT1-MMP^{I167A} displayed a similar pattern, residing on the cell periphery and the intracellular space (green fluorescence in the top panel). In addition, we observed partial co-localization of the wild-type MT1-MMP and MT1-MMP^{I167A} with Na⁺/K⁺-ATPase (yellow fluorescence in the bottom panel). Next, we employed a trans-well migration assay to assess the impact of mutation I167A on MT1-MMP promoted cell migration. We observed that the relative cell numbers migrated through type 1 collagen coated inserts were comparable in cells transfected with the wild-type MT1-MMP and MT1-MMP^{I167A}. Both significantly promoted cell migration compared to the control (**Figure 11B**). Therefore, replacement of Ile167 with Ala does not affect the trafficking of MT1-MMP to the cell surface or its ability to promote cell migration.

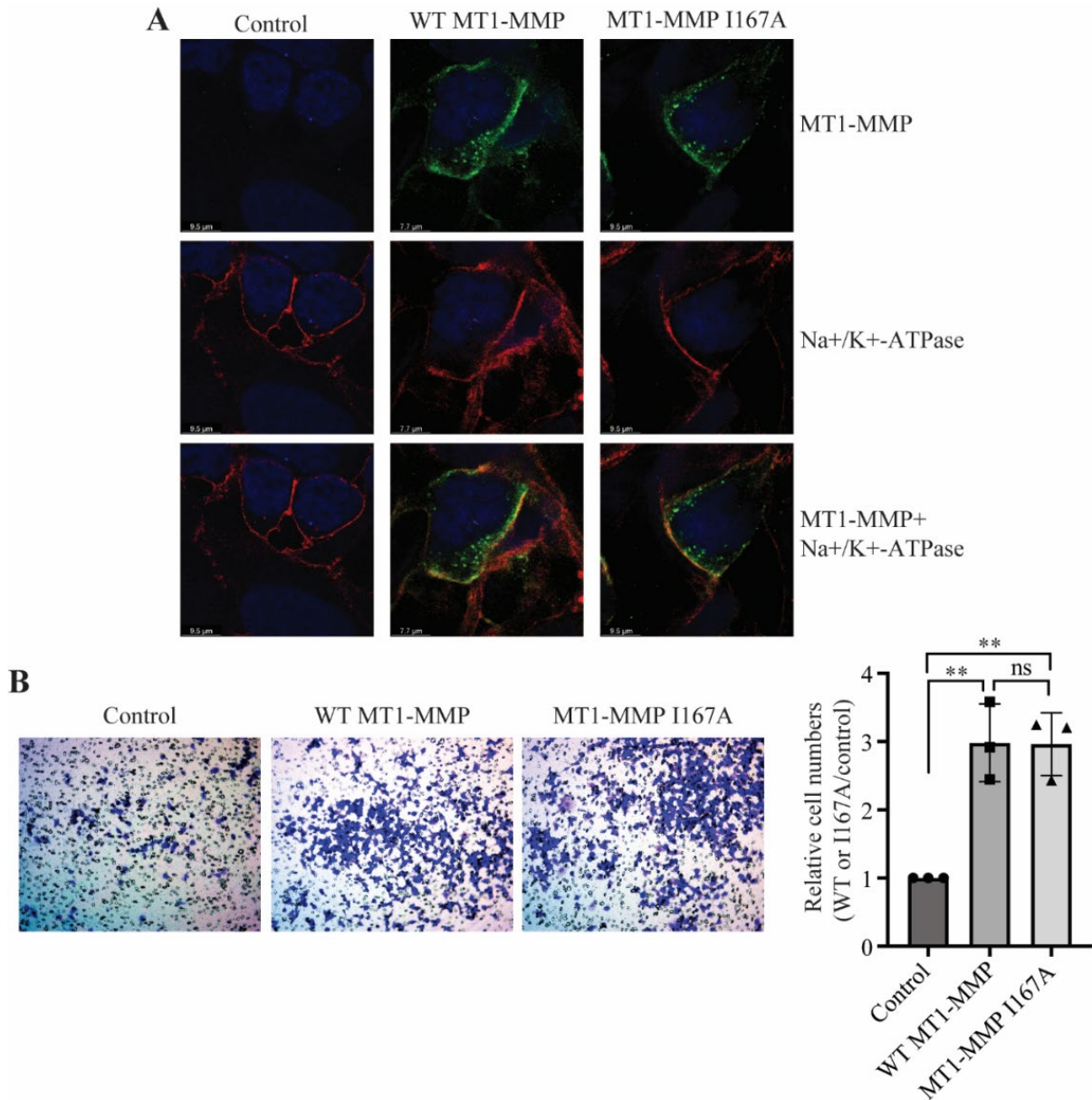


Figure 11. Effects of I167A on MT1-MMP trafficking and cell migration. (A) Confocal microscopy.

HEK293 cells transfected with empty plasmid (Control) or plasmid containing the HA-tagged wild-type or I167A mutant MT1-MMP were subjected to confocal microscopy. MT1-MMP was detected with a rabbit anti-HA antibody (Proteintech) and showed in green fluorescence (top and bottom panels). Na⁺/K⁺-ATPase was detected by a mouse monoclonal antibody and showed in red fluorescence (bottom panel). Nuclei were visualized with DAPI (blue). An x-y optical section of the cells illustrates the

distribution of the wild-type and mutant proteins (magnification: 325X). **(B) Transwell assay.** HEK293 cells transfected with empty plasmid (Control) or plasmid containing the HA-tagged wild-type or I167A mutant MT1-MMP were placed on a type 1 collagen coated insert. After 48 h, cells were stained with crystal violet. After removal of cell on the top of the insert, cells on the bottom of the insert were imaged on an OMAX M837ZL-C140U3 microscope. Cell number was counted, and then divided by image area. Relative cell numbers are the ratio of the cell numbers of cells transfected with the wild-type or I167A MT1-MMP to that of cells transfected with the empty vector (control), which was defined as 1. Representative images are shown.

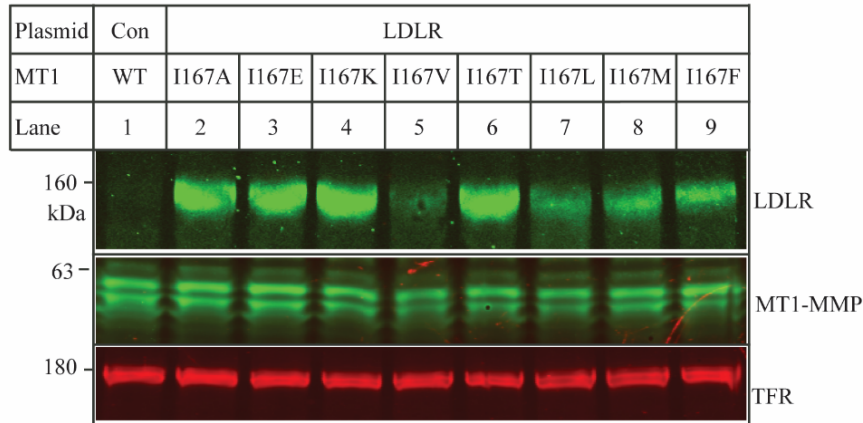
3.2.4 Detailed Mutational Analysis of Ile167

Ile in the MT-loop of MT1-MMP is highly conserved in different species except for alligators and turtles. Instead of Ile, they have another hydrophobic residue, valine (**Figure 12A**). Therefore, we investigated how specific the requirement was for Ile167 to contribute to MT1-MMP's ability to promote LDLR cleavage. To assess whether another non-polar residue at position 167 could substitute for Ile, we replaced Ile167 with a hydrophobic amino acid residue, including Leu, Val, Met, and Phe. We also mutated Ile167 to a polar residue, including Glu, Lys, and Thr, which has a negatively charged, a positively charged, and a polar side chain, respectively. These mutant MT1-MMPs were then co-expressed with LDLR in HEK293 cells. As shown in **Figures 12B and C**, mutations I167E, I167K and I167T, like I167A, significantly impaired MT1-MMP induced LDLR cleavage, whereas substitution of Ile with a hydrophobic residue (mutations I167V, I167L, I167M, and I167F) retained the ability to cleave LDLR. These findings indicate that a hydrophobic residue at position 167 in the MT-loop appears to be required for MT1-MMP promoted LDLR cleavage.

A

Human.	iqnytpkvgeyatyeairkafvrwesatplrfr evpyayireg hekqadi
Chimpanzee.	iqnytpkvgeyatyeairkafvrwesatplrfr evpyayireg hekqadi
Monkey.	iqnytpkvgeyatyeairkafvrwesatplrfr evpyayireg hekqadi
Cow.	iqnytpnvgeyatfeairkafvrwesatplrfr evpyayireg hekqadi
Sheep.	iqnytpkvgeyatfeairkafvrwesatplrfr evpyayireg hekqadi
Goat.	iqnytpkvgeyatfeairkafvrwesatplrfr evpyayireg hekqadv
Deer.	iqnytpkvgeyatfeairkafvrwesatplrfr evpyayireg hekqadi
Fox.	iqnytpkvgeyatfeairkafvrwesatplrfr evpyayireg hekqadi
Dog.	iqnytpkvgeyatfeairkafvrwesatplrfr evpyayireg hekqadi
Seal.	iqnytpkvgeyatfeairkafvrwesatplrfr evpyayireg hekqadi
Cat.	iqnytpkvgehatfeairkafvrwesatplrfr evpyayireg hekqadi
Horse.	iqnytpkvgeyatfeairkafvrwesatplrfr evpyayireg hekqadi
Wild boar.	iqnytpkvgeyatfeairkafvrwesatplrfr evpyayireg hekqadi
Porpoise.	iqnytpkvgeyatfeairkafvrwesatplhfr evpyayireg hekqadi
Whale.	iqnytpkvgeyatfeairkafvrwesatplhfr evpyayireg hekqadi
Elephant.	iqnytpkvgeyatfeairkafvrwesatplhfr evpyayireg hekqadi
Mouse.	iqnytpkvgeyatfeairkafvrwesatplrfr evpyayireg hekqadi
Rat.	iqnytpkvgeyatfeairkafvrwesatplrfr evpyayireg hekqadi
Beaver.	iqnytpkvgeyatfeairkafvrwesatplrfr evpyayireg hekqadi
Chinese hamster	iqnytpkvgeyatfeairkafvrwesatplrfr evpyayireg hekqadi
Squirrel.	iqnytpkvgeyatfeairkafvrwesatplrfr evpyayireg hekqadi
Guinea pig.	iqnytpkvgeyatfeairkafvrwesatplrfr evpyayireg hekqadi
Armadillo.	iqnytpkvgeyatleairkafvrwesatplrfr evpyayireg hekqadi
Rabbit.	iqnytpkvgeyatfeairkafvrwesatplrfr evhyayirdg regkqadi
Puma.	iqnytpkvgehatfeairkafvrwesatplrfr evpyayireg hekqadi
Alligator.	iqnytpkvgehatfeairafvrwqkatplrvfr evpyayvreg repqadi
Turtle.	iqnytpkvgevatfeairafgvwgaatplrfr evpyahvrqgr apqadi
Lizard.	iqnytpkvgehatysairrafsvwqsvtplrfr evpyssireg hepqadi
Frog.	iqnytpkigeystyeairrafkwesvtplrfr evryvdikdgyt khadi
Cyno. Semi.	iqnytpkvgehatyeairkafvrwesaipltfr evipysqirgkvd kyadi
Zebrofish.	iqnytpkvgeyetfeairkafkwesvtplrfr evsysdir kvdfadi
Jan. rice fish.	iqnytpkvgeyetheairrafkiwekvtplrfr evipysyirdk vekfadi

B



C

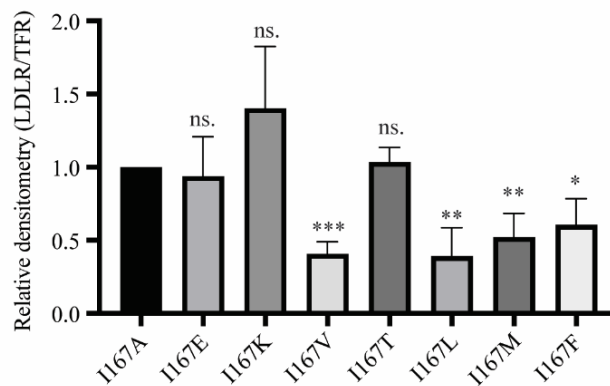


Figure 12. Mutational analysis of I167. (A) Alignment of partial MT1-MMP sequence of different species. The MT-loop of human MT1-MMP was bolded. The alignment was performed using Multiple Alignment using Fast Fourier Transform (MAFFT)FFT-NS-I (v7.429). Human MT1-MMP: NP_004986. Chimpanzee MT1-MMP: XP_001157686. Monkey MT1-MMP: NP_001253793. Cow MT1-MMP: NP_776815. Sheep MT1-MMP: NP_001159653. Goat MT1-MMP: NP_001272694. Deer MT1-MMP: XP_020765064. Fox MT1-MMP: XP_025863277. Dog MT1-MMP: XP_022277499. Seal MT1-MMP: XP_025726135. Cat MT1-MMP: XP_003987503. Horse MT1-MMP: XP_023477731. Wild boar MT1-MMP: NP_999404. Porpoise MT1-MMP: XP_024597443. Whale MT1-MMP: XP_007100541. Elephant MT1-MMP: XP_010598801. Mouse MT1-MMP: NP_032634. Rat MT1-MMP: NP_112318. Beaver MT1-MMP: JAV38019.1. Chinese hamster MT1-MMP: NP_001233698. Squirrel MT1-MMP: XP_026261904. Guinea pig MT1-MMP: XP_003474550. Armadillo MT1-MMP: XP_004474626. Rabbit MT1-MMP: NP_001076262. Puma MT1-MMP: XP_025775067. Alligator MT1-MMP: XP_006037158. Turtle MT1-MMP: XP_005290198. Lizard MT1-MMP: XP_020665388. Frog MT1-MMP: XP_025863277. Cynoglossus semilaevis (Cyno. Semi.) MT1-MMP: XP_008321358. Zebrafish MT1-MMP: NP_919395. Japanese rich fish (Jan. rice fish) MT1-MMP: NP_001098357. **(B to C) Immunoblotting and quantification.** Equal amounts of plasmid DNA containing wild-type LDLR was co-expressed with the wild-type or mutant MT1-MMP in HEK293 cells. 48 h later, whole cell lysate was isolated. Equal amounts of total proteins in whole cell lysate were applied to immunoblotting with antibodies as indicated. TFR, transferrin receptor (TFR). Representative images are shown. Densitometry was determined by a Li-Cor Odyssey Infrared Imaging System. Relative densitometry was defined as the ratio of the densitometry of LDLR to that of TFR at the same condition. Values were mean \pm S.D. of ≥ 3 experiments. The significant difference between two groups (mutations vs. I167A) was determined via Student's *t*-test. no significance (ns), $p > 0.05$. *, $p < 0.05$. **, $p < 0.01$. ***, $p < 0.001$.

3.3 Discussion

Our previous findings suggest that hepatic MT1-MMP is a promising target for raising hepatic LDLR levels and reducing plasma LDL-C levels (Alabi et al., 2021). However, given the presence of 23 MMP family members and the highly conserved catalytic region among these MMPs, a highly specific and selective MT1-MMP inhibitor is needed to avoid potential off-target effects. This requires an in-depth understanding of the specificity of the protease cleavage site. While no consensus cleavage site for MMPs has been identified, it is believed that MMPs preferentially cleave specific substrates at certain sites containing specific amino acid residues (Eckhard et al., 2016). Therefore, we first sought to identify the cleavage site of MT1-MMP on LDLR. We found that removal of each of the functional domains in LDLR or disruption of each of the predicted cleavage sites with site-directed mutagenesis did not abolish MT1-MMP induced cleavage of the receptor. Furthermore, we observed multiple cleaved LDLR bands with different molecular mass in the cell culture medium. These findings suggest that MT1-MMP appears to cleave LDLR at multiple sites and may not strictly require specific amino acid residues at the cleavage sites.

MT1-MMP contains several functional domains. For example, the hemopexin domain contributes to the interaction of MT1-MMP with its substrates, such as CD44 and collagen (Marcink et al., 2019; Tam et al., 2004; Van Doren et al., 2017; Zarrabi et al., 2011). The cytoplasmic tail plays an important role in the endocytosis of MT1-MMP and the localization of MT1-MMP on the specific microdomains in the plasma membrane (Castro-Castro et al., 2016; Feinberg et al., 2018; Houghton, 2015; Xia, Alabi, et al., 2021a). Deletion of the cytoplasmic tail did not affect the trafficking of MT1-MMP to the plasma membrane nor its ability to activate pro-MMP2, but the mutant proteins displayed a different distribution pattern on the cell surface and an impaired ability to mediate cell invasion compared to the wild-type protein (Lehti et al., 2000; Rozanov, Deryugina, et al., 2004). Therefore, we sought to define determinants in MT1-MMP that are critical for its action on LDLR. We found that deletion of hemopexin domain and the C-terminal cytoplasmic tail of MT1-MMP did not significantly impair its

ability to cleave LDLR, indicating a negligible role of these two functional domains in this process. Conversely, deletion of the entire catalytic domain essentially abolished the ability of MT1-MMP to cleave LDLR, which is consistent with our previous finding that the catalytic activity of MT1-MMP is required for LDLR cleavage (Alabi et al., 2021). Interestingly, we found that the MT-loop within the catalytic domain plays an important role in MT1-MMP mediated LDLR cleavage.

Although the X-ray crystallographic structure of the full-length MT1-MMP or its intact extracellular domain is currently unavailable, the crystallographic structure of the catalytic domain of MT1-MMP and the predicted structure of the full-length protein by AlphaFold reveal that the MT-loop sticks out from the main structure and is stabilized via a hydrogen bond between the NH group of Ala165 and the thiol group of Cys127 (Decaneto et al., 2017; Fernandez-Catalan et al., 1998; Grossman et al., 2010; Jumper et al., 2021) (**Figure 13**). Deletion of the entire MT-loop had no significant effect on the expression, trafficking, processing, or the proteolytic activity of MT1-MMP (English et al., 2001; Lang et al., 2004), but significantly reduced the association of MT1-MMP with TIMP-2 and pro-MMP2 activation. It also inhibited MT1-MMP mediated degradation of the ECM and cellular invasion (English et al., 2001; Woskowicz et al., 2013). In addition, it has been reported that the MT-loop together with the hemopexin domain was required for the translocation of MT1-MMP from the apical to the basal membrane in polarized epithelial cells during tubulogenesis (Weaver et al., 2014). The MT-loop is flexible and displays different conformations among different MT-MMPs (Lang et al., 2004). Thus, its specificity and accessibility represent a potential target for the development of selective MT1-MMP inhibitors. Indeed, an antibody specifically against the MT-loop has been developed and can block the binding of pro-MMP2 to MT1-MMP and inhibit pro-MMP2 activation (Shiryaev et al., 2013). In this study, we reported the critical role of the MT-loop in MT1-MMP promoted LDLR cleavage. Furthermore, we found that Ile167 within the MT-loop plays an essential role in the effective cleavage of LDLR induced by MT1-MMP. Detailed analysis revealed the requirement of a hydrophobic side chain at position 167 for MT1-MMP's action on LDLR. Structurally, Ile167 is situated in the middle of a small

α -helix in the MT-loop. The hydrophobic side chain of Ile167 positions inside the loop even though the entire MT-loop sticks out from the main structure (**Figure 13**). How exactly Ile167 contributes to MT1-MMP promoted LDLR cleavage is unclear. We observed that mutation I167A showed a similar distribution pattern as the wild-type protein in confocal microscopy, indicating that the mutant MT1-MMP could be delivered to the plasma membrane. Mutation I167A also had no notable effect on MT1-MMP induced cell migration. These strongly suggest that I167A does not cause a major perturbation of the protein structure. However, we cannot exclude the possibility that I167A may result in a subtle structural change in the MT-loop.

In summary, although we did not find a specific cleavage site of MT1-MMP on LDLR, our study clearly showed that an amino acid residue with a hydrophobic side chain at position 167 of the MT-loop is essential for MT1-MMP induced LDLR cleavage. Removal of the hydrophobic side chain causes a significant reduction in LDLR cleavage but does not notably affect the trafficking of MT1-MMP or MT1-MMP's ability to mediate cell migration. Therefore, our findings may provide fundamental information for the future design of highly sensitive and specific inhibitors for MT1-MMP.

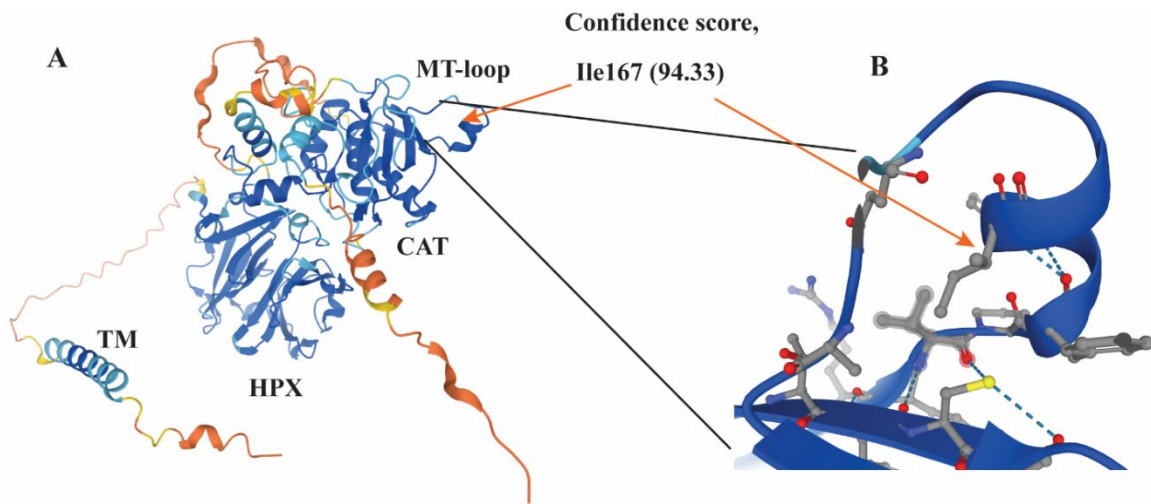


Figure 13. Structure of MT1-MMP (A) and enlarged view of the MT-loop (B). The structure was adopted from AlphaFold (<https://alphafold.ebi.ac.uk/search/text/MT1-MMP>) (Jumper et al., 2021). The model confidence scores of Ile167 are very high (94.33). The side chain of Ile167 is pointed to the inside of the MT-loop.

Chapter 4: Determining Hepatic Membrane Type 1 Matrix Metalloproteinase's Effect on ECM Degradation in Liver Fibrosis

4.1 Introduction

Hepatic LDLR is a major player in the primary pathway for plasma LDL clearance. Decreased levels of functional LDLR increase plasma LDL-C levels, thereby increasing the risk for atherosclerosis. MT1-MMP cleaves hepatic LDLR at multiple sites, generating sLDLR fragments that are positively associated with a decrease in functional LDLR. Conversely, knocking down hepatic MT1-MMP increases hepatic LDLR levels (Alabi et al., 2021). However, MT1-MMP shares a highly conserved catalytic domain with other MMPs, which makes the development of MT1-MMP specific inhibitors difficult (Xia, Alabi, et al., 2021b). We found that the MT-loop within the catalytic domain of MT1-MMP is essential for LDLR cleavage induced by MT1-MMP. Considering the specificity and high accessibility of the MT-loop, our findings reveal that MT1-MMP is a viable target for lipid lowering therapies.

MT1-MMP also plays an important role in ECM degradation under both physiological and pathological conditions, such as liver fibrosis. Liver fibrosis is defined by the upregulation of the pro-inflammatory and pro-fibrotic pathways and the accumulation of fibrillar ECM due to an imbalance between ECM deposition and degradation (Acharya et al., 2021; Gressner et al., 2007). MT1-MMP cleaves multiple ECM substrates including fibronectin, fibrillar type 2 and type 1 collagen found in the fibrotic liver (Benyon & Arthur, 2001; Gifford & Itoh, 2019; Sodek et al., 2007). MT1-MMP cleaves type 1 collagen at Gly775-Ile776 on the $\alpha 1$ chain and Gly775-Leu776 on the $\alpha 2$ chain. MT1-MMP's proteolytic activity on ECM components is important in regulating the balance between ECM deposition and degradation in the normal wound healing response for liver cells. MT1-MMP also regulates levels of active MMP2 by cleaving pro-MMP2. MMP2 is a gelatinase that cleaves type 4 collagen in the basement membrane to promote cell invasion (Benyon & Arthur, 2001; Takawale et al., 2015).

Furthermore, MT1-MMP is found to activate TGF- β , an important pro-fibrotic and pro-inflammatory cytokine in liver fibrosis that upregulates the ECM producing MFB phenotype in liver cells. Latent TGF- β is typically sequestered on the ECM and can be activated via proteolytic action (Dewidar et al., 2019; Nakerakanti & Trojanowska, 2012; Takawale et al., 2015). Integrin $\alpha\beta 8$ was found to interact with LAP on its RGD binding motif and recruit MT1-MMP to activate TGF- β on the cell surface (Mu et al., 2002). Active TGF- β can then proceed to bind to T β R II and activate the downstream SMAD pathway to upregulate TGF- β 's target genes (Dewidar et al., 2019). Additionally, multiple studies have found that MT1-MMP expression was increased in all liver cells during liver injury (Benyon & Arthur, 2001; Knittel et al., 1999). Therefore, impaired hepatic MT1-MMP activity may affect to the development of liver fibrosis.

To establish hepatic MT1-MMP as a viable target for lowering plasma lipids, we must establish its specificity and understand possible off-target effects. For this purpose, we tried to establish a diet induced liver fibrosis mouse model as described (Clapper et al., 2013; Kim et al., 2017; Tetri et al., 2008). Both *Mmp14^{Flox}* and *Mmp14^{LKO}* mice were subjected to a 42 week high cholesterol, high fructose, and high fat GAN diet. The combinations of fructose, cholesterol, and fat in *ad libitum* diets can induce liver steatosis in mice and reflect the human clinical progression for liver fibrosis (Clapper et al., 2013; Hansen et al., 2020; Kim et al., 2017; Tetri et al., 2008). However, we found that the GAN diet did not induce notable liver fibrosis in *Mmp14^{Flox}* and *Mmp14^{LKO}* mice even though the mice appeared to develop steatosis. We also did not observe any significant difference in liver lipid levels and expression of genes involved in lipid metabolism, inflammation, and fibrosis between *Mmp14^{Flox}* and *Mmp14^{LKO}* mice.

4.2 Results

4.2.1 Physical Parameters and Plasma Lipids of *Mmp14^{Flox}* and *Mmp14^{LKO}* Mice

We sought to determine how MT1-MMP affected the development of liver fibrosis under the stress of a high caloric diet. Thus, *Mmp14^{Flox}* (age 15 to 18 weeks, 12 male and 12 female) and *Mmp14^{LKO}* (age 16 to 22 weeks, 10 male and 7 female) mice were fed *ad libitum* on the GAN diet for 42 weeks. 9 mice (1 male *Mmp14^{Flox}*, 3 male *Mmp14^{LKO}*, 2 female *Mmp14^{Flox}*, 3 female *Mmp14^{LKO}*) were euthanized before reaching endpoint due to development of severe dermatitis. 2 male *Mmp14^{Flox}* and 1 female *Mmp14^{LKO}* developed liver tumor or liver carcinoma and were also excluded from the study (**Table 3**).

At baseline, body weight was very similar for *Mmp14^{Flox}* and *Mmp14^{LKO}* mice, where they were respectively, 23.83g ± 3.32 vs 24.28g ± 3.53 (P>0.05). At the endpoint, body weight for *Mmp14^{Flox}* and *Mmp14^{LKO}* mice was 42.43g ± 6.21 and 46.98g ± 8.66 (P>0.05) respectively (**Table 3**). We did not observe a significant difference in body weight and liver weight/body weight ratio for *Mmp14^{Flox}* and *Mmp14^{LKO}* mice. Fasting blood glucose and plasma levels of TC, TG, HDL-C, and non-HDL-C were measured, and we did not observe any significant difference between *Mmp14^{Flox}* and *Mmp14^{LKO}* mice (**Table 4**). Therefore, knock out of hepatic MT1-MMP does not significantly affect blood glucose and plasma lipid levels, body weight, and ratio of liver weight/body weight.

Table 3. Mice physiological parameters at endpoint. Body weight was measured at the beginning and end of the experiment. Liver weight was measured only at the end. Statistical analysis was done on GraphPad Prism version 9.0. The significant difference (Flox vs LKO, Female Flox vs Female LKO, Male Flox vs Male LKO) was determined via Student's *t*-test. not significance (ns), $p > 0.05$.

Parameters	Mean Values \pm Standard Deviation		Significant difference
	Flox	LKO	
Included (mice)			-
Male	9	7	
Female	10	3	
Total	19	10	
Excluded (mice)			-
Male	3	3	
Female	2	4	
Total	5	7	
Body Weight (g)			
Male	46.57 \pm 3.53	48.58 \pm 9.24	ns
Female	38.33 \pm 5.61	43.26 \pm 7.18	ns
Total	42.43 \pm 6.21	46.98 \pm 8.66	ns
Liver Weight/Body Weight Ratio (n=12)			
Total	0.062 \pm 0.012	0.077 \pm 0.11	ns

Table 4. Blood glucose and plasma lipids. Blood glucose was measured on Contour ® Blood Glucose Monitor. Plasma levels of TC, TG, and HDL-C were measured using their specific kits. Non-HDL-C was calculated by subtracting HDL-C from TC. Values were mean ± SD. Statistical analysis was done on GraphPad Prism version 9.0. The significant difference (Flox vs LKO, Female Flox vs Female LKO, Male Flox vs Male LKO) was determined via Student's *t*-test. not significance (ns), $p > 0.05$

Parameters	Mean Values ± Standard Deviation		Significant difference
	Flox	LKO	
Blood Glucose (mmol/L)			
Male	10.79±3.46	10.73±2.79	ns
Female	9.01±0.93	9.67±1.34	ns
Total	9.80±2.49	10.41 ±2.42	ns
Triglyceride (mmol/L)			
Male	2.32±1.48	1.97±0.72	ns
Female	2.18±1.40	1.32±0.72	ns
Total	2.25±1.40	1.77±0.88	ns
Total Cholesterol (mg/dL)			
Male	224.49±50.03	237.97±106.75	ns
Female	117.53±38.86	183.86±69.13	ns
Total	168.25±69.81	221.73±96.65	ns
HDL-C (mg/dL)			
Male	116.80±21.79	125.77±26.01	ns
Female	77.15±23.56	83.39±61.43	ns
Total	95.93±30.04	113.05±41.34	ns
Non-HDL-C (mg/dL)			
Male	107.60±61.58	112.2±98.46	ns
Female	40.38±19.12	100.5±9.62	ns
Total	72.22±55.29	108.67±80.72	ns

4.2.2 Histological Stains of *Mmp14^{Flox}* and *Mmp14^{LKO}* Livers

Next, we assessed the histology of liver samples. Visually compared to the liver of *Mmp14^{Flox}* and *Mmp14^{LKO}* mice on a regular chow diet, livers of *Mmp14^{Flox}* and *Mmp14^{LKO}* mice on the GAN diet were larger and pale in colour (**Figure 14A**).

Livers were then subjected to sectioning for H&E and Picrosirius Red staining. In the liver of *Mmp14^{Flox}* and *Mmp14^{LKO}* mice, H&E staining revealed the presence of many macro and micro-vacuoles. However, we did not observe a notable difference between *Mmp14^{Flox}* and *Mmp14^{LKO}* mice (**Figure 14B**). Picrosirius Red staining was then used to assess liver fibrosis. Fibrogenesis in the liver typically occurs as part of the wound healing response (Acharya et al., 2021; Yanguas et al., 2016). While we did observe some collagen staining around blood vessels, there was no notable fibrosis in the liver of *Mmp14^{Flox}* and *Mmp14^{LKO}* mice (**Figure 14B**). These findings showed that the GAN diet caused liver steatosis but not notable fibrosis in our mouse model. They also suggest that lacking hepatic MT1-MMP does not promote the development of liver fibrosis in mice fed the GAN diet.

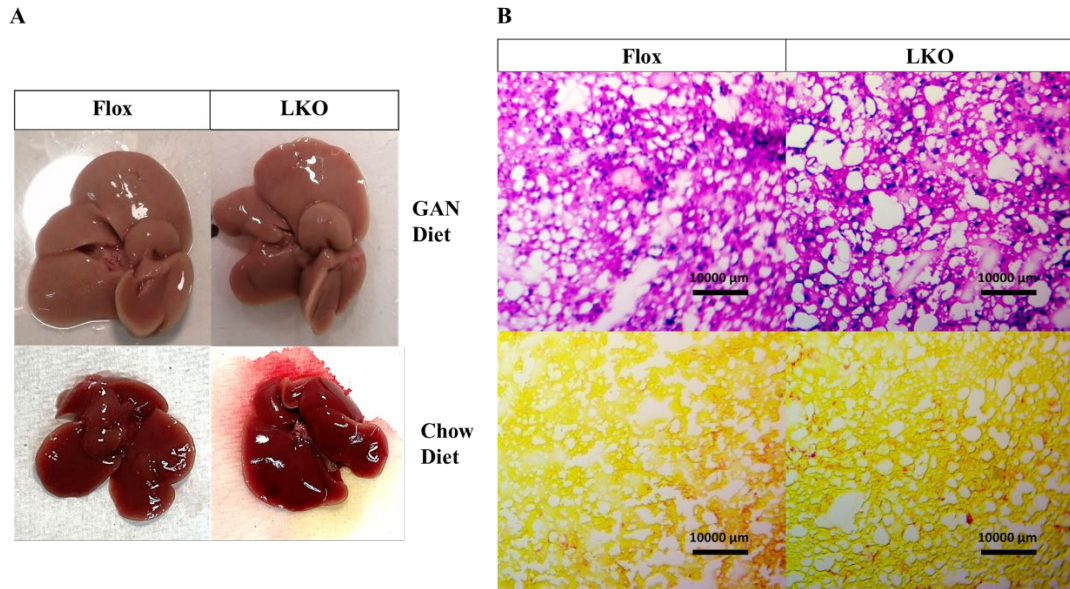


Figure 14. Histology of liver. (A) Mice liver. Pictures of *Mmp14^{Flox}* and *Mmp14^{LKO}* mice liver on chow and GAN diet. **(B) Staining of liver sections.** Liver samples were preserved in Cryomatrix™ and then sectioned for H&E (top) and Picrosirius Red staining (bottom) by the Histology facility at the Alberta Diabetes Institute. Images were taken at 10X magnification on OMAX M837ZL-C140U3 microscope.

4.2.3 Liver TC and TG

We then determined whether deficiency of hepatic MT1-MMP affected hepatic lipid levels. Oil-Red O staining confirmed severe accumulation of neutral lipids in the liver of *Mmp14^{Flox}* and *Mmp14^{LKO}* mice (**Figure 15A**). Total lipids were then extracted from liver samples, and TC and TG were measured by their specific kits. As shown in **Figure 15B**, hepatic TC and TG levels significantly increased in both *Mmp14^{Flox}* and *Mmp14^{LKO}* mice on the GAN diet, similar to that of previous studies (Boland et al., 2019; Hansen et al., 2020). Hepatic TC and TG were comparable in the liver of *Mmp14^{Flox}* and *Mmp14^{LKO}* mice. Therefore, lacking hepatic MT1-MMP does not appear to affect the development of liver steatosis in mice fed the GAN diet.

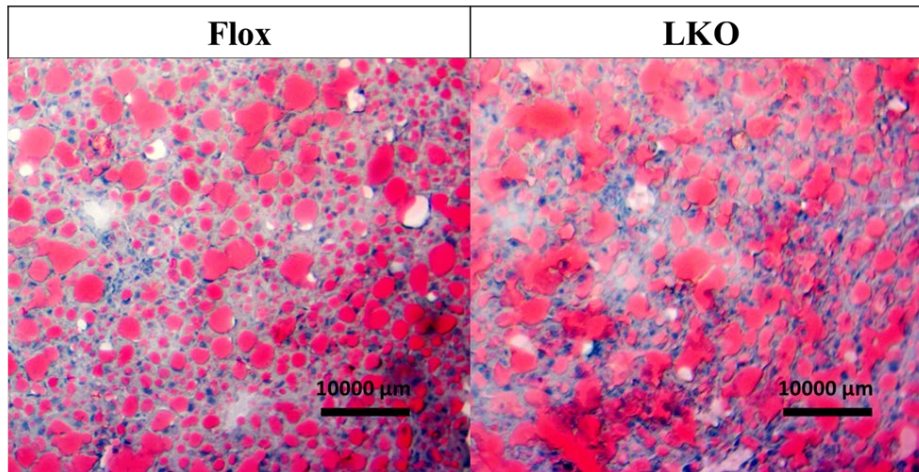
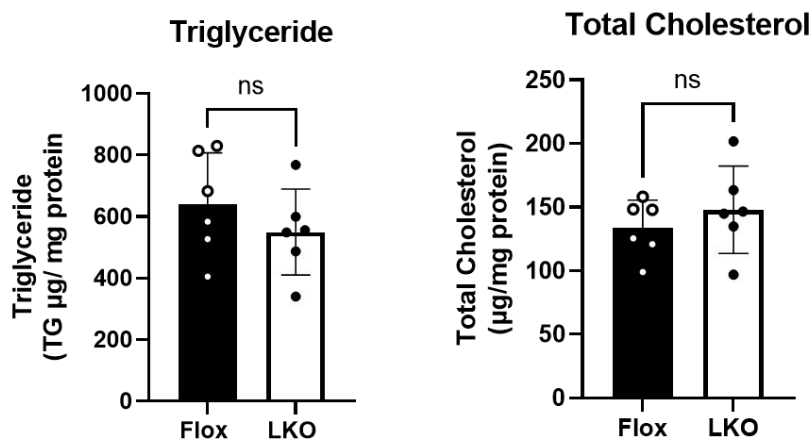
A**B**

Figure 15. Hepatic lipid levels. (A) Oil-Red O staining of liver sections. (B) Hepatic TC and TG levels.

100 mg of liver samples (6 mice per group) for lipid extraction. Liver TC and TG were measured using their kits on a Spectra Max 250 plate reader at wavelength 600 nm and 540 nm respectively. Lipid levels were normalized to protein concentration and presented as μg/mg total proteins. Images were taken at 10X magnification on OMAX M837ZL-C140U3 microscope. The significant difference (Flox vs LKO) was determined via Student's *t*-test. no significance (ns), $p > 0.05$.

4.2.4 Gene Expression

We also determined mRNA levels of genes involved in lipid metabolism, inflammation, and fibrosis via RT-PCR. The mRNA level of *Mmp14* was markedly reduced in the liver of *Mmp14^{LKO}* mice, confirming the successful silencing of hepatic MT1-MMP (**Figure 16A**). SREBP-2 primarily regulates transcription of proteins required for cholesterol pathways, such as LDLR, PCSK9, and HMGCR. (Luo et al., 2020; Xue et al., 2020; Yang et al., 2020). PCSK9 promotes hepatic LDLR degradation and plays a central role in regulating plasma LDL-C levels (Xia, Peng, et al., 2021). SREBP-1c activates transcription of genes required for lipogenesis, such as fatty acid synthase (FASN), a multi-complex enzyme that catalyzes fatty acid synthesis (DeBose-Boyd & Ye, 2018; Fhu & Ali, 2020; Su et al., 2020). Peroxisome proliferator-activated receptor alpha (PPAR- α) can upregulate transcription of genes involved in fatty acid β -oxidation such as carnitine palmitoyltransferase-1a (CPT1a) (Pawlak et al., 2015). CPT1a is the key rate limiting enzyme and the carnitine shuttle that transfers fatty acids into the mitochondria for β -oxidation (Schlaepfer & Joshi, 2020). *Srebp2*, *Srebp1c*, *Pcsk9*, *Fasn*, *Ppara*, and *Cpt1a* encode important factors involved in lipid metabolism. As shown in **Figure 16B**, deficiency of hepatic MT1-MMP did not significantly affect the mRNA levels of these genes. We then looked at changes in the mRNA levels of pro-inflammatory factors such as Tnf- α and interleukin 1-beta (Il-1 β). Tnf- α is an important pro-inflammatory that can activate HSC for increased inflammation in the context of steatosis, NASH, and liver fibrosis (Knittel et al., 1999; Musso et al., 2013). *Tnfa* and *Il1b* encode factors that play important roles in inflammation. TGF- β is the main pro-fibrotic factor for HSC to initiate ECM deposition and *Coll1a1* is the gene expressing type 1 collagen (Karsenty & Park, 1995; Knittel et al., 1999). *Tgfb* and *Coll1a1* were investigated as genes involved in fibrosis. As shown in **Figures 16C and 16D**, there was no significant difference in mRNA levels of these genes tested between *Mmp14^{Flox}* and *Mmp14^{LKO}* mice. Therefore, our findings suggest that knocking out MT1-MMP specifically in the

liver does not affect the expression of genes encoding important factors in lipid metabolism, inflammation, and fibrosis.

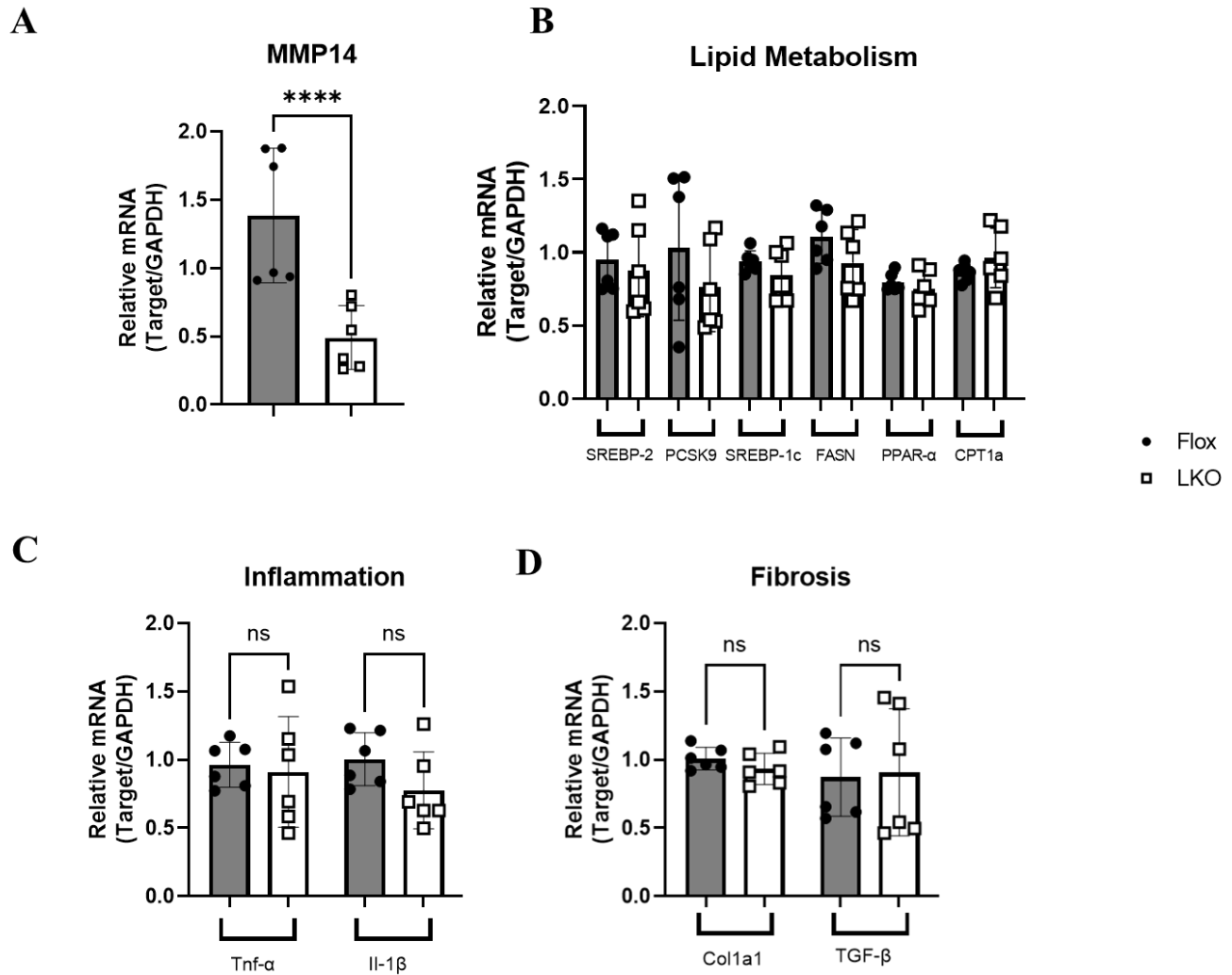


Figure 16. mRNA levels. Total RNA was extracted from mouse livers (n=6) and subjected to RT-PCR using StepOne Plus RT-PCR machine and SYBR Green Master Mix. The mRNA levels of (A) *Mmp14*, (B) genes associated with lipid metabolism, (C) inflammation, and (D) fibrosis were normalized to Gapdh. Statistical analysis was done on GraphPad Prism version 9.0. The significant difference (Flox vs LKO) was determined via Student's *t*-test. no significance (ns), $p > 0.05$. ****, $p < 0.0001$

4.3 Discussion

MT1-MMP cleaves type 1 collagen and plays a critical role in ECM degradation and activation of pro-fibrotic processes during liver fibrosis (Benyon & Arthur, 2001; Mu et al., 2002; Takawale et al., 2015). In this section we sought to determine how liver MT1-MMP influence the development of the liver fibrosis in mice on the GAN diet.

In human pathology, factors like poor diet, smoking, or sedentary lifestyle induce liver steatosis. NAFLD is defined as the excess accumulation of TG in the liver (Engin, 2017; Francque et al., 2021; Friedman et al., 2018). Under normal conditions, acute liver injury recruits and activates pro-inflammatory and fibrotic factors, such as TNF- α and TGF- β as part of the wound healing response. However, chronic injury, such as perpetuating liver steatosis, upregulates inflammation and fibrillar ECM deposition, thus propagating the development of liver fibrosis (Acharya et al., 2021; Buzzetti et al., 2016).

In our study, both *Mmp14^{Flox}* and *Mmp14^{LKO}* mice became equally obese with no significant difference in body weight, liver weight/body weight ratio, blood glucose, plasma levels of TC, TG, HDL-C, and non-HDL-C. Both *Mmp14^{Flox}* and *Mmp14^{LKO}* livers were equally fatty and double in size compared to *Mmp14^{Flox}* and *Mmp14^{LKO}* mice on the chow diet. Analysis of Oil-Red O stains alongside liver TC and TG levels indicated that both *Mmp14^{Flox}* and *Mmp14^{LKO}* mice showed comparable levels of liver steatosis (Friedman et al., 2018). Picosirius Red staining revealed negligible levels and no significant difference in expression of collagen for both *Mmp14^{Flox}* and *Mmp14^{LKO}* mice. Lacking hepatic MT1-MMP also did not significantly affect the expression of gene encoding factors involved in lipid metabolism, inflammation, and fibrosis. Therefore, our findings suggest that hepatic MT1-MMP does not affect the development of liver steatosis nor accelerates fibrosis in mice. However, more experiments are needed to ascertain these possibilities.

In this study, all mice were on an *ad libitum* diet in the same housing conditions and care. Both *Mmp14^{Flox}* and *Mmp14^{LKO}* mice developed atopic dermatitis, a chronic inflammatory skin disease typical in mice from inbreeding and/or high-fat diets (Kim et al., 2019). We observed dermatitis in 3 *Mmp14^{Flox}* mice (1 male and 2 females) and 6 *Mmp14^{LKO}* mice (3 males and 3 females). We also observed severe liver carcinoma in 2 male *Mmp14^{Flox}*, but not in *Mmp14^{LKO}* mice. However, 1 female *Mmp14^{LKO}* mice did develop liver tumor. We cannot draw a conclusion on these observations due to the small sample size. However, it would be of interest to further study the impact of the deficiency of hepatic MT1-MMP on the development of dermatitis and liver cancer.

Clapper et al reported that C57BL/6 mice on the 30-week amylin liver NASH diet showed a significant difference in levels of fibrosis compared to a low-fat diet group (10% kcal with no cholesterol or fructose). However, levels of fibrosis were low and could not be established as fibrotic liver (Clapper et al., 2013). In our study, both *Mmp14^{Flox}* and *Mmp14^{LKO}* mice did not exhibit notable liver fibrosis after a 42 week GAN diet feeding. All mice by the end of the study were around 12 to 13 months old and displayed signs of severe obesity where it significantly decreased their quality of life. We also observed a negligible difference in mRNA levels for factors of inflammation, lipid metabolism, and fibrosis between *Mmp14^{Flox}* and *Mmp14^{LKO}* groups. Therefore, even though our findings cannot elucidate the exact role of hepatic MT1-MMP in the development of liver fibrosis, it suggests that inhibition of hepatic MT1-MMP does not progress liver steatosis nor stimulate the development of liver fibrosis for mice fed on the GAN diet. This implicates the therapeutic potential of hepatic MT1-MMP inhibition as a lipid lowering strategy. However, further studies using other liver fibrosis mouse models such as chemical toxin induction by carbon tetrachloride (CCl₄) or thioacetamide (TAA) are needed. CCl₄ and TAA work by rapidly inducing similar patterns of significant liver fibrosis (Dong et al., 2016; Kim et al., 2017; Tetri et al., 2008).

Chapter 5 Discussion, Conclusion, and Future Directions

Hepatic LDLR is a major player in regulating lipid metabolism, where dysfunction in LDLR results in pathologies denoted by increased plasma LDL-C (Defesche et al., 2017; Xia, Alabi, et al., 2021a; Youngblom et al., 1993). Statins and PCSK9 inhibitors function by increasing the levels of LDLR to increase plasma LDL-C clearance. However, the caveat is that statins are less than 50% efficient, can induce adverse side effects as well as cause statin intolerance (Ahmad, 2014; Fitchett et al., 2015; Xia, Alabi, et al., 2021a). Meanwhile, PCSK9 inhibitors are expensive and thus inaccessible for many patients (Fitchett et al., 2015; Kolber et al., 2018; Sabatine, 2019). Therefore, the search for alternative therapies is crucial.

In our previous *in vitro* and *in vivo* studies, we found that knocking down hepatic MT1-MMP increased LDLR levels, thus decreasing the risk for atherosclerosis (Alabi et al., 2021). MT1-MMP therefore presents as a potential target for lowering lipids. However, MT1-MMP's catalytic domain is highly conserved in other MMPs, as exhibited by past failed clinical drug trials for cancer, due to non-specific inhibition (Fields, 2019; Page-McCaw et al., 2007; Vandenbroucke & Libert, 2014). Therefore, in this project, we first investigated the determinants of LDLR that allowed for MT1-MMP mediated LDLR cleavage and found that LDLR has no specific cleavage residue or domain. Furthermore, MT1-MMP appears to cleave LDLR at multiple sites. On the other hand, the MT-loop within the catalytic domain of MT1-MMP is required for its action on LDLR. We further demonstrated the importance of Ile167 within the MT-loop in MT1-MMP induced LDLR cleavage.

The MT-loop is a unique structure only found in MT-MMPs and displays different conformations among different MT-MMPs, indicating MT-loop's specificity (English et al., 2001; Lang et al., 2004; Xia, Alabi, et al., 2021a). It has been reported that deleting the MT-loop did not inactivate MT-MMP's catalytic activity, but instead decreased their targeting for specific substrates. For example, studies in

cancer metastases found that while MT-loop deletion did not affect protease expression, processing, or catalytic function, the association between MT1-MMP and TIMP-2 for MMP2 activation decreased (English et al., 2001; Woskowicz et al., 2013). Structurally, the MT-loop protrudes from the molecular surface, indicating its accessibility. Therefore, the MT-loop represents a potential target for the development of selective MT1-MMP inhibitors. Currently, there is an antibody that has been developed to work specifically against the MT-loop. It has been found to block pro-MMP2 binding to MT1-MMP and thereby inhibit pro-MMP2 activation (Shiryaev et al., 2013). It would be interesting to observe whether this antibody can block MT1-MMP mediated cleavage of LDLR.

In this project, we analyzed protein levels in whole cell lysate which contained the membrane-bound MT1-MMP and membrane-bound segment of cleaved LDLR. To ascertain an accurate representation of soluble products from MT1-MMP actions, the cell culture medium should be investigated. MMP2 is a soluble protein that is activated by MT1-MMP cleavage of its pro-MMP2 form (Takawale et al., 2015). Thus, for future studies, we plan to use the cell culture medium from transfections of WT-MT1-MMP and MT1-MMP^{H167A} with WT-LDLR to assess soluble LDLR fragments and activation of pro-MMP2. Protocols we can consider are gel zymography to visualize active MMP2 activity (Snoek-van Beurden & Von den Hoff, 2005; Wilkesman & Kurz, 2017).

Another possible study to assess how mutations in the MT-loop affect the ability of MT1-MMP to mediate cell invasion is through 3D collagen matrix. The 3D collagen matrix is a good representation of how mutant MT1-MMP affects *in vivo* cell invasion (Ebine et al., 2019; Sakai et al., 2011). For example, we can observe the effects of the wild-type and mutant MT1-MMP in proteolytic tracks of invading cells (Ebine et al., 2019; Weaver et al., 2014).

To assess hepatic MT1-MMP's potential as a target for specific lipid lowering inhibitors, we then focused on possible off-target effects when specifically inhibiting hepatic MT1-MMP. MT1-MMP cleaves type 1 collagen, a fibrillar ECM component in the pathology of liver fibrosis (Acharya et al.,

2021; Benyon & Arthur, 2001). MT1-MMP has also been implicated in the activation of TGF- β , a critical pro-fibrotic cytokine, in promoting the development of pro-fibrotic myofibroblasts (Mu et al., 2002). Furthermore, MT1-MMP expression is increased in all liver cells during the wound healing response (Benyon & Arthur, 2001; Knittel et al., 1999). Therefore, hepatic MT1-MMP may play a role in ECM degradation during pathological liver fibrosis, which is defined by a significant increase in deposition of fibrillar ECM in end stage liver disease (Acharya et al., 2021; Dewidar et al., 2019; Friedman et al., 2018).

In the second part of this project, we observed severe obesity in the mice after feeding them the GAN diet for 42 weeks. However, we found that there was no significant difference in blood glucose and levels of plasma TC, TG, HDL-C, and Non-HDL-C, as well as hepatic TC and TG between *Mmp14^{Flox}* and *Mmp14^{LKO}* mice. Body weight, liver weight/body weight ratio, histology of the liver, and expression of genes encoding factors of lipid metabolism, inflammation, and fibrosis were also comparable in the two genotypes. These findings suggest that hepatic MT1-MMP deficiency does not promote liver steatosis. As we did not observe notable liver fibrosis in both *Mmp14^{Flox}* and *Mmp14^{LKO}* mice, our data also suggests that lacking hepatic MT1-MMP does not promote the development of liver fibrosis in mice fed the GAN diet. However, to further establish MT1-MMP's potential, *Mmp14^{LKO}* will have to be tested on other mouse models.

One future study is to induce liver fibrosis using CCl₄ and TAA. CCl₄ is a haloalkane that produces a trichloromethyl radical under oxidative stress which causes lipid peroxidation, resulting in liver cell apoptosis, necrosis, and fibrosis. Similarly, TAA is also activated via oxidation and reacts with amines on proteins and lipids to promote liver damage and fibrosis (Kim et al., 2017; Tetri et al., 2008). While chemical induction of liver fibrosis does not reflect the natural clinical progression seen in humans, it is worth investigating CCl₄ and TAA models to observe the extent of influence hepatic MT1-MMP may have on the development of liver fibrosis. Another diet-induced model we can test is through using

phosphatidylethanolamine N-methyltransferase (PEMT) knockout or knockdown mice. Hepatic PEMT catalyses the conversion of phosphatidylethanolamine (PE) to phosphatidylcholine (PC) as the only source of *de novo* choline (Zia et al., 2018). PC is critical for lipoprotein assembly and secretion, where deficiency in PC can decrease circulating lipoproteins. It has been shown that PEMT knockout protects against obesity and diet-induced atherosclerosis in LDLR^{-/-} mice (Vance, 2013). However, the trade-off for this protection is liver steatosis as low PC:PE contributes to compromised hepatocyte membranes (Vance, 2013). PEMT knockout or knockdown mice on a high-fat diet develop notable steatosis and fibrosis (Vance, 2013; Zia et al., 2018). Therefore, we can knock down PEMT in *Mmp14*^{LKO} and *Mmp14*^{Flox} mice and subject them to a high-fat diet to further elucidate MT1-MMP's role in lipid metabolism and ECM regulation in liver fibrosis.

Atherosclerosis is the main risk factor for CVD and is driven by high levels of plasma cholesterol, such as LDL-C (Lu & Daugherty, 2015; Xia, Alabi, et al., 2021b). MT1-MMP cleaves LDLR and increase plasma LDL-C, resulting in an increased risk of atherosclerosis (Alabi et al., 2021). Therefore, hepatic MT1-MMP is a viable target to lower plasma lipids. In summary, we discovered that deleting the MT-loop impairs MT1-MMP mediated LDLR cleavage without abolishing MT1-MMP's catalytic function. Furthermore, the hydrophobicity of Ile167 is critical for MT-loop function (**Figure 17**). From our animal study component, specifically knocking out hepatic MT1-MMP and subjecting the mice to the GAN diet did not induce liver fibrosis or worsen liver steatosis (**Figure 17**). Thus, our findings supply fundamental knowledge for future research on hepatic MT1-MMP as a viable candidate in developing specific and sensitive inhibitors for patients intolerant to current lipid-lowering strategies.

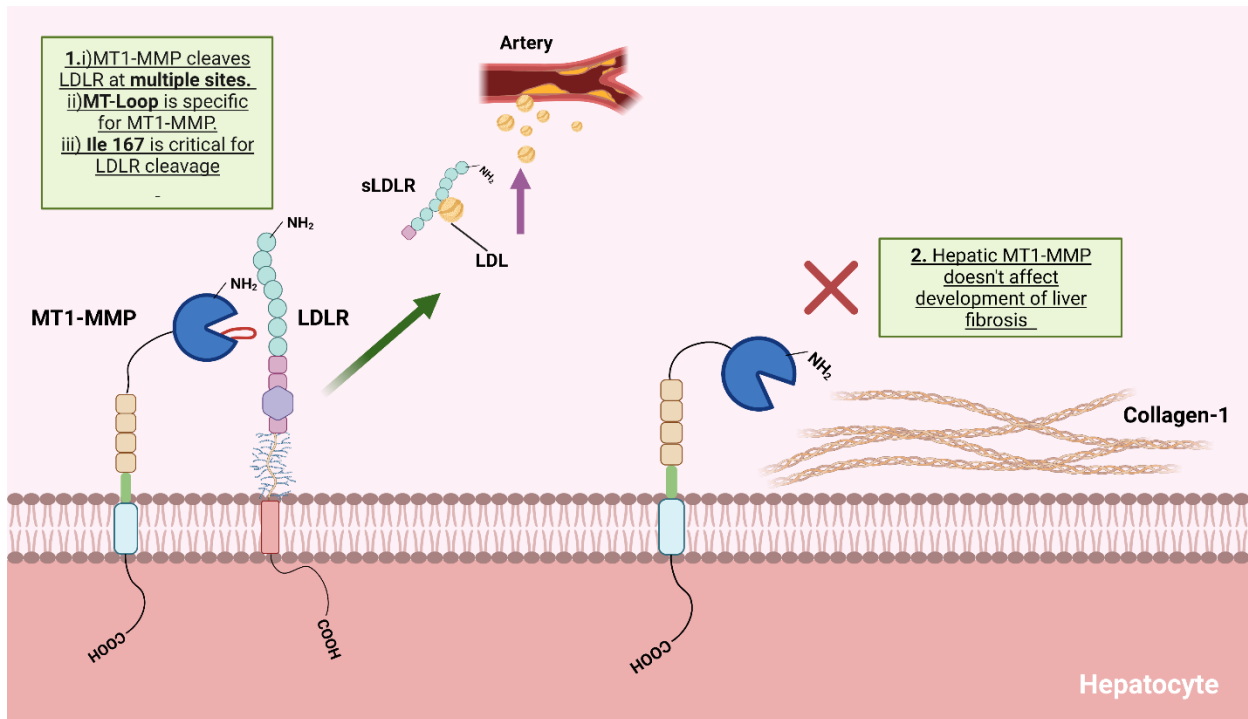


Figure 17. Project findings. Part 1: MT1-MMP cleaves LDLR at multiple sites and generates sLDLR. Plasma sLDLR levels are positively correlated with the increased risk towards atherosclerosis. The MT-loop structure is specific for LDLR cleavage and deletion of the MT-loop impairs LDLR cleavage but retains MT1-MMP's catalytic activity. The hydrophobicity of isoleucine at position 167 in the MT-Loop is important for LDLR cleavage. **Part 2:** Hepatic MT1-MMP does not affect the development of liver steatosis and liver fibrosis. (Figure made by Maggie Wang on BioRender)

References

- Acharya, P., Chouhan, K., Weiskirchen, S., & Weiskirchen, R. (2021). Cellular Mechanisms of Liver Fibrosis. *Front Pharmacol*, *12*, 671640. <https://doi.org/10.3389/fphar.2021.671640>
- Ahmad, Z. (2014). Statin intolerance. *Am J Cardiol*, *113*(10), 1765-1771. <https://doi.org/10.1016/j.amjcard.2014.02.033>
- Alabi, A., Xia, X. D., Gu, H. M., Wang, F., Deng, S. J., Yang, N., Adijiang, A., Douglas, D. N., Kneteman, N. M., Xue, Y., Chen, L., Qin, S., Wang, G., & Zhang, D. W. (2021). Membrane type 1 matrix metalloproteinase promotes LDL receptor shedding and accelerates the development of atherosclerosis. *Nat Commun*, *12*(1), 1889. <https://doi.org/10.1038/s41467-021-22167-3>
- Amar, S., Smith, L., & Fields, G. B. (2017a). Matrix metalloproteinase collagenolysis in health and disease. *Biochim Biophys Acta*. <https://doi.org/10.1016/j.bbamcr.2017.04.015>
- Amar, S., Smith, L., & Fields, G. B. (2017b). Matrix metalloproteinase collagenolysis in health and disease. *Biochim Biophys Acta Mol Cell Res*, *1864*(11 Pt A), 1940-1951. <https://doi.org/10.1016/j.bbamcr.2017.04.015>
- Amar, S., Smith, L., & Fields, G. B. (2017c). Matrix metalloproteinase collagenolysis in health and disease. *Biochim Biophys Acta*, *1864*(11 Pt A), 1940-1951. <https://doi.org/10.1016/j.bbamcr.2017.04.015>
- Beglova, N., & Blacklow, S. C. (2005). The LDL receptor: how acid pulls the trigger. *Trends Biochem Sci*, *30*(6), 309-317. <https://doi.org/10.1016/j.tibs.2005.03.007>
- Beglova, N., Jeon, H., Fisher, C., & Blacklow, S. C. (2004). Cooperation between fixed and low pH-inducible interfaces controls lipoprotein release by the LDL receptor. *Mol Cell*, *16*(2), 281-292. <https://doi.org/S1097276504005519> [pii]
- 10.1016/j.molcel.2004.09.038
- Bentzon, J. F., Otsuka, F., Virmani, R., & Falk, E. (2014). Mechanisms of plaque formation and rupture. *Circ Res*, *114*(12), 1852-1866. <https://doi.org/10.1161/CIRCRESAHA.114.302721>
- Benyon, R. C., & Arthur, M. J. (2001). Extracellular matrix degradation and the role of hepatic stellate cells. *Semin Liver Dis*, *21*(3), 373-384. <https://doi.org/10.1055/s-2001-17552>
- Boland, M. L., Oro, D., Tolbol, K. S., Thrane, S. T., Nielsen, J. C., Cohen, T. S., Tabor, D. E., Fernandes, F., Tovchigrechko, A., Veidal, S. S., Warren, P., Sellman, B. R., Jelsing, J., Feigh, M., Vrang, N., Trevaskis, J. L., & Hansen, H. H. (2019). Towards a standard diet-induced and biopsy-confirmed mouse model of non-alcoholic steatohepatitis: Impact of dietary fat source. *World J Gastroenterol*, *25*(33), 4904-4920. <https://doi.org/10.3748/wjg.v25.i33.4904>
- Brown, M. S., & Goldstein, J. L. (1997). The SREBP pathway: regulation of cholesterol metabolism by proteolysis of a membrane-bound transcription factor. *Cell*, *89*(3), 331-340. [https://doi.org/10.1016/s0092-8674\(00\)80213-5](https://doi.org/10.1016/s0092-8674(00)80213-5)
- Buzzetti, E., Pinzani, M., & Tsochatzis, E. A. (2016). The multiple-hit pathogenesis of non-alcoholic fatty liver disease (NAFLD). *Metabolism*, *65*(8), 1038-1048. <https://doi.org/10.1016/j.metabol.2015.12.012>
- Calabro, S. R., Maczurek, A. E., Morgan, A. J., Tu, T., Wen, V. W., Yee, C., Mridha, A., Lee, M., d'Avigdor, W., Locarnini, S. A., McCaughan, G. W., Warner, F. J., McLennan, S. V., & Shackel, N. A. (2014). Hepatocyte produced matrix metalloproteinases are regulated by CD147 in liver fibrogenesis. *PLoS One*, *9*(7), e90571. <https://doi.org/10.1371/journal.pone.0090571>

- Cao, J., Drews, M., Lee, H. M., Conner, C., Bahou, W. F., & Zucker, S. (1998). The propeptide domain of membrane type 1 matrix metalloproteinase is required for binding of tissue inhibitor of metalloproteinases and for activation of pro-gelatinase A. *J Biol Chem*, 273(52), 34745-34752. <https://www.ncbi.nlm.nih.gov/pubmed/9856998>
- Castro-Castro, A., Marchesin, V., Monteiro, P., Lodillinsky, C., Rosse, C., & Chavrier, P. (2016). Cellular and Molecular Mechanisms of MT1-MMP-Dependent Cancer Cell Invasion. *Annu Rev Cell Dev Biol*, 32, 555-576. <https://doi.org/10.1146/annurev-cellbio-111315-125227>
- Chiang, D. J., Pritchard, M. T., & Nagy, L. E. (2011). Obesity, diabetes mellitus, and liver fibrosis. *Am J Physiol Gastrointest Liver Physiol*, 300(5), G697-702. <https://doi.org/10.1152/ajpgi.00426.2010>
- Clapper, J. R., Hendricks, M. D., Gu, G., Wittmer, C., Dolman, C. S., Herich, J., Athanacio, J., Villescaz, C., Ghosh, S. S., Heilig, J. S., Lowe, C., & Roth, J. D. (2013). Diet-induced mouse model of fatty liver disease and nonalcoholic steatohepatitis reflecting clinical disease progression and methods of assessment. *Am J Physiol Gastrointest Liver Physiol*, 305(7), G483-495. <https://doi.org/10.1152/ajpgi.00079.2013>
- Davis, C. G., Goldstein, J. L., Sudhof, T. C., Anderson, R. G., Russell, D. W., & Brown, M. S. (1987). Acid-dependent ligand dissociation and recycling of LDL receptor mediated by growth factor homology region. *Nature*, 326(6115), 760-765. <https://doi.org/10.1038/326760a0>
- Davis, C. G., Lehrman, M. A., Russell, D. W., Anderson, R. G., Brown, M. S., & Goldstein, J. L. (1986). The J.D. mutation in familial hypercholesterolemia: amino acid substitution in cytoplasmic domain impedes internalization of LDL receptors. *Cell*, 45(1), 15-24. [https://doi.org/0092-8674\(86\)90533-7](https://doi.org/0092-8674(86)90533-7)
- Davis, C. G., van Driel, I. R., Russell, D. W., Brown, M. S., & Goldstein, J. L. (1987). The low density lipoprotein receptor. Identification of amino acids in cytoplasmic domain required for rapid endocytosis. *J Biol Chem*, 262(9), 4075-4082. http://www.ncbi.nlm.nih.gov/entrez/query.fcgi?cmd=Retrieve&db=PubMed&dopt=Citation&list_uids=3104336
- DeBose-Boyd, R. A., & Ye, J. (2018). SREBPs in Lipid Metabolism, Insulin Signaling, and Beyond. *Trends Biochem Sci*, 43(5), 358-368. <https://doi.org/10.1016/j.tibs.2018.01.005>
- Decaneto, E., Vasilevskaya, T., Kutin, Y., Ogata, H., Grossman, M., Sagi, I., Havenith, M., Lubitz, W., Thiel, W., & Cox, N. (2017). Solvent water interactions within the active site of the membrane type I matrix metalloproteinase. *Phys Chem Chem Phys*, 19(45), 30316-30331. <https://doi.org/10.1039/c7cp05572b>
- Defesche, J. C., Gidding, S. S., Harada-Shiba, M., Hegele, R. A., Santos, R. D., & Wierzbicki, A. S. (2017). Familial hypercholesterolaemia. *Nat Rev Dis Primers*, 3, 17093. <https://doi.org/10.1038/nrdp.2017.93>
- Dewidar, B., Meyer, C., Dooley, S., & Meindl-Beinker, A. N. (2019). TGF-beta in Hepatic Stellate Cell Activation and Liver Fibrogenesis-Updated 2019. *Cells*, 8(11). <https://doi.org/10.3390/cells8111419>
- Dong, S., Chen, Q. L., Song, Y. N., Sun, Y., Wei, B., Li, X. Y., Hu, Y. Y., Liu, P., & Su, S. B. (2016). Mechanisms of CCl4-induced liver fibrosis with combined transcriptomic and proteomic analysis. *J Toxicol Sci*, 41(4), 561-572. <https://doi.org/10.2131/jts.41.561>
- Dufour, A., Sampson, N. S., Zucker, S., & Cao, J. (2008). Role of the hemopexin domain of matrix metalloproteinases in cell migration. *J Cell Physiol*, 217(3), 643-651. <https://doi.org/10.1002/jcp.21535>
- Ebine, K., Chow, C. R., & Munshi, H. G. (2019). Quantitative Method to Track Proteolytic Invasion in 3D Collagen. *Methods Mol Biol*, 1882, 161-169. https://doi.org/10.1007/978-1-4939-8879-2_15
- Eckhard, U., Huesgen, P. F., Schilling, O., Bellac, C. L., Butler, G. S., Cox, J. H., Dufour, A., Goebeler, V., Kappelhoff, R., Keller, U. A. D., Klein, T., Lange, P. F., Marino, G., Morrison, C.

- J., Prudova, A., Rodriguez, D., Starr, A. E., Wang, Y., & Overall, C. M. (2016). Active site specificity profiling of the matrix metalloproteinase family: Proteomic identification of 4300 cleavage sites by nine MMPs explored with structural and synthetic peptide cleavage analyses. *Matrix Biol*, 49, 37-60. <https://doi.org/10.1016/j.matbio.2015.09.003>
- Engin, A. (2017). Non-Alcoholic Fatty Liver Disease. *Adv Exp Med Biol*, 960, 443-467. https://doi.org/10.1007/978-3-319-48382-5_19
- English, W. R., Holtz, B., Vogt, G., Knauper, V., & Murphy, G. (2001). Characterization of the role of the "MT-loop": an eight-amino acid insertion specific to progelatinase A (MMP2) activating membrane-type matrix metalloproteinases. *J Biol Chem*, 276(45), 42018-42026. <https://doi.org/10.1074/jbc.M107783200>
- Fabregat, I., & Caballero-Diaz, D. (2018). Transforming Growth Factor-beta-Induced Cell Plasticity in Liver Fibrosis and Hepatocarcinogenesis. *Front Oncol*, 8, 357. <https://doi.org/10.3389/fonc.2018.00357>
- Feinberg, T. Y., Zheng, H., Liu, R., Wicha, M. S., Yu, S. M., & Weiss, S. J. (2018). Divergent Matrix-Remodeling Strategies Distinguish Developmental from Neoplastic Mammary Epithelial Cell Invasion Programs. *Dev Cell*, 47(2), 145-160 e146. <https://doi.org/10.1016/j.devcel.2018.08.025>
- Fernandez-Catalan, C., Bode, W., Huber, R., Turk, D., Calvete, J. J., Lichte, A., Tschesche, H., & Maskos, K. (1998). Crystal structure of the complex formed by the membrane type 1-matrix metalloproteinase with the tissue inhibitor of metalloproteinases-2, the soluble progelatinase A receptor. *EMBO J*, 17(17), 5238-5248. <https://doi.org/10.1093/emboj/17.17.5238>
- Ferre, P., Phan, F., & Foufelle, F. (2021). SREBP-1c and lipogenesis in the liver: an update1. *Biochem J*, 478(20), 3723-3739. <https://doi.org/10.1042/BCJ20210071>
- Fhu, C. W., & Ali, A. (2020). Fatty Acid Synthase: An Emerging Target in Cancer. *Molecules*, 25(17). <https://doi.org/10.3390/molecules25173935>
- Fields, G. B. (2019). The Rebirth of Matrix Metalloproteinase Inhibitors: Moving Beyond the Dogma. *Cells*, 8(9). <https://doi.org/10.3390/cells8090984>
- Fitchett, D. H., Hegele, R. A., & Verma, S. (2015). Cardiology patient page. Statin intolerance. *Circulation*, 131(13), e389-391. <https://doi.org/10.1161/CIRCULATIONAHA.114.013189>
- Franque, S., Szabo, G., Abdelmalek, M. F., Byrne, C. D., Cusi, K., Dufour, J. F., Roden, M., Sacks, F., & Tacke, F. (2021). Nonalcoholic steatohepatitis: the role of peroxisome proliferator-activated receptors. *Nat Rev Gastroenterol Hepatol*, 18(1), 24-39. <https://doi.org/10.1038/s41575-020-00366-5>
- Friedman, S. L., Neuschwander-Tetri, B. A., Rinella, M., & Sanyal, A. J. (2018). Mechanisms of NAFLD development and therapeutic strategies. *Nat Med*, 24(7), 908-922. <https://doi.org/10.1038/s41591-018-0104-9>
- Gao, X., Gu, H., Li, G., Rye, K. A., & Zhang, D. W. (2012). Identification of an amino acid residue in ATP-binding cassette transport G1 critical for mediating cholesterol efflux. *Biochim Biophys Acta*, 1821(3), 552-559. <https://doi.org/10.1016/j.bbaliip.2011.07.012>
- Ghosh, S. S., Wang, J., & Ghosh, S. (2022). Measurement of In Vivo VLDL and Chylomicron Secretion. *Methods Mol Biol*, 2455, 63-71. https://doi.org/10.1007/978-1-0716-2128-8_6
- Gifford, V., & Itoh, Y. (2019). MT1-MMP-dependent cell migration: proteolytic and non-proteolytic mechanisms. *Biochem Soc Trans*, 47(3), 811-826. <https://doi.org/10.1042/BST20180363>
- Go, G. W., & Mani, A. (2012). Low-density lipoprotein receptor (LDLR) family orchestrates cholesterol homeostasis. *Yale J Biol Med*, 85(1), 19-28. <https://www.ncbi.nlm.nih.gov/pubmed/22461740>
- Goldstein, J. L., & Brown, M. S. (2009). The LDL receptor. *Arterioscler Thromb Vasc Biol*, 29(4), 431-438. <https://doi.org/10.1161/ATVBAHA.108.179564>

- Goldstein, J. L., & Brown, M. S. (2015). A century of cholesterol and coronaries: from plaques to genes to statins. *Cell*, 161(1), 161-172. <https://doi.org/10.1016/j.cell.2015.01.036>
- Gressner, O. A., Weiskirchen, R., & Gressner, A. M. (2007). Biomarkers of hepatic fibrosis, fibrogenesis and genetic pre-disposition pending between fiction and reality. *J Cell Mol Med*, 11(5), 1031-1051. <https://doi.org/10.1111/j.1582-4934.2007.00092.x>
- Gross, J., & Lapiere, C. M. (1962). Collagenolytic activity in amphibian tissues: a tissue culture assay. *Proc Natl Acad Sci U S A*, 48, 1014-1022. <https://doi.org/10.1073/pnas.48.6.1014>
- Grossman, M., Tworowski, D., Dym, O., Lee, M. H., Levy, Y., Murphy, G., & Sagi, I. (2010). The intrinsic protein flexibility of endogenous protease inhibitor TIMP-1 controls its binding interface and affects its function. *Biochemistry*, 49(29), 6184-6192. <https://doi.org/10.1021/bi902141x>
- Gu, H. M., Adijiang, A., Mah, M., & Zhang, D. W. (2013). Characterization of the role of EGF-A of low-density lipoprotein receptor in PCSK9 binding. *J Lipid Res*, 54(12), 3345-3357. <https://doi.org/10.1194/jlr.M041129>
- Gu, H. M., Li, G., Gao, X., Berthiaume, L. G., & Zhang, D. W. (2013). Characterization of palmitoylation of ATP binding cassette transporter G1: effect on protein trafficking and function. *Biochim Biophys Acta*, 1831(6), 1067-1078. <https://doi.org/10.1016/j.bbalip.2013.01.019>
- Gu, H. M., Wang, F., Alabi, A., Deng, S., Qin, S., & Zhang, D. W. (2016). Identification of an Amino Acid Residue Critical for Plasma Membrane Localization of ATP-Binding Cassette Transporter G1. *Arterioscler Thromb Vasc Biol*, 36(2), 253-255. <https://doi.org/10.1161/ATVBAHA.115.306592>
- Gu, H. M., Wang, F. Q., & Zhang, D. W. (2014). Caveolin-1 interacts with ATP binding cassette transporter G1 (ABCG1) and regulates ABCG1-mediated cholesterol efflux. *Biochim Biophys Acta*, 1841(6), 847-858. <https://doi.org/10.1016/j.bbalip.2014.02.002>
- Guo, S., Xia, X. D., Gu, H. M., & Zhang, D. W. (2020). Proprotein Convertase Subtilisin/Kexin-Type 9 and Lipid Metabolism. *Adv Exp Med Biol*, 1276, 137-156. https://doi.org/10.1007/978-981-15-6082-8_9
- Hansen, H. H., HM, A. E., Oro, D., Evers, S. S., Heeboll, S., Eriksen, P. L., Thomsen, K. L., Bengtsson, A., Veidal, S. S., Feigh, M., Suppli, M. P., Knop, F. K., Gronbaek, H., Miranda, D., Trevaskis, J. L., Vrang, N., Jelsing, J., & Rigbolt, K. T. G. (2020). Human translatability of the GAN diet-induced obese mouse model of non-alcoholic steatohepatitis. *BMC Gastroenterol*, 20(1), 210. <https://doi.org/10.1186/s12876-020-01356-2>
- Heart&Stroke, H. a. S. F. (2022). *Atherosclerosis*. Retrieved March 15, 2022 from https://www.heartandstroke.ca/heart-disease/conditions/atherosclerosis?gclid=Cj0KCQjw0PWRBhDKARIsAPKHFGiG9ZTKaxcHTsddDuF9WMI2zCKkbK6jgr4MI5S-ZcF59QS_L8CJ5FcaAibGEALw_wcB&gclsrc=aw.ds
- Henriksson, E., & Andersen, B. (2020). FGF19 and FGF21 for the Treatment of NASH-Two Sides of the Same Coin? Differential and Overlapping Effects of FGF19 and FGF21 From Mice to Human. *Front Endocrinol (Lausanne)*, 11, 601349. <https://doi.org/10.3389/fendo.2020.601349>
- Holmbeck, K., Bianco, P., Caterina, J., Yamada, S., Kromer, M., Kuznetsov, S. A., Mankani, M., Robey, P. G., Poole, A. R., Pidoux, I., Ward, J. M., & Birkedal-Hansen, H. (1999). MT1-MMP-deficient mice develop dwarfism, osteopenia, arthritis, and connective tissue disease due to inadequate collagen turnover. *Cell*, 99(1), 81-92. <http://www.ncbi.nlm.nih.gov/pubmed/10520996>
- Horton, J. D., Cohen, J. C., & Hobbs, H. H. (2009). PCSK9: a convertase that coordinates LDL catabolism. *J Lipid Res*, 50 Suppl, S172-177. <https://doi.org/10.1194/jlr.R800091-JLR200>
- Horton, J. D., Shah, N. A., Warrington, J. A., Anderson, N. N., Park, S. W., Brown, M. S., & Goldstein, J. L. (2003). Combined analysis of oligonucleotide microarray data from transgenic

and knockout mice identifies direct SREBP target genes. *Proc Natl Acad Sci U S A*, 100(21), 12027-12032. <https://doi.org/10.1073/pnas.1534923100>

1534923100 [pii]

- Houghton, A. M. (2015). Matrix metalloproteinases in destructive lung disease. *Matrix Biol*, 44-46, 167-174. <https://doi.org/10.1016/j.matbio.2015.02.002>
- Iida, J., Wilhelmson, K. L., Price, M. A., Wilson, C. M., Pei, D., Furcht, L. T., & McCarthy, J. B. (2004). Membrane type-1 matrix metalloproteinase promotes human melanoma invasion and growth. *J Invest Dermatol*, 122(1), 167-176. <https://doi.org/10.1046/j.0022-202X.2003.22114.x>
- Itoh, Y. (2015). Membrane-type matrix metalloproteinases: Their functions and regulations. *Matrix Biol*, 44-46, 207-223. <https://doi.org/10.1016/j.matbio.2015.03.004>
- Itoh, Y., Ito, N., Nagase, H., & Seiki, M. (2008). The second dimer interface of MT1-MMP, the transmembrane domain, is essential for ProMMP-2 activation on the cell surface. *J Biol Chem*, 283(19), 13053-13062. <https://doi.org/10.1074/jbc.M709327200>
- Jahn, D., Kircher, S., Hermanns, H. M., & Geier, A. (2019). Animal models of NAFLD from a hepatologist's point of view. *Biochim Biophys Acta Mol Basis Dis*, 1865(5), 943-953. <https://doi.org/10.1016/j.bbadis.2018.06.023>
- Jeon, H., & Blacklow, S. C. (2005). Structure and physiologic function of the low-density lipoprotein receptor. *Annu Rev Biochem*, 74, 535-562. <https://doi.org/10.1146/annurev.biochem.74.082803.133354>
- Jumper, J., Evans, R., Pritzel, A., Green, T., Figurnov, M., Ronneberger, O., Tunyasuvunakool, K., Bates, R., Zidek, A., Potapenko, A., Bridgland, A., Meyer, C., Kohl, S. A. A., Ballard, A. J., Cowie, A., Romera-Paredes, B., Nikolov, S., Jain, R., Adler, J., . . . Hassabis, D. (2021). Highly accurate protein structure prediction with AlphaFold. *Nature*, 596(7873), 583-589. <https://doi.org/10.1038/s41586-021-03819-2>
- Karsenty, G., & Park, R. W. (1995). Regulation of type I collagen genes expression. *Int Rev Immunol*, 12(2-4), 177-185. <https://doi.org/10.3109/08830189509056711>
- Kim, D., Kobayashi, T., & Nagao, K. (2019). Research Techniques Made Simple: Mouse Models of Atopic Dermatitis. *J Invest Dermatol*, 139(5), 984-990 e981. <https://doi.org/10.1016/j.jid.2019.02.014>
- Kim, Y. O., Popov, Y., & Schuppan, D. (2017). Optimized Mouse Models for Liver Fibrosis. *Methods Mol Biol*, 1559, 279-296. https://doi.org/10.1007/978-1-4939-6786-5_19
- Knittel, T., Mehde, M., Kobold, D., Saile, B., Dinter, C., & Ramadori, G. (1999). Expression patterns of matrix metalloproteinases and their inhibitors in parenchymal and non-parenchymal cells of rat liver: regulation by TNF-alpha and TGF-beta1. *J Hepatol*, 30(1), 48-60. [https://doi.org/10.1016/s0168-8278\(99\)80007-5](https://doi.org/10.1016/s0168-8278(99)80007-5)
- Kolber, M. R., Nickonchuk, T., & Turgeon, R. (2018). Do PCSK9 inhibitors reduce cardiovascular events? *Can Fam Physician*, 64(9), 669. <https://www.ncbi.nlm.nih.gov/pubmed/30209099>
- Krstic, J., & Santibanez, J. F. (2014). Transforming growth factor-beta and matrix metalloproteinases: functional interactions in tumor stroma-infiltrating myeloid cells. *ScientificWorldJournal*, 2014, 521754. <https://doi.org/10.1155/2014/521754>
- Kumar, S., Ratnikov, B. I., Kazanov, M. D., Smith, J. W., & Cieplak, P. (2015). CleavPredict: A Platform for Reasoning about Matrix Metalloproteinases Proteolytic Events. *PLoS One*, 10(5), e0127877. <https://doi.org/10.1371/journal.pone.0127877>
- Lagace, T. A. (2014). PCSK9 and LDLR degradation: regulatory mechanisms in circulation and in cells. *Curr Opin Lipidol*, 25(5), 387-393. <https://doi.org/10.1097/MOL.0000000000000114>
- Lang, R., Braun, M., Sounni, N. E., Noel, A., Frankenne, F., Foidart, J. M., Bode, W., & Maskos, K. (2004). Crystal structure of the catalytic domain of MMP-16/MT3-MMP: characterization of

- MT-MMP specific features. *J Mol Biol*, 336(1), 213-225.
<https://doi.org/10.1016/j.jmb.2003.12.022>
- Lehti, K., Valtanen, H., Wickstrom, S. A., Lohi, J., & Keski-Oja, J. (2000). Regulation of membrane-type-1 matrix metalloproteinase activity by its cytoplasmic domain. *J Biol Chem*, 275(20), 15006-15013. <https://doi.org/10.1074/jbc.M910220199>
- Libby, P. (2021). The changing landscape of atherosclerosis. *Nature*, 592(7855), 524-533.
<https://doi.org/10.1038/s41586-021-03392-8>
- Lohi, J., Lehti, K., Valtanen, H., Parks, W. C., & Keski-Oja, J. (2000). Structural analysis and promoter characterization of the human membrane-type matrix metalloproteinase-1 (MT1-MMP) gene. *Gene*, 242(1-2), 75-86. [https://doi.org/10.1016/s0378-1119\(99\)00549-1](https://doi.org/10.1016/s0378-1119(99)00549-1)
- Lu, H., & Daugherty, A. (2015). Atherosclerosis. *Arterioscler Thromb Vasc Biol*, 35(3), 485-491.
<https://doi.org/10.1161/ATVBAHA.115.305380>
- Luo, J., Yang, H., & Song, B. L. (2020). Mechanisms and regulation of cholesterol homeostasis. *Nat Rev Mol Cell Biol*, 21(4), 225-245. <https://doi.org/10.1038/s41580-019-0190-7>
- Marcink, T. C., Simoncic, J. A., An, B., Knapinska, A. M., Fulcher, Y. G., Akkaladevi, N., Fields, G. B., & Van Doren, S. R. (2019). MT1-MMP Binds Membranes by Opposite Tips of Its beta Propeller to Position It for Pericellular Proteolysis. *Structure*, 27(2), 281-292 e286.
<https://doi.org/10.1016/j.str.2018.10.008>
- Mayne, J., Ooi, T. C., Tepliakova, L., Seebun, D., Walker, K., Mohottalage, D., Ning, Z., Abujrad, H., Mbikay, M., Wassef, H., Chretien, M., & Figeys, D. (2018). Associations Between Soluble LDLR and Lipoproteins in a Caucasian Cohort and The Effect of PCSK9 Loss-of-Function. *J Clin Endocrinol Metab*. <https://doi.org/10.1210/jc.2018-00777>
- Mayne, J., Raymond, A., Chaplin, A., Cousins, M., Kaefer, N., Gyamera-Acheampong, C., Seidah, N. G., Mbikay, M., Chretien, M., & Ooi, T. C. (2007). Plasma PCSK9 levels correlate with cholesterol in men but not in women. *Biochem Biophys Res Commun*, 361(2), 451-456.
http://www.ncbi.nlm.nih.gov/entrez/query.fcgi?cmd=Retrieve&db=PubMed&dopt=Citation&list_uids=17645871
- Mori, H., Lo, A. T., Inman, J. L., Alcaraz, J., Ghajar, C. M., Mott, J. D., Nelson, C. M., Chen, C. S., Zhang, H., Bascom, J. L., Seiki, M., & Bissell, M. J. (2013). Transmembrane/cytoplasmic, rather than catalytic, domains of Mmp14 signal to MAPK activation and mammary branching morphogenesis via binding to integrin beta1. *Development*, 140(2), 343-352.
<https://doi.org/10.1242/dev.084236>
- Mori, H., Tomari, T., Koshikawa, N., Kajita, M., Itoh, Y., Sato, H., Tojo, H., Yana, I., & Seiki, M. (2002). CD44 directs membrane-type 1 matrix metalloproteinase to lamellipodia by associating with its hemopexin-like domain. *EMBO J*, 21(15), 3949-3959.
<https://doi.org/10.1093/emboj/cdf411>
- Mu, D., Cambier, S., Fjellbirkeland, L., Baron, J. L., Munger, J. S., Kawakatsu, H., Sheppard, D., Broaddus, V. C., & Nishimura, S. L. (2002). The integrin alpha(v)beta8 mediates epithelial homeostasis through MT1-MMP-dependent activation of TGF-beta1. *J Cell Biol*, 157(3), 493-507. <https://doi.org/10.1083/jcb.200109100>
- Musso, G., Gambino, R., & Cassader, M. (2013). Cholesterol metabolism and the pathogenesis of non-alcoholic steatohepatitis. *Prog Lipid Res*, 52(1), 175-191.
<https://doi.org/10.1016/j.plipres.2012.11.002>
- Nakerakanti, S., & Trojanowska, M. (2012). The Role of TGF-beta Receptors in Fibrosis. *Open Rheumatol J*, 6, 156-162. <https://doi.org/10.2174/1874312901206010156>
- Newberry, E. P., Hall, Z., Xie, Y., Molitor, E. A., Bayguinov, P. O., Strout, G. W., Fitzpatrick, J. A. J., Brunt, E. M., Griffin, J. L., & Davidson, N. O. (2021). Liver-Specific Deletion of Mouse Tm6sf2 Promotes Steatosis, Fibrosis, and Hepatocellular Cancer. *Hepatology*, 74(3), 1203-1219. <https://doi.org/10.1002/hep.31771>

- Osenkowski, P., Toth, M., & Fridman, R. (2004). Processing, shedding, and endocytosis of membrane type 1-matrix metalloproteinase (MT1-MMP). *J Cell Physiol*, 200(1), 2-10. <https://doi.org/10.1002/jcp.20064>
- Page-McCaw, A., Ewald, A. J., & Werb, Z. (2007). Matrix metalloproteinases and the regulation of tissue remodelling. *Nat Rev Mol Cell Biol*, 8(3), 221-233. <https://doi.org/10.1038/nrm2125>
- Pahwa, S., Stawikowski, M. J., & Fields, G. B. (2014). Monitoring and Inhibiting MT1-MMP during Cancer Initiation and Progression. *Cancers (Basel)*, 6(1), 416-435. <https://doi.org/10.3390/cancers6010416>
- Panera, N., Gnani, D., Crudele, A., Ceccarelli, S., Nobili, V., & Alisi, A. (2014). MicroRNAs as controlled systems and controllers in non-alcoholic fatty liver disease. *World J Gastroenterol*, 20(41), 15079-15086. <https://doi.org/10.3748/wjg.v20.i41.15079>
- Pawlak, M., Lefebvre, P., & Staels, B. (2015). Molecular mechanism of PPARalpha action and its impact on lipid metabolism, inflammation and fibrosis in non-alcoholic fatty liver disease. *J Hepatol*, 62(3), 720-733. <https://doi.org/10.1016/j.jhep.2014.10.039>
- Petta, S., Marchesini, G., Caracausi, L., Macaluso, F. S., Camma, C., Ciminnisi, S., Cabibi, D., Porcasi, R., Craxi, A., & Di Marco, V. (2013). Industrial, not fruit fructose intake is associated with the severity of liver fibrosis in genotype 1 chronic hepatitis C patients. *J Hepatol*, 59(6), 1169-1176. <https://doi.org/10.1016/j.jhep.2013.07.037>
- Pijuan, J., Barcelo, C., Moreno, D. F., Maiques, O., Siso, P., Marti, R. M., Macia, A., & Panosa, A. (2019). In vitro Cell Migration, Invasion, and Adhesion Assays: From Cell Imaging to Data Analysis. *Front Cell Dev Biol*, 7, 107. <https://doi.org/10.3389/fcell.2019.00107>
- Quintero-Fabian, S., Arreola, R., Becerril-Villanueva, E., Torres-Romero, J. C., Arana-Argaez, V., Lara-Riegos, J., Ramirez-Camacho, M. A., & Alvarez-Sanchez, M. E. (2019). Role of Matrix Metalloproteinases in Angiogenesis and Cancer. *Front Oncol*, 9, 1370. <https://doi.org/10.3389/fonc.2019.01370>
- Ra, H. J., & Parks, W. C. (2007). Control of matrix metalloproteinase catalytic activity. *Matrix Biol*, 26(8), 587-596. <https://doi.org/10.1016/j.matbio.2007.07.001>
- Rawson, R. B. (2003). The SREBP pathway--insights from Insigs and insects. *Nat Rev Mol Cell Biol*, 4(8), 631-640. <https://doi.org/10.1038/nrm1174>
- Rosselli, M., Lotersztajn, S., Vizzutti, F., Arena, U., Pinzani, M., & Marra, F. (2014). The metabolic syndrome and chronic liver disease. *Curr Pharm Des*, 20(31), 5010-5024. <https://doi.org/10.2174/1381612819666131206111352>
- Rozañov, D. V., Deryugina, E. I., Monosov, E. Z., Marchenko, N. D., & Strongin, A. Y. (2004). Aberrant, persistent inclusion into lipid rafts limits the tumorigenic function of membrane type-1 matrix metalloproteinase in malignant cells. *Exp Cell Res*, 293(1), 81-95. <https://doi.org/10.1016/j.yexcr.2003.10.006>
- Rozañov, D. V., Deryugina, E. I., Ratnikov, B. I., Monosov, E. Z., Marchenko, G. N., Quigley, J. P., & Strongin, A. Y. (2001). Mutation analysis of membrane type-1 matrix metalloproteinase (MT1-MMP). The role of the cytoplasmic tail Cys(574), the active site Glu(240), and furin cleavage motifs in oligomerization, processing, and self-proteolysis of MT1-MMP expressed in breast carcinoma cells. *J Biol Chem*, 276(28), 25705-25714. <https://doi.org/10.1074/jbc.M007921200>
- Rozañov, D. V., Hahn-Dantona, E., Strickland, D. K., & Strongin, A. Y. (2004). The low density lipoprotein receptor-related protein LRP is regulated by membrane type-1 matrix metalloproteinase (MT1-MMP) proteolysis in malignant cells [In Vitro
- Research Support, Non-U.S. Gov't
- Research Support, U.S. Gov't, P.H.S.]. *J Biol Chem*, 279(6), 4260-4268. <https://doi.org/10.1074/jbc.M311569200>

- Rudenko, G., Henry, L., Henderson, K., Ichtchenko, K., Brown, M. S., Goldstein, J. L., & Deisenhofer, J. (2002). Structure of the LDL receptor extracellular domain at endosomal pH. *Science*, 298(5602), 2353-2358. <https://doi.org/10.1126/science.1078124>
- Russell, D. W., Brown, M. S., & Goldstein, J. L. (1989). Different combinations of cysteine-rich repeats mediate binding of low density lipoprotein receptor to two different proteins. *J Biol Chem*, 264(36), 21682-21688. http://www.ncbi.nlm.nih.gov/entrez/query.fcgi?cmd=Retrieve&db=PubMed&dopt=Citation&list_uids=2600087
- Sabatine, M. S. (2019). PCSK9 inhibitors: clinical evidence and implementation. *Nat Rev Cardiol*, 16(3), 155-165. <https://doi.org/10.1038/s41569-018-0107-8>
- Sakai, K., Nakamura, T., Suzuki, Y., Imizu, T., & Matsumoto, K. (2011). 3-D collagen-dependent cell surface expression of MT1-MMP and MMP-2 activation regardless of integrin beta1 function and matrix stiffness. *Biochem Biophys Res Commun*, 412(1), 98-103. <https://doi.org/10.1016/j.bbrc.2011.07.050>
- Sato, H., Takino, T., Okada, Y., Cao, J., Shinagawa, A., Yamamoto, E., & Seiki, M. (1994). A matrix metalloproteinase expressed on the surface of invasive tumour cells. *Nature*, 370(6484), 61-65. <https://doi.org/10.1038/370061a0>
- Schlaepfer, I. R., & Joshi, M. (2020). CPT1A-mediated Fat Oxidation, Mechanisms, and Therapeutic Potential. *Endocrinology*, 161(2). <https://doi.org/10.1210/endo/bqz046>
- Schwabe, R. F., Tabas, I., & Pajvani, U. B. (2020). Mechanisms of Fibrosis Development in Nonalcoholic Steatohepatitis. *Gastroenterology*, 158(7), 1913-1928. <https://doi.org/10.1053/j.gastro.2019.11.311>
- Seidah, N. G. (2017). The PCSK9 revolution and the potential of PCSK9-based therapies to reduce LDL-cholesterol. *Glob Cardiol Sci Pract*, 2017(1), e201702. <https://doi.org/10.21542/gcsp.2017.2>
- Seidah, N. G., Awan, Z., Chretien, M., & Mbikay, M. (2014). PCSK9: a key modulator of cardiovascular health. *Circ Res*, 114(6), 1022-1036. <https://doi.org/10.1161/CIRCRESAHA.114.301621>
- Shen, Y., Wang, B., Deng, S., Zhai, L., Gu, H. M., Alabi, A., Xia, X., Zhao, Y., Chang, X., Qin, S., & Zhang, D. W. (2020). Surf4 regulates expression of proprotein convertase subtilisin/kexin type 9 (PCSK9) but is not required for PCSK9 secretion in cultured human hepatocytes. *Biochim Biophys Acta Mol Cell Biol Lipids*, 1865(2), 158555. <https://doi.org/10.1016/j.bbalip.2019.158555>
- Shimano, H., & Sato, R. (2017). SREBP-regulated lipid metabolism: convergent physiology - divergent pathophysiology. *Nat Rev Endocrinol*, 13(12), 710-730. <https://doi.org/10.1038/nrendo.2017.91>
- Shimohiro, H., Taniguchi, S. I., Koda, M., Sakai, C., & Yamada, S. (2014). Association Between Serum Soluble Low-Density Lipoprotein Receptor Levels and Metabolic Factors in Healthy Japanese Individuals. *J Clin Lab Anal*, 29(1), 52-56. <https://doi.org/10.1002/jcla.21727>
- Shiryayev, S. A., Remacle, A. G., Golubkov, V. S., Ingvarsen, S., Porse, A., Behrendt, N., Cieplak, P., & Strongin, A. Y. (2013). A monoclonal antibody interferes with TIMP-2 binding and incapacitates the MMP-2-activating function of multifunctional, pro-tumorigenic MMP-14/MT1-MMP. *Oncogenesis*, 2, e80. <https://doi.org/10.1038/oncsis.2013.44>
- Snoek-van Beurden, P. A., & Von den Hoff, J. W. (2005). Zymographic techniques for the analysis of matrix metalloproteinases and their inhibitors. *Biotechniques*, 38(1), 73-83. <https://doi.org/10.2144/05381RV01>
- Sodek, K. L., Ringuette, M. J., & Brown, T. J. (2007). MT1-MMP is the critical determinant of matrix degradation and invasion by ovarian cancer cells. *Br J Cancer*, 97(3), 358-367. <https://doi.org/10.1038/sj.bjc.6603863>

- Stancu, C., & Sima, A. (2001). Statins: mechanism of action and effects. *J Cell Mol Med*, 5(4), 378-387. <https://doi.org/10.1111/j.1582-4934.2001.tb00172.x>
- Su, S., Tian, H., Jia, X., Zhu, X., Wu, J., Zhang, Y., Chen, Y., Li, Z., & Zhou, Y. (2020). Mechanistic insights into the effects of SREBP1c on hepatic stellate cell and liver fibrosis. *J Cell Mol Med*, 24(17), 10063-10074. <https://doi.org/10.1111/jcmm.15614>
- Takawale, A., Sakamuri, S. S., & Kassiri, Z. (2015). Extracellular matrix communication and turnover in cardiac physiology and pathology. *Compr Physiol*, 5(2), 687-719. <https://doi.org/10.1002/cphy.c140045>
- Tam, E. M., Moore, T. R., Butler, G. S., & Overall, C. M. (2004). Characterization of the distinct collagen binding, helicase and cleavage mechanisms of matrix metalloproteinase 2 and 14 (gelatinase A and MT1-MMP): the differential roles of the MMP hemopexin c domains and the MMP-2 fibronectin type II modules in collagen triple helicase activities. *J Biol Chem*, 279(41), 43336-43344. <https://doi.org/10.1074/jbc.M407186200>
- Tetri, L. H., Basaranoglu, M., Brunt, E. M., Yerian, L. M., & Neuschwander-Tetri, B. A. (2008). Severe NAFLD with hepatic necroinflammatory changes in mice fed trans fats and a high-fructose corn syrup equivalent. *Am J Physiol Gastrointest Liver Physiol*, 295(5), G987-995. <https://doi.org/10.1152/ajpgi.90272.2008>
- Tochowicz, A., Goettig, P., Evans, R., Visse, R., Shitomi, Y., Palmisano, R., Ito, N., Richter, K., Maskos, K., Franke, D., Svergun, D., Nagase, H., Bode, W., & Itoh, Y. (2011). The dimer interface of the membrane type 1 matrix metalloproteinase hemopexin domain: crystal structure and biological functions. *J Biol Chem*, 286(9), 7587-7600. <https://doi.org/10.1074/jbc.M110.178434>
- Toth, M., Hernandez-Barrantes, S., Osenkowski, P., Bernardo, M. M., Gervasi, D. C., Shimura, Y., Meroueh, O., Kotra, L. P., Galvez, B. G., Arroyo, A. G., Mobashery, S., & Fridman, R. (2002). Complex pattern of membrane type 1 matrix metalloproteinase shedding. Regulation by autocatalytic cells surface inactivation of active enzyme. *J Biol Chem*, 277(29), 26340-26350. <https://doi.org/10.1074/jbc.M200655200>
- Van Doren, S. R., Marcink, T. C., Koppiseti, R. K., Jurkevich, A., & Fulcher, Y. G. (2017). Peripheral membrane associations of matrix metalloproteinases. *Biochim Biophys Acta Mol Cell Res*, 1864(11 Pt A), 1964-1973. <https://doi.org/10.1016/j.bbamcr.2017.04.013>
- van Driel, I. R., Davis, C. G., Goldstein, J. L., & Brown, M. S. (1987). Self-association of the low density lipoprotein receptor mediated by the cytoplasmic domain. *J Biol Chem*, 262(33), 16127-16134. http://www.ncbi.nlm.nih.gov/entrez/query.fcgi?cmd=Retrieve&db=PubMed&dopt=Citation&list_uids=3680245
- Vance, D. E. (2013). Physiological roles of phosphatidylethanolamine N-methyltransferase. *Biochim Biophys Acta*, 1831(3), 626-632. <https://doi.org/10.1016/j.bbali.2012.07.017>
- Vandenbroucke, R. E., & Libert, C. (2014). Is there new hope for therapeutic matrix metalloproteinase inhibition? *Nat Rev Drug Discov*, 13(12), 904-927. <https://doi.org/10.1038/nrd4390>
- Vuorio, A., Kuoppala, J., Kovanen, P. T., Humphries, S. E., Tonstad, S., Wiegman, A., Drogari, E., & Ramaswami, U. (2017). Statins for children with familial hypercholesterolemia. *Cochrane Database Syst Rev*, 7, CD006401. <https://doi.org/10.1002/14651858.CD006401.pub4>
- Wang, F., Li, G., Gu, H. M., & Zhang, D. W. (2013). Characterization of the role of a highly conserved sequence in ATP binding cassette transporter G (ABCG) family in ABCG1 stability, oligomerization and trafficking. *Biochemistry*, 52(52), 9497-9509. <https://doi.org/10.1021/bi401285j>
- Wang, M., Zhao, D., Spinetti, G., Zhang, J., Jiang, L. Q., Pintus, G., Monticone, R., & Lakatta, E. G. (2006). Matrix metalloproteinase 2 activation of transforming growth factor-beta1 (TGF-beta1)

- and TGF-beta1-type II receptor signaling within the aged arterial wall. *Arterioscler Thromb Vasc Biol*, 26(7), 1503-1509. <https://doi.org/10.1161/01.ATV.0000225777.58488.f2>
- Wang, Y., Dubland, J. A., Allahverdian, S., Asonye, E., Sahin, B., Jaw, J. E., Sin, D. D., Seidman, M. A., Leeper, N. J., & Francis, G. A. (2019). Smooth Muscle Cells Contribute the Majority of Foam Cells in ApoE (Apolipoprotein E)-Deficient Mouse Atherosclerosis. *Arterioscler Thromb Vasc Biol*, 39(5), 876-887. <https://doi.org/10.1161/ATVBAHA.119.312434>
- Weaver, S. A., Wolters, B., Ito, N., Woskowicz, A. M., Kaneko, K., Shitomi, Y., Seiki, M., & Itoh, Y. (2014). Basal localization of MT1-MMP is essential for epithelial cell morphogenesis in 3D collagen matrix. *J Cell Sci*, 127(Pt 6), 1203-1213. <https://doi.org/10.1242/jcs.135236>
- WHO, N.-c. d. W. H. O. (2022). *Cardiovascular diseases*. Retrieved March 15, 2022 from <https://www.who.int/health-topics/cardiovascular-diseases>
- Wilkesman, J., & Kurz, L. (2017). Zymography Principles. *Methods Mol Biol*, 1626, 3-10. https://doi.org/10.1007/978-1-4939-7111-4_1
- Woskowicz, A. M., Weaver, S. A., Shitomi, Y., Ito, N., & Itoh, Y. (2013). MT-LOOP-dependent localization of membrane type I matrix metalloproteinase (MT1-MMP) to the cell adhesion complexes promotes cancer cell invasion. *J Biol Chem*, 288(49), 35126-35137. <https://doi.org/10.1074/jbc.M113.496067>
- Xia, X. D., Alabi, A., Wang, M., Gu, H. M., Yang, R. Z., Wang, G., & Zhang, D. W. (2021a). Membrane-type I matrix metalloproteinase (MT1-MMP), lipid metabolism and therapeutic implications. *J Mol Cell Biol*, 13(7), 513-526. <https://doi.org/10.1093/jmcb/mjab048>
- Xia, X. D., Alabi, A., Wang, M., Gu, H. M., Yang, R. Z., Wang, G. Q., & Zhang, D. W. (2021b). Membrane-type I matrix metalloproteinase (MT1-MMP), lipid metabolism, and therapeutic implications. *J Mol Cell Biol*, 13(7), 513-526. <https://doi.org/10.1093/jmcb/mjab048>
- Xia, X. D., Peng, Z. S., Gu, H. M., Wang, M., Wang, G. Q., & Zhang, D. W. (2021). Regulation of PCSK9 Expression and Function: Mechanisms and Therapeutic Implications. *Front Cardiovasc Med*, 8, 764038. <https://doi.org/10.3389/fcvm.2021.764038>
- Xue, L., Qi, H., Zhang, H., Ding, L., Huang, Q., Zhao, D., Wu, B. J., & Li, X. (2020). Targeting SREBP-2-Regulated Mevalonate Metabolism for Cancer Therapy. *Front Oncol*, 10, 1510. <https://doi.org/10.3389/fonc.2020.01510>
- Yanez-Mo, M., Barreiro, O., Gonzalo, P., Batista, A., Megias, D., Genis, L., Sachs, N., Sala-Valdes, M., Alonso, M. A., Montoya, M. C., Sonnenberg, A., Arroyo, A. G., & Sanchez-Madrid, F. (2008). MT1-MMP collagenolytic activity is regulated through association with tetraspanin CD151 in primary endothelial cells. *Blood*, 112(8), 3217-3226. <https://doi.org/10.1182/blood-2008-02-139394>
- Yang, H. X., Zhang, M., Long, S. Y., Tuo, Q. H., Tian, Y., Chen, J. X., Zhang, C. P., & Liao, D. F. (2020). Cholesterol in LDL receptor recycling and degradation. *Clin Chim Acta*, 500, 81-86. <https://doi.org/10.1016/j.cca.2019.09.022>
- Yanguas, S. C., Cogliati, B., Willebrords, J., Maes, M., Colle, I., van den Bossche, B., de Oliveira, C., Andraus, W., Alves, V. A. F., Leclercq, I., & Vinken, M. (2016). Experimental models of liver fibrosis. *Arch Toxicol*, 90(5), 1025-1048. <https://doi.org/10.1007/s00204-015-1543-4>
- Youngblom, E., Pariani, M., & Knowles, J. W. (1993). Familial Hypercholesterolemia. In M. P. Adam, H. H. Ardinger, R. A. Pagon, S. E. Wallace, L. J. H. Bean, G. Mirzaa, & A. Amemiya (Eds.), *GeneReviews((R))*. <https://www.ncbi.nlm.nih.gov/pubmed/24404629>
- Zarrabi, K., Dufour, A., Li, J., Kuscu, C., Pulkoski-Gross, A., Zhi, J., Hu, Y., Sampson, N. S., Zucker, S., & Cao, J. (2011). Inhibition of matrix metalloproteinase 14 (MMP-14)-mediated cancer cell migration. *J Biol Chem*, 286(38), 33167-33177. <https://doi.org/10.1074/jbc.M111.256644>
- Zhang, D. W., Garuti, R., Tang, W. J., Cohen, J. C., & Hobbs, H. H. (2008). Structural requirements for PCSK9-mediated degradation of the low-density lipoprotein receptor. *Proc Natl Acad Sci U S A*, 105(35), 13045-13050.

http://www.ncbi.nlm.nih.gov/entrez/query.fcgi?cmd=Retrieve&db=PubMed&dopt=Citation&list_uids=18753623

Zhang, D. W., Lagace, T. A., Garuti, R., Zhao, Z., McDonald, M., Horton, J. D., Cohen, J. C., & Hobbs, H. H. (2007). Binding of proprotein convertase subtilisin/kexin type 9 to epidermal growth factor-like repeat A of low density lipoprotein receptor decreases receptor recycling and increases degradation. *J Biol Chem*, 282(25), 18602-18612.

http://www.ncbi.nlm.nih.gov/entrez/query.fcgi?cmd=Retrieve&db=PubMed&dopt=Citation&list_uids=17452316

Zhou, Z., Apte, S. S., Soininen, R., Cao, R., Baaklini, G. Y., Rauser, R. W., Wang, J., Cao, Y., & Tryggvason, K. (2000). Impaired endochondral ossification and angiogenesis in mice deficient in membrane-type matrix metalloproteinase I. *Proc Natl Acad Sci U S A*, 97(8), 4052-4057.

<https://doi.org/10.1073/pnas.060037197>

Zia, Y., Al Rajabi, A., Mi, S., Ju, T., Leonard, K. A., Nelson, R., Thiesen, A., Willing, B. P., Field, C. J., Curtis, J. M., van der Veen, J. N., & Jacobs, R. L. (2018). Hepatic Expression of PEMT, but Not Dietary Choline Supplementation, Reverses the Protection against Atherosclerosis in Pemt^{-/-}/Ldlr^{-/-} Mice. *J Nutr*, 148(10), 1513-1520. <https://doi.org/10.1093/jn/nxy165>

Zucker, S., Hymowitz, M., Conner, C. E., DiYanni, E. A., & Cao, J. (2002). Rapid trafficking of membrane type 1-matrix metalloproteinase to the cell surface regulates progelatinase activation [Research Support, Non-U.S. Gov't

Research Support, U.S. Gov't, Non-P.H.S.]. *Lab Invest*, 82(12), 1673-1684.

<http://www.ncbi.nlm.nih.gov/pubmed/12480917>